Examining Chromatin Modifiers Essential for Glioma Growth and Drug Response

by

Ezgi Yağmur Kala Kalkan

A Dissertation Submitted to the

Graduate School of Health Sciences

in Partial Fulfillment of the Requirements for

the Degree of

Doctor of Philosophy

In

Cellular and Molecular Medicine

December 25, 2023

Examining Chromatin Modifiers Essential for Glioma Growth and Drug Response

Koç University

Graduate School of Health Sciences

This is to certify that I have examined this copy of a doctoral dissertation by

Ezgi Yağmur KALA KALKAN

and have found that it is complete and satisfactory in all respects,
and that any and all revisions required by the final
examining committee has been made.

Committee Members:

_____

Prof. Tuğba Bağcı Önder (Advisor)

_____

Assoc. Prof. Umut Şahin

_____

Assist. Prof. Gözde Korkmaz

_____

Prof. Tamer Önder

_____

Assoc. Prof. Nihal Karakaş

Date: 25.12.2023

I dedicate this thesis to

My mother, Tenzile, for her endless support,

My brother, Çağrı, for always being there for me,

For my husband, Batu, for being my forever lab partner,

And finally, to my father, Mustafa, for everything he taught me about life.

ABSTRACT

Examining Chromatin Modifiers Essential for Glioma Growth and Drug Response

Ezgi Yağmur Kala Kalkan

Doctor of Philosophy in Cellular and Molecular Medicine

25.12.2023

Glioblastoma (GBM) is a highly aggressive primary brain tumor associated with low survival rates. Standard-of-care involves surgery, irradiation, and chemotherapy utilizing Temozolomide (TMZ), a DNA alkylating agent. Despite its high effectiveness, the efficacy of TMZ can be compromised by various epigenetic mechanisms, including the transcriptional regulation of 0-6-methylguanine methyltransferase (MGMT) enzyme expression. The promoter methylation status of *MGMT* is a crucial prognostic factor, as its epigenetic suppression enhances the response to TMZ. Novel epigenetic factors regulating the survival and resistance to therapy in GBM remain undiscovered.

To explore resistance mechanisms in GBM, we first generated TMZ-resistant cell lines starting from naïve cells and escalating TMZ doses over a long period. We demonstrated that TMZ-resistance phenotype was sustainable both *in vitro* and *in vivo*. Transcriptome analysis revealed *MGMT* as an upregulated gene in TMZ-resistant models along with many differentially expressed genes. Considering that resistance may be associated with adaptive epigenetic changes, we investigated the functional roles of chromatin regulators in TMZ-resistant cells. To this end, we employed a targeted CRISPR/Cas9-based screen with our Epigenetic Knock-Out sgRNA Library (EPIKOL), focusing on various chromatin modifiers and epigenetic enzymes. Applying EPIKOL screens in multiple naïve and TMZ-resistant cell lines, we first identified key epigenetic factors regulating GBM cell viability. We then explored selective vulnerability of TMZ-resistant cell lines and identified Retinoblastoma Binding Protein 4 (RBBP4) as a regulator of acquired TMZ resistance. Knock-out of RBBP4 in resistant models resulted in increased apoptosis and G2/M arrest. RNA sequencing of control and RPPB4 knock-out cells revealed G2/M checkpoint and E2F targets as downregulated pathways. We demonstrated that the expression of *MGMT* was not significantly altered by RBBP4 in

TMZ-resistant models, providing strong evidence for RBBP4-mediated regulation of cell proliferation and TMZ response in an MGMT-independent manner.

Overall, our findings hold promise for the development of innovative epigenetic-based therapeutic strategies targeting GBM in the future.

ÖZETÇE

Glioma Büyümesi ve İlaç Direncinde Kromatin Düzenleyicilerin Araştırılması

Ezgi Yağmur Kala Kalkan

Hücresel ve Moleküler Tıp, Doktora

25.12.2023

Glioblastoma (GBM), düşük sağkalım oranları ile ilişkilendirilen son derece agresif bir primer beyin tümörüdür. Standart terapi yöntemleri cerrahi, radyoterapi ve DNA alkillendirici ajan olarak Temozolomide (TMZ) kemoterapisini içerir. TMZ'nin etkinliği, MGMT gen ekspresyonunun düzenlenmesi gibi çeşitli epigenetik mekanizmalar tarafından olumsuz etkilenebilir ve *MGMT'nin* promotör metilasyon durumu TMZ yanıtında önemli bir prognostik faktördür. GBM'de sağkalımı ve terapiye direnci düzenleyen yeni epigenetik faktörler henüz keşfedilmemiştir. Bu çalışmada, GBM'deki direnç mekanizmalarını keşfetmek amacıyla TMZ dirençli hücre hatları oluşturduk. Direnç fenotipini *in vitro* ve *in vivo* deneylerle gösterdik. Geliştirilen TMZ-dirençli hücre hatlarında transkriptom analizi yaptık ve birçok farklı ifade edilen genler ile birlikte MGMT seviyesinin de önemli ölçüde arttığını gözlemledik. TMZ direncinin epigenetik değişiliklerle ilişkili olabileceğini düşünerek, çeşitli kromatin düzenleyici ve epigenetik enzimlerin hedeflendiği CRISPR/cas9 kütüphanesi EPIKOL ile tarama yaptık. Yapılan taramalar sonucunda, RBBP4 genini TMZ-dirençli hücreler için potansiyel bir hedef olarak belirledik. RBBP4 geninin susturulması sonucu hücre ölümünün arttığı ve hücre bölünmesinin G2/M fazlarında akümüle olduğunu gösterdik. Sonrasında yaptığımız RNA dizileme sonucunda G2/M ve E2F hedef yolaklarının önemli oranda azaldığını tespit ettik. RBBP4 susturulması sonucunda MGMT ekspresyon seviyesinin önemli oranda düşmediğini göstererek, MGMT'den bağımsız bir yolla dirençli hücrelerde hassasiyet oluşturma potansiyelini ortaya koyduk.

Transkriptom analizi, MGMT'nin TMZ dirençli modellerde artan bir gen olarak ortaya çıkmasını ve birçok farklı ifade edilen geni içeriyordu. Direncin adaptif epigenetik değişikliklerle ilişkili olabileceğini düşünerek, TMZ dirençli hücrelerde kromatin düzenleyicilerinin rollerini araştırdık. Çeşitli kromatin düzenleyicilerini ve epigenetik

enzimleri hedefleyen Epigenetik Knock-Out sgRNA Kütüphanemiz (EPIKOL) ile odaklı bir CRISPR/Cas9 tabanlı tarama yaptık. TMZ dirençli hücre hatlarının seçici hassasiyetini keşfettik ve Retinoblastoma Binding Protein 4 (RBBP4) genini kazanılmış TMZ direncinin bir düzenleyicisi olarak belirledik. Dirençli modellerde RBBP4'in knock-out'u, artan apoptoz ve G2/M tutuklanmasına neden oldu. RNA sekanslama analizi, G2/M kontrol noktası ve E2F hedeflerinin düşük olduğu yolları ortaya koydu. RBBP4 knock-out sonrası MGMT ekspresyonunun önemli ölçüde değişmediğini göstererek, RBBP4'un TMZ-dirençli hücrelerde MGMT'den bağımsız bir düzenleme gerçekleştirdiğine dair kanıt sunduk.

Elde ettiğimiz bulgular, gelecekte GBM'yi hedefleyen yenilikçi epigenetik tabanlı tedavi stratejilerinin gelişimi için umut verici bir potansiyel taşımaktadır.

ACKNOWLEDGEMENT

First, I would like to express my deepest gratitude to my PI, Prof. Tuğba Bağcı Önder. She has been incredibly supportive, and she has been there for me at all ups and downs throughout my thesis journey. I will always remember how understanding and supportive she was during my bad days and how happy and excited she was during my good days. I wouldn't be the scientist I am today without her; therefore, I will always be grateful.

I would like to thank my thesis committee members Assoc. Prof. Umut Şahin and Assist. Prof. Gözde Korkmaz for their guidance over the years. Their ideas were incredible valuable for me, and they help shaping my thesis. I would also like to acknowledge my thesis defence members Prof. Tamer Önder and Assoc. Prof. Nihal Karakaş for their valuable contributions.

I wish to thank by TBO Lab family, this PhD would not be completed without them. Biggest thanks go out to EPIKOL team, Dr. Özlem Yedier-Bayram and Dr. Göktuğ Karabıyık. The journal we embarked on together was challenging, however we always supported each other and got each other's backs. Özlem and Göktuğ became my companions and whenever I was in doubt or had a question, they were the first people I would go to. Next thank you is for my girls, Nareg Değirmenci, Ebru Yılmaz and Canan Bayraktar, for being the greatest friends anyone can ask for in both inside and outside of the lab. Dr. Ahmet Cingöz has been there for me whenever I needed, I will always remember our chats while having coffee. Beyza Nur Köseoğlu has been a companion for me while working over the weekends and thesis writing process, she made these difficult tasks fun and easy. I would also like to thank İpek Kök, Sedef Saraç and Aksel Çelikkol for their friendships and support. I am grateful to have Defne Yığcı as an undergraduate student over the years as she is an incredible smart person and helped me with many projects.

Besides the current members of TBO Lab, there are several alumni that made an impact in my life. Our recent MSc graduates, Mina Küçüktaş and Beril Esin are two amazing young scientists with a promising future ahead. I am very proud of them, and I miss having fun and listening to weird songs with both. Dr. Filiz Şenbabaoğlu-Aksu and Dr. Ali Cenk Aksu are the two amazing people that deserves a big thank you for their

endless support, friendship, and mentorship. I wish them a wonderful life. Dr. Ezgi Özyerli-Göknar will have a special place in my life as we supported each other and completed a challenging project while on different countries. I would also like to acknowledge Dr. Alişan Kayabölen and Dr. Fidan Şeker-Polat as great lab mates who were always helpful and supportive.

I would like to express my gratitude to my family for their patience and love. My mother Tenzile and my brother Çağrı never stopped believing in me and they have been my biggest supporters. I wish to believe that my father, Mustafa can see my accomplishments. He was the best father anyone can ask for, and I loved him very much. I hope that I made all of you proud.

Finally, I wish to thank my husband, Dr. Batuhan Mert Kalkan. I would not have done this without him. Life has not been easy for both of us, but we managed, and still managing, to overcome all the obstacles that is put in front of us. With our little family of three, including our cat Odin (A.K.A. Tospik Bey), we can face the world and embark on new adventures.

TABLE OF CONTENTS

LIST OF TABLES

LIST OF FIGURES

ABBREVIATIONS

ATRX	Alpha Thalassemia X-linked Mental Retardation Protein
BER	Base Excision Repair
CAF1	Chromatin Associated Factor 1
Cas9	CRISPR associated endonuclease 9
cDNA	Complementary DNA
CHD	Chromodomain Helicase DNA binding
CNS	Central Nervous System
CREBBP	CREB Binding Protein
CRISPR	Clustered Regularly Interspaced Short Palindromic Repeats
dCas9	Dead Cas9
DEG	Differentially Expressed Genes
DNMT	DNA Methyltransferase
DREAM	Dimerization Partner, RB-like, E2F and Multi-Vulval Class B
DSB	Double Strand Break
EP300	E1A Binding Protein P300
EPIKOL	Epigenetic Knockout Library
EZH2	Enhancer of Zeste Homolog 2
GBM	Glioblastoma
gRNA	Guide RNA
GSEA	Gene Set Enrichment Analysis
HAT	Histone Acetyltransferase
HDAC	Histone Deacethylase
HDM	Histone Demethylase
HMT	Histone Methyltransferase
HR	Homologous Repair
ISWI	Imitation Switch
KDM	Lysine Demethylase
KRAB	Kruppel-Associated Box
LFC	Log2 Fold Change
MGMT	O6 Methylguanine Methyltransferase

MMR	Mismatch Repair
MTIC	5-(3- methyltriazen-1-yl) imidazole-4-carboxamide
MuvB	Multi-Vulval Class B
NES	Negative Enrichment Score
NHEJ	Non-Homologous End Joining
NT	Non-Targeting
NuRD	Nucleosome remodeling and deacetylase
NuRF	Nucleosome Remodeling Factor
PAM	Protospacer Adjacent Motif
PARP1	Poly (ADP-ribose) Polymerase 1
PRC	Polycomb Repressive Complex
RB	Retinoblastoma
RBBP4	Retinoblastoma Binding Protein 4
RTK	Receptor Tyrosine Kinase
RT-qPCR	Reverse Transcriptase Quantitative PCR
SAM	S- adenosylmethionine
SSB	Single Strand Break
SWI/SNF	Switch/Sucrose Non-Fermentable
TCGA	The Cancer Genome Atlas
TERT	Telomerase Reverse Transcriptase
TET	Ten-Eleven Translocation
TMZ	Temozolomide
TTF	Tumor Treating Field
WHO	World Health Organization

1 INTRODUCTION

1.1 Glioblastoma (GBM)

Adult-type diffuse gliomas comprise the most malignant tumors in all central nervous systems tumors. According to the 2021 World Health Organization (WHO) classifications, adult-type diffuse gliomas are separated into three main categories as Astrocytoma (IDH-mutant), oligodendroglioma (IDH-mutant, 1p/19q-codeleted) and Glioblastoma (IDH-wildtype) (Louis et al., 2021). Among these CNS tumors, Glioblastoma is the most common and lethal primary brain tumor and characterized as Grade 4 according to the WHO (Louis et al., 2016).

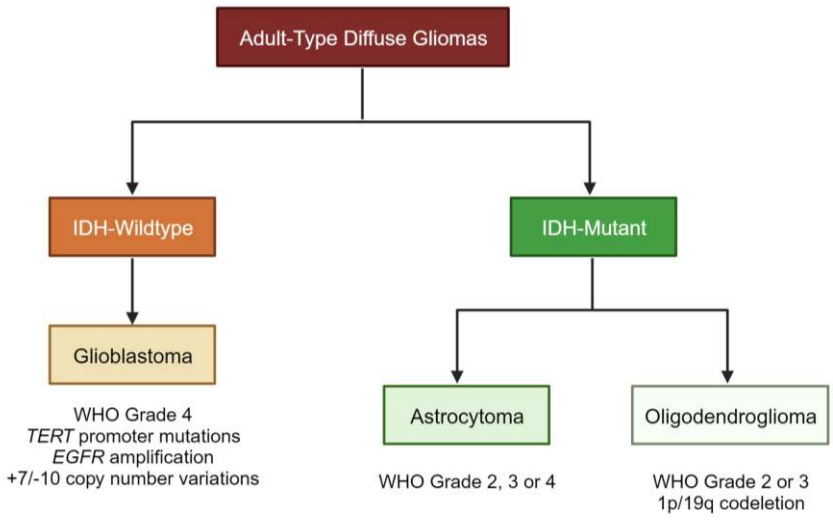

Figure 1.1: Adult-Type Diffuse Glioma Types. Adapted from **(Schaff & Mellinghoff, 2023)**. Figure created in Biorender.com.

Despite being the most common malignant brain tumor, Glioblastoma is considered to be a rare tumor with an incidence rate of 3.22 per 100.000 people in the US (Ostrom et al., 2019). Incidence rate increases with age, GBM is mostly seen in males, and most cases do not have any familial history for the disease (Wen et al., 2020).

According to the CBTRUS report, 5-year survival rate was 6.8% for Glioblastoma patients with the lowest rate in CNS tumors (Ostrom et al., 2019).

GBMs can be divided into two groups as primary and secondary GBMs. Primary GBMs arise as *de novo* and show characteristics of a highly aggressive tumor with no demonstration of prior symptoms. Primary GBMs advance rapidly and are seen mostly in elderly patients. Secondary GBMs derive from lower grade gliomas and are seen mostly in younger patients. These two types of GBMs show different genomic characteristics and altered pathways (Crespo et al., 2015).

Glioblastoma was the first cancer studied for The Cancer Genome Atlas (TCGA)(McLendon et al., 2008). Key pathways in glioma tumorigenesis were identified as receptor tyrosine kinase (RTK) pathway, retinoblastoma (RB), and p53(J. Chen et al., 2012). Revised WHO classifications included several molecular key characteristics for the diagnosis of Glioblastoma. Epidermal growth factor receptor (*EGFR*) amplification, telomerase reverse transcriptase (*TERT*) promoter methylation and gain of chromosome 7 together with loss of chromosome 10 (+7/-10) are the characteristically altered molecular signatures in Glioblastoma, IDH-wildtype (Louis et al., 2021).

Isocitrate Dehydrogenase *IDH1/IDH2* mutations are observed in GBM patients, which results in epigenetic dysregulation due to the formation of 2-hydroxy glutarate (2-HG) (Parsons et al., 2008),(Crespo et al., 2015). This metabolite disrupts the function of DNA demethylases such as TET enzymes and leads to DNA hypermethylation. GBM Patients with IDH mutations shown to survival longer with better clinical outcome compared to IDH-wildtype patients (Yan et al., 2009). In 2021 WHO classification, all IDH-mutated subtype gliomas were removed from Glioblastoma classification and grouped under different gliomas, hence GBM was defined as IDH-wildtype (Louis et al., 2021).

Another important factor in GBM is the O^6-methylguanine methyltransferase enzyme (MGMT). *MGMT* promoter hypermethylation is an important prognostic factor for GBM (Hegi et al., 2005). MGMT reverts the activity of TMZ, which is the alkylating

agent used worldwide for the treatment of GBM. Hypermethylated *MGMT* promoter is associated with TMZ sensitivity and better response (Gusyatiner & Hegi, 2018).

1.2 Glioblastoma Treatment Options

Initial symptoms for GBM involve patients suffering from headaches, neurological discomfort, and epileptic symptoms due to the expansion of tumor, leading to increased pressure in the brain (Wen et al., 2020). Diagnosis of glioblastoma is performed by MRI imaging in the absence and presence of a contrast agent (Weller et al., 2021). The standard-of-care for the treatment of GBM includes surgical resection of the tumor, radiation therapy, and chemotherapy (Holland, 2000). Unfortunately, even with the treatment, GBM recurrence is very common. In the case of recurrent progression of the disease, re-surgery, TMZ rechallenge, and different experimental therapies are considered; however, impact of these treatments on the overall survival rate is yet to be proven (Weller et al., 2021).

1.2.1. Surgery

The first line of defense against GBM is the surgical removal of the tumor. Due to the invasiveness of the tumor that spreads from the initial tumor area, this is difficult. However, the removal of the tumor mass as much as possible without damaging the normal brain functions remains crucial. Tumor tissue is later used for the assessment of genetic markers such as IDH mutation status and *MGMT* promoter methylation for the best post-surgical therapy options. Verification of resection of the tumor is determined using MRI within 48 hours after surgery.

1.2.2. Radiation Therapy (RT)

Standard radiotherapy regimen for GBM treatment post-surgery is 2 Gy fractions for 5 days with total of 60 Gy over 6 weeks (Breen et al., 2020). Concomitant TMZ treatment shows an improved overall survival rate of patients compared to RT treatment alone (Stupp et al., n.d.). However, the treatment regimen differs based on favorable/unfavorable factors of the tumor such as age and MGMT status. These factors determine if RT alone or RT+TMZ will be administered to the patient (Mann et al., 2018).

RT works by inducing DNA damage, which leads to impaired replication capacity followed by cell death. There are three main DNA damage types caused by irradiation: base and sugar damage, single-strand breaks (SSBs) and double-strand breaks (DSBs) (R. X. Huang & Zhou, 2020). Cell activates DNA damage response (DDR) pathways to repair the damage caused by irradiation. DSBs constitute a major part of the damage caused by RT and repair is done by two pathways as non-homologous end joining (NHEJ) and homologous recombination (HR) (Jackson & Bartek, 2009).

Basic principle behind NHEJ is that the end of the broken DNA needs to be sealed together. This mechanism can take place at any point in the cell cycle, but it is error prone(Aleksandrov et al., 2020) . NHEJ pathway starts by the recruitment of Ku70/Ku80 proteins as heterodimers to the broken ends, followed by recruited DNA dependent protein kinases (DNA-PKcs) to the damaged area. The processing also includes kinases such as Artemis which can trim the ends of the DNA. Ligation of the broken ends is completed via XRCC4-Ligase4-XLF complex (Pilié et al., 2019).

HR pathway on the other hand, uses sister chromatid as a temple to accurately repair the damage caused by irradiation. The shortcoming of this pathway is that since sister chromatid is used, this repair mechanism can only be active during 2 and G2 phases (Aleksandrov et al., 2020). MRN complex is recruited to the damaged site and creates single stranded DNA via GtBP. ssDNA is then coated with the RPA protein until BRCA2 is recruited and RPA is replaced with RAD51 protein. Led by RAD51, homologous template is invaded, and D-loop is formed. DNA polymerases complete the sequence based on the template and repair of the broken DNA is completed (Brandsma & Gent, 2012a).

1.2.3. Temozolomide

Temozolomide (TMZ) is a DNA alkylating agent that is used for the treatment of Glioblastoma. TMZ is a small, lipophilic drug that is administrated orally and absorbed through the intestines, due to its small size, it can pass through the blood brain barrier easily (Wesolowski et al., 2010). Within the cell, TMZ is hydrolyzed to 5-(3-methyltriazen-1-yl) imidazole-4-carboxamide (MTIC). MTIC translocate to the nucleus

and adds methyl groups to N3-methyladenine, N7-methylguanine, and O6-methylguanine (S. Y. Lee, 2016). Cells with active Mismatch Repair (MMR), Base Excision Repair (BER) and O-6-Methylguanine DNA methyltransferase (MGMT) enzyme activities can repair the damage caused by TMZ. MGMT repairs the methylated residues on O6-methylguanine by transferring the added methyl group to itself. Therefore, methylated MGMT protein cannot function and is eventually degraded. Cells with defective DNA repair mechanisms cannot repair the methylated residues, and this leads to apoptosis (Villano et al., 2009) (**Figure 1.2**).

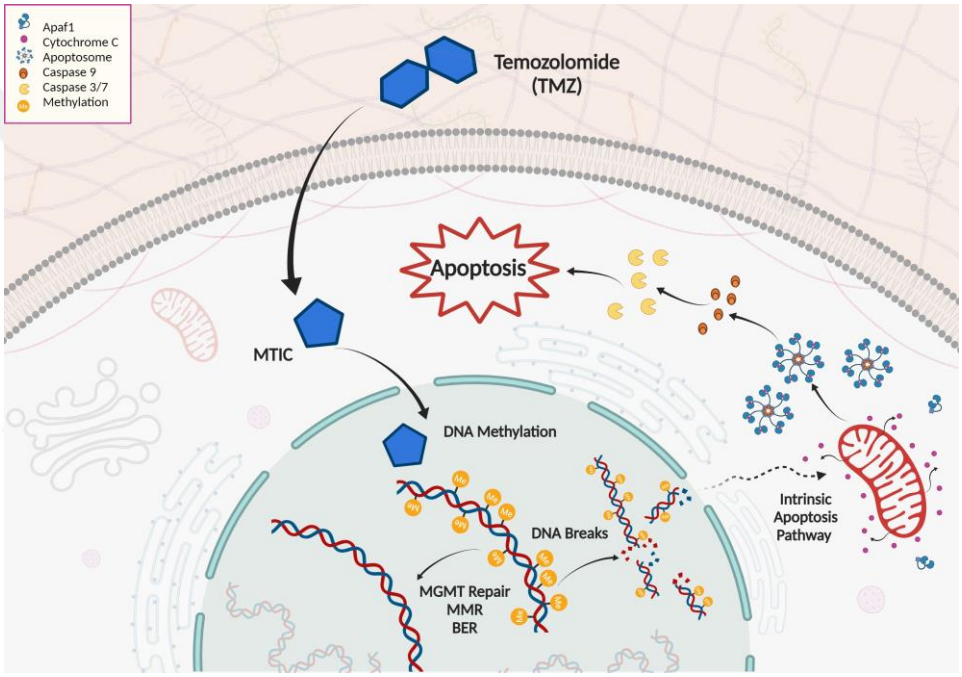

Figure 1.2: Temozolomide working principle. Adapted from (Tomar et al., 2021). Figure created in Biorender.com.

Temozolomide (or Temodar) is administered orally and the dose of TMZ is determined as 75 mg/m^2 of body surface area per day and it is taken 7 days a week along with RT. TMZ is maintained with 150-200 mg/m^2 of body surface area per day for 5 days with 28-day cycles as adjuvant therapy (Stupp et al., n.d.). As all chemotherapeutic agents, TMZ has side effects and toxicity, such as nausea, vomiting and risk of thrombocytopenia (Wesolowski et al., 2010).

MGMT promoter methylation status is important for the determination of TMZ administration to the patient. Methylated *MGMT* leads to better outcomes than unmethylated, as overall survival of a patient with methylated *MGMT* status is 21.7 months whereas 12.7 months for a patient with unmethylated *MGMT* (Hegi et al., 2005). For administration of TMZ, if the patient has poor outcome (age>70, unmethylated *MGMT*), instead of TMZ, patient can be placed in clinical trial or only RT treatment can be applied (Weller et al., 2021).

1.2.4. Other Therapies

Nitrosoureas are a group of DNA alkylating agents, which were used for the treatment of GBM in 1970-80s (Brandes et al., 2016). Lomustine, carmustine and fetomustine are the common nitrosoureas used for GBM, however different countries apply different regimens with these agents. For example, fetomustine is not approved in the US (Wen et al., 2020). Nitrosoureas are BBB permeable, however they have severe toxic side effects(Fisher & Adamson, 2021) . For GBM patients, this treatment option is mostly taken for recurrent or progressed GBM (Weller et al., 2021).

Another therapeutic option mostly taken for recurrent GBM patients is bevacizumab treatment. Bevacizumab is a vascular endothelial growth factor (VEGF) antibody that is used as an anti-angiogenic agent (Yang et al., 2022). However, although progression free survival was improved, no significant results were obtained about overall survival in patients treated with this antibody (Fisher & Adamson, 2021). This therapy is approved in many countries including the US; however, it's not approved in the UN.

Tumor-treating fields (TTF) provide antimitotic effects due to the induced electric fields by intermediate-frequency (200kHz) (Stupp et al., 2012). TTFs are used for GBM treatment in combination with TMZ. In 2011, TTF received FDA approval for its usage in recurrent GBM and in 2015 for newly diagnosed GBM. Results of clinical trials for TTFs show increased overall survival with TMZ compared to TMZ alone (Stupp et al., 2015). Despite its promising effects, TTF therapy is not included in the standard-of-care regimen for GBM treatment (Mehta et al., 2017).

1.3 Temozolomide Resistance in GBM

TMZ is the first line of defense for GBM treatment however, TMZ resistance is very common and seen in most recurrent GBM patients. As mentioned in TMZ working mechanism in **Figure 1.2**, several pathways and enzymes are responsible for the repair of DNA damage caused by TMZ activity. TMZ exposure can lead to mutations in some of these genes, leading to active repair of the damage. Repair of DNA adducts unfortunately leads to decreased TMZ effect, leading to decreased survival.

1.3.1. MGMT

The methylation status of the *MGMT* promoter is a prognostic factor, where hypermethylated *MGMT* promoter provides a survival benefit for patients (Fisher & Adamson, 2021). *MGMT* promoter methylation is an important factor for TMZ resistance. Methylation status determines the expression of MGMT protein, when methylated, less MGMT is expressed therefore better TMZ response is observed in patients. However, when unmethylated, MGMT is highly expressed leading to the repair of O6-guanine residues.

Cells with acquired TMZ resistance show increased MGMT expression (S. Y. Lee, 2016). It was shown that an enhancer activates the expression MGMT and induces TMZ resistance, which the enhancer itself is activated by H3K27ac through the recruitment of p300 (X. Chen et al., 2018). Different strategies are being used to overcome TMZ resistance in GBM, including MGMT inhibition. MGMT is a suicidal protein, meaning to repair the effect caused by TMZ, MGMT protein itself needs to be destroyed by taking up the methyl adduct. This mechanism is exploited for the development of inhibitor strategies (L. Liu & Gerson, 2006). O6-benzylguanine is one of the inhibitors for MGMT silencing that shows good potential for GBM along with other cancer types however there many reported side effects (W. Yu et al., 2020). The most effective treatment strategy is yet to be determined.

1.3.2. Base Excision Repair (BER)

BER pathway is initiated for the removal of N3-methyladenine, N7-methylguanine residues caused by TMZ. Key component of BER pathway, Poly (ADP-ribose) polymerase 1 (PARP1) is recruited to the damaged area and signals for the recruitment of BER components for active repair (Ortiz et al., 2020). Even though they constitute around 90% of the adducts, N-purine adducts are less toxic for the cells with intact BER system due to rapid repair mechanism(Singh et al., 2021) . PARP inhibitors are shown to be effective for impaired BER pathway and are being investigated for GBM treatment (Villano et al., 2009).

1.3.3. Mismatch Repair (MMR)

MMR pathway is initiated for O6-methylguanine adduct. Thymine is mismatched with the O6-methyguanine, and this mismatch is recognized by the functional MMR system during DNA replication. Following recognition, a futile repair cycle is initiated which results in DSBs followed by apoptosis (Tomar et al., 2021). When members of MMR pathway are not functional or mutated, replication continues and TMZ resistance is observed (Woo et al., 2019). Although MMR pathway is involved in TMZ resistance, no direct therapy option is available (Ortiz et al., 2020).

1.4 Epigenetics

Epigenetics is defined as the changes on DNA and histones without changing the DNA sequence itself. These changes affect the accessibility of the chromatin leading to euchromatin (active) and heterochromatin (repressed) states (Allis & Jenuwein, 2016). Chromatin is composed of DNA and histones, packed together to form nucleosome. H2A, H2B, H3 and H4 form an octamer and 146 bp of DNA is wrapped around in each octamer (Hyun et al., 2017). Linker DNA is present between each nucleosome complex. Epigenetic alterations are induced mostly by DNA methylation and histone modifications shown in **Figure 1.3** (Bates, 2020).

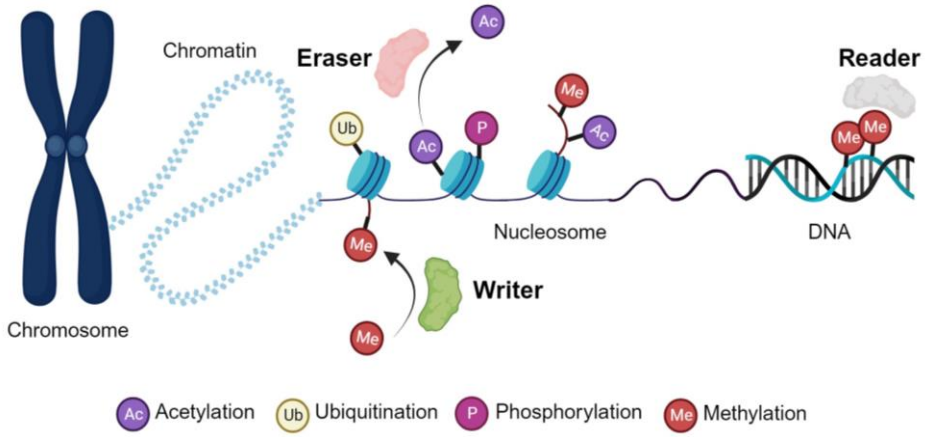

Figure 1.3: Epigenetic Alterations. Modifications on histone tails and methylation on DNA are added via writer enzymes (green). These marks are recognized by reader proteins (gray) and removed by erasers (pink). Figure created in Biorender.com.

1.4.1. DNA Methylation

DNA methylation is linked to the expression of genes as the DNA methylation patterns include promoter hypermethylation and genome-wide hypomethylation (Allis & Jenuwein, 2016). Promoter hypermethylation occurs at the CpG islands that produce 5-methylcytosine (5mC), and the methyl groups are added by DNA methyltransferase enzymes (DNMTs) which uses S-adenosylmethionine (SAM) as the methyl donor (Plass et al., 2013). Loss-of-function mutations of TET enzymes or DNMT overexpression can lead to hypermethylated promoters, which leads to gene silencing. DNA hypomethylation, on the other hand, results from the loss-of-function mutation in genes encoding DNMTs that leads to genomic instability along with altered expression patterns (Jones et al., 2016), (Pfister & Ashworth, 2017).

In cancer, various mutations in enzymes involved in DNA methylation process are identified. DNMT3A, which is a writer, is found to be mutated in around 20% of AML patients (Roberti et al., 2019). Changes in methylation pattern for promoters and gene bodies are also highly seen in cancer patients. Hypermethylation of tumor suppressor genes such as p16 and DNA damage response proteins are frequently observed

in tumors. To reverse these effects, DNMT inhibitors are used in clinical trials for cancer treatment. Azacitidine and decitabine are two FDA approved inhibitors used for leukemia (Bates, 2020).

1.4.2. Histone Modifications

N-terminal tails of the histones are extended out of the nucleosome complex; therefore, these tails can be modified. These modifications are methylations, acetylations, phosphorylations, ubiquitinations, and sumoylations (Henikoff & Smith, 2015). Histone Methyltransferases (HMTs) add methyl groups on histone tails at lysine or arginine residues, whereas histone demethylases (HDMs) remove the methyl marks. For example, methylation that leads to repressive mark H3K27me3 is added by EZH2 enzyme and removed by KDM6A (Romani et al., 2018). There are several reader families for the recognition of methyl marks on lysine or arginine. These are proteins that contain Tudor domain, PHD fingers, Chromo domain and MBT domains (Musselman et al., 2012).

Histone acetylation is achieved by histone acetyltransferases (HATs), such as EP300 and CREBBP, and removed by histone deacetylases (HDACs). HATs use Acetyl-CoA as the cofactor for the acetyl group (Bannister & Kouzarides, 2011). Readers of the acetyl mark on histone tails are bromodomain containing proteins, such as the BET family (Dawson & Kouzarides, 2012).

Mutations in histone modifying enzymes may lead to decreased expression of certain genes, such as tumor suppressors or induced activation of oncogenes (Pfister & Ashworth, 2017). HDAC inhibitors have gained FDA approval and currently used in clinics for T-cell lymphoma and multiple myeloma (Berdasco & Esteller, 2019).

1.4.3. Chromatin Remodelers

Chromatin remodeling complexes allow the mobilization of nucleosomes as well as nucleosome reconstruction by using ATP in the process. Chromatin remodeling enzymes are divided into four main groups as INO80, switch/sucrose non-fermentable

(SWI/SNF), chromodomain helicase DNA-binding (CHD), and imitation switch (ISWI) families (Clapier et al., 2017).

Mutations in chromatin remodeling complex members lead to tumor formation by alterations in the transcription of genes essential for cell survival (Plass et al., 2013). A synthetic lethal interaction between EZH2 and SWI/SNF complex members is studied, however no direct inhibitor targeting such chromatin remodelers are in clinics (Pfister & Ashworth, 2017).

1.5 Glioblastoma Epigenetics

Epigenetic alterations are frequently identified in GBM patients. *MGMT* promoter hypermethylation is an example of these epigenetic alterations, as discussed earlier. In recent years, it has been shown that mutations in genes coding isocitrate dehydrogenase enzymes *IDH1* and *IDH2* results in the production of 2-hydroxyglutarate (2-HG) (Gusyatiner & Hegi, 2018). 2-HG works by impairing the Ten-eleven translocation (TET) enzymes, therefore resulting in hypermethylated DNA phenotype (A. Liu et al., 2016). Tumors with IDH mutations are shown to display glioma CpG island methylator phenotype (G-CIMP) due to impaired TET enzyme activity that results in global DNA methylation alterations(Malta et al., 2018). Until 2021, IDH mutated, and wildtype subgroups were included in GBM classifications, however as mentioned above, new WHO classification dictates that only IDH wild type is considered for glioblastoma characterization (Louis et al., 2021).

Increased histone deacetylase (HDAC) expression was identified in GBM. Study conducted by Brennan et al has identified various HDAC inhibitors, which are under investigation for the treatment of glioblastoma (Romani et al., 2018). HDAC inhibitor Vorinostat (SAHA) and Belinostat are among the inhibitors that are used for the treatment of GBM in combination with TMZ. Several other inhibitors are in the clinical trials (Kunadis et al., 2021).

EZH2 is a component of PRC (polycomb repressive complex) and is highly associated with H2K27me3 mark (Kondo et al., 2014). EZH2 overexpression is found in

GBM patients however recent studies by de Vries et al demonstrated that long term exposure to EZH2 inhibitors results in tumor progression due to increased DNA damage response (de Vries et al., 2015).

ATRX (alpha thalassemia X-linked mental retardation protein) functions as a remodeler in SWI/SNF2 complex and is found to be mutated in secondary GBMs (Haase et al., 2018). Study conducted by Qin et al has shown that loss of ATRX leads to altered cell-cycle phase transition (Qin et al., 2022). Although ATRX mutations were included for GBM classification in 2016 WHO CNS classifications, ATRX alterations are currently associated with only IDH-mutant astrocytoma (Louis et al., 2021).

Another group of enzymes that are upregulated in GBM is histone demethylases. KDM6A/6B are associated with H3K27 methylation, like EZH2 (Romani et al., 2018). An inhibitor for KDM6A/6B, GSKJ4, has been studied in DIPG and was shown to reverse the methylation phenotype (Hashizume et al., 2014). Kayabolen A et al demonstrated that GSKJ4 is an important inhibitor that downregulates metabolic activities in IDH-mutant glioma models (Kayabolen et al., n.d.). Recent studies showed that KDM5A overexpression is associated with increased drug resistance independent from MGMT expression (Banelli et al., 2015). Later, the same group demonstrated that KDM inhibitor JIN04 can kill naïve and TMZ-resistant cells, can pass through BBB and synergize with TMZ, providing a potential target for clinical applications (Banelli et al., 2017).

It is clear that epigenetic modifications are important players in GBM progression. However, there are still many unclarified mechanisms regulating GBM progression and/or therapy response. Therefore, new studies are required to identify novel regulators and targets.

1.6 CRISPR/Cas9

CRISPR stands for Clustered Regularly Interspaced Short Palindromic Repeats, and Cas9 is the CRISPR associated protein 9. CRISPR/Cas9 system is part of the bacterial adaptive immune system, which allows the bacterium to defend itself from invaders. It does so by integrating part of the viral DNA into its CRISPR array. Transcription of the

CRISPR array results in short CRISPR RNAs or crRNAs. crRNA, along with Cas9 endonuclease, allows bacteria to recognize and cleave the DNA if the same invader infects the cell (Jiang & Doudna, 2017).

CRISPR/Cas9 system requires two basic elements, a guide RNA that is engineered to target the desired sequence and the Cas9 endonuclease. As the name implies, gRNA guides the Cas9 to the target site. Cas9 recognizes the protospacer adjacent motif (PAM), which is located downstream of the target site. Upon binding, Cas9 uses its nuclease domains HNH and RuvC to cleave complementary and noncomplementary DNA strands, respectively (Jinek et al., 2012). Double strand breaks generated by Cas9 can be repaired by two different DNA repair mechanisms, NHEJ pathway or homology directed repair (HDR) pathway. NHEJ pathway is error prone, usually inducing deletions or insertions at the cut site. However, HDR uses a donor DNA template or the sister chromatid to repair the break (Brandsma & Gent, 2012b). This template can be engineered to introduce any desired modifications into the target locus.

The endless possibilities of CRISPR/Cas9 system allowed scientists all around the world to engineer new mechanisms such as gene activation, repression, epigenetic alterations, and imaging (Barrangou & Doudna, 2016).

One of the engineered systems is called CRISPR inhibition (CRISPRi). This technology uses a catalytically inactive form of Cas9, called dead Cas9 (dCas9) fused with Kruppel-associated box (KRAB) protein. dCas9-KRAB system recognizes the region of interest via gRNA however instead of inducing a DSB, KRAB blocks the transcription of the gene of interest, therefore gene is inhibited. Another engineered system is CRISPR activation (CRISPRa), which uses an activator protein, such as VP64 fused with dCAS9 to activate the expression of a specific gene (Dominguez et al., 2016). One other use of inactive Cas9 is to induce epigenetic alterations via using various modifiers such as DNMTs or TETs. This way, methylation or demethylation of gene promoter is controlled (Nakamura et al., 2021). These applications allow scientists to manipulate and study gene functions without the damaging effects of DSBs (Alyateem et al., 2023)**(Figure 1.4).**

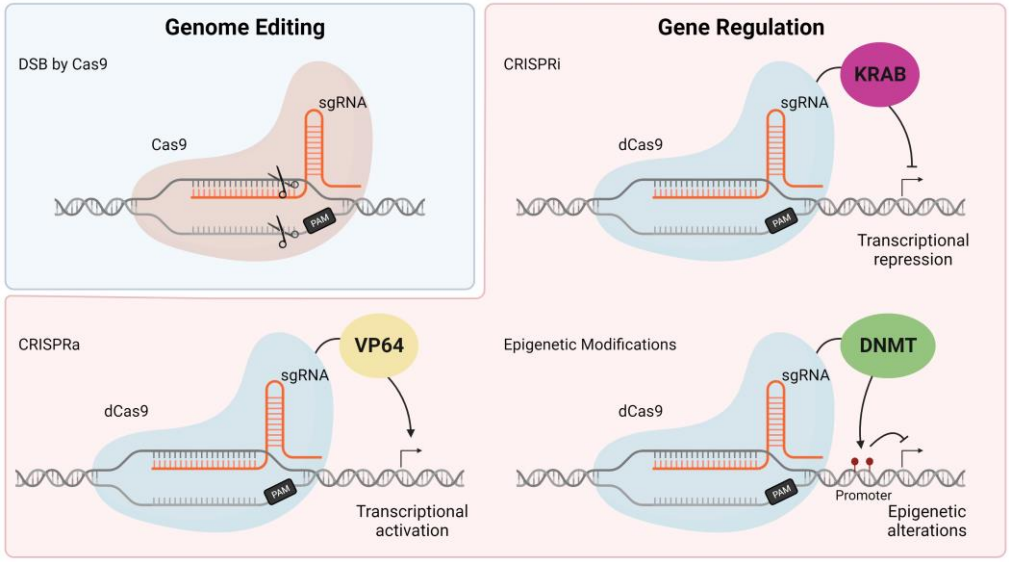

Figure 1.4: CRISPR/Cas9 systems. Genome editing system uses Cas9 enzyme and functions via inducing DSBs. For gene regulation, dead Cas9 is used, and gene expression is modulated via effectors fused to dCas9. Adapted from (Alyateem et al., 2023) (Awwad et al., 2023). Figure created in Biorender.com.

Following the discovery of CRISPR/Cas9 and its experimental applications, genome-wide CRISPR/Cas9 knock-out screens in human cells were made possible and several important studies have been published for functional genetic screens (Shalem et al., 2014),(T. Wang et al., 2014). Genetic screens involve the introduction of a pooled gRNA library to cells via viral vectors that results in perturbations within the genome (Doench, 2018). CRISPR screens are separated into two different strategies as positive screens (or enrichment) and negative screens (or drop-out). In positive screens, cells that have survival pressure such as drug treatment are studied. In negative screens, cells that have been depleted from the population allowing us to understand which genes regulate cell survival (Miles et al., 2016). Both strategies are used to identify new mechanisms in different diseases.

1.7 Focused CRISPR/Cas9 Screens

Even though genome-wide screens are frequently used, more custom and small-scale libraries are generated over the years. These libraries are designed specific to a

group of genes, such as kinases (Doench et al., 2016). Focused CRISPR/Cas9 libraries have several advantages over genome-wide libraries. They are smaller in size, therefore less labor intensive. The small scale allows the cost of experimentation to decrease as well (Miles et al., 2016). Since the number of genes are limited to researchers' interest, number of gRNAs/genes is higher compared to genome-wide libraries, which contain around only 4-10 gRNAs/gene (Iyer et al., 2020). The shortcomings of custom libraries include the fact that their scope is focused on a specific target, and this may lead the user to miss out on different genes and mechanisms that can be exploited using genome-wide libraries (Bock et al., 2022).

Screens strategies have been used for glioblastoma studies over the past years. Both genome-wide and focused libraries are utilized for this purpose. For example, Toledo et al used a genome-wide library in glioblastoma stem cells (GSCs) to identify lethality genes and as a result they identified PKMYT1 as a candidate gene (Toledo et al., 2015). Dmello et al performed an *in vivo* screen using Kinome Library and demonstrated that Checkpoint kinase 1/2 is a potential target for sensitization of glioblastoma to immune checkpoint blockade (Dmello et al., 2023). Glioblastoma and therapy resistance has also been investigated using CRISPR screening approaches. MacLeod et al has utilized genome-wide CRISPR/Cas9 library to identify both fitness genes and TMZ response genes in patient-derived glioblastoma stem cells. Important stemness genes and stress pathways have been identified as genetic vulnerabilities of GSCs, and several pathways including homology directed repair and mismatch repair pathways were demonstrated to be modulators of TMZ response (MacLeod et al., 2019). Another important study on TMZ resistance was performed by Huang et al and identified E2F6 as a potential target in EGFRvIII-expressing glioblastomas using genome-wide screening approach (K. Huang et al., 2019). Overall, it is seen that CRISPR/Cas9 screening has been used widely in the context of therapy resistance, immunotherapy, lethality for glioblastoma therapy.

1.8 Epigenetic Knock-Out Library (EPIKOL)

An epigenetics focused library is generated in KUTTAM, called Epigenetic Knock-Out Library (EPIKOL) (Yedier-Bayram et al., 2022). EPIKOL targets 719 epigenetic modifiers along with 35 essentiality genes and 25 context genes. With 10 gRNAs/gene and 80 non-targeting gRNA controls, it contains 7870 gRNAs in total. gRNA sequences employed in EPIKOL curation were extracted from previously published genome-wide libraries. In case 10 gRNAs were not sufficed or overlapped, remaining gRNAs were hand-designed.

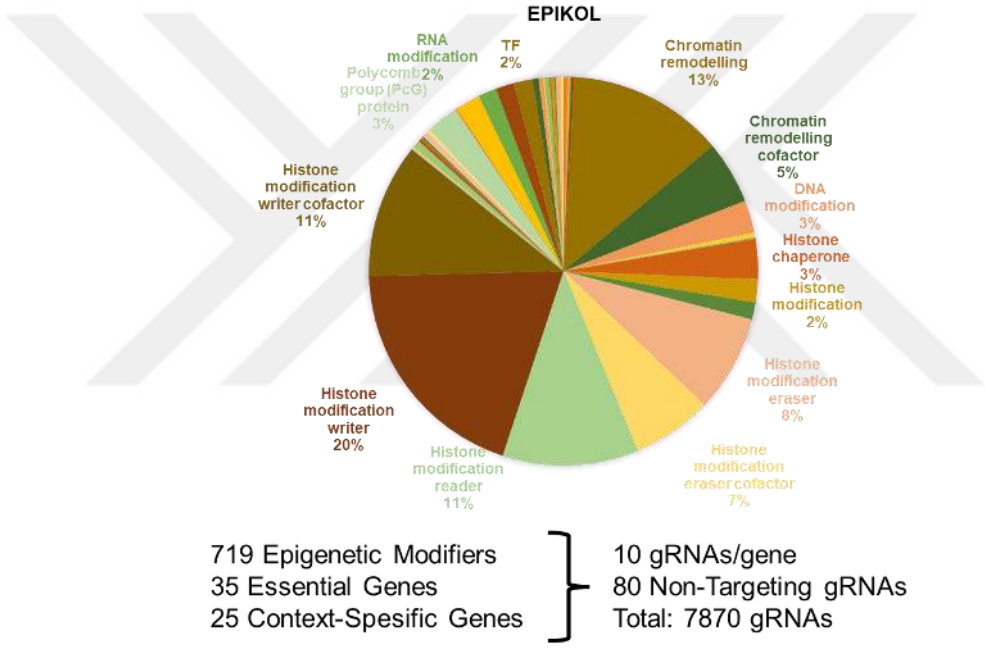

Figure 1.5: EPIKOL content. Venn diagram showing the major factors in EPIKOL. A total of 7870 gRNAs are present in the library.

1.9 Retinoblastoma Binding Protein 4 (RBBP4)

RBBP4 is a member of the retinoblastoma binding protein family. Within this family, RBBP4 and RBBP7 share high sequence similarities, up to 92%, therefore they are homologous proteins (Millard et al., n.d.). RBBP4 protein contains 425 amino acids and is part of the WD-repeat domain family (**Figure 1.6.A**). The protein structure of RBBP4 allows it to act as a scaffold for protein-protein interactions (Cai et al., 2023). As

a WD-repeat protein, RBBP4 has β-propeller structure with hole in the middle, and N-terminus and C-terminus α-helices (Qian & Lee, 1995). Proteins besides histones can bind and interact with RBBP4 via around the β-propeller but not inside the hole, which is the central channel. Binding of histones, however, occurs via the PP loop located in the β-propeller channel (Stirnimann et al., 2010). These binding mechanisms allow RBBP4 to interact with various proteins, bind to histones and act in many epigenetic alterations.

RBBP4, along with RBBP7, is found in many complexes, which are the chromatin assembly factor 1 (CAF1), polycomb repressive complex 2 (PRC2), nucleosome remodeling and deacetylase (NuRD), and the DREAM complex (Cai et al., 2023) as shown in **Figure 1.6.B**.

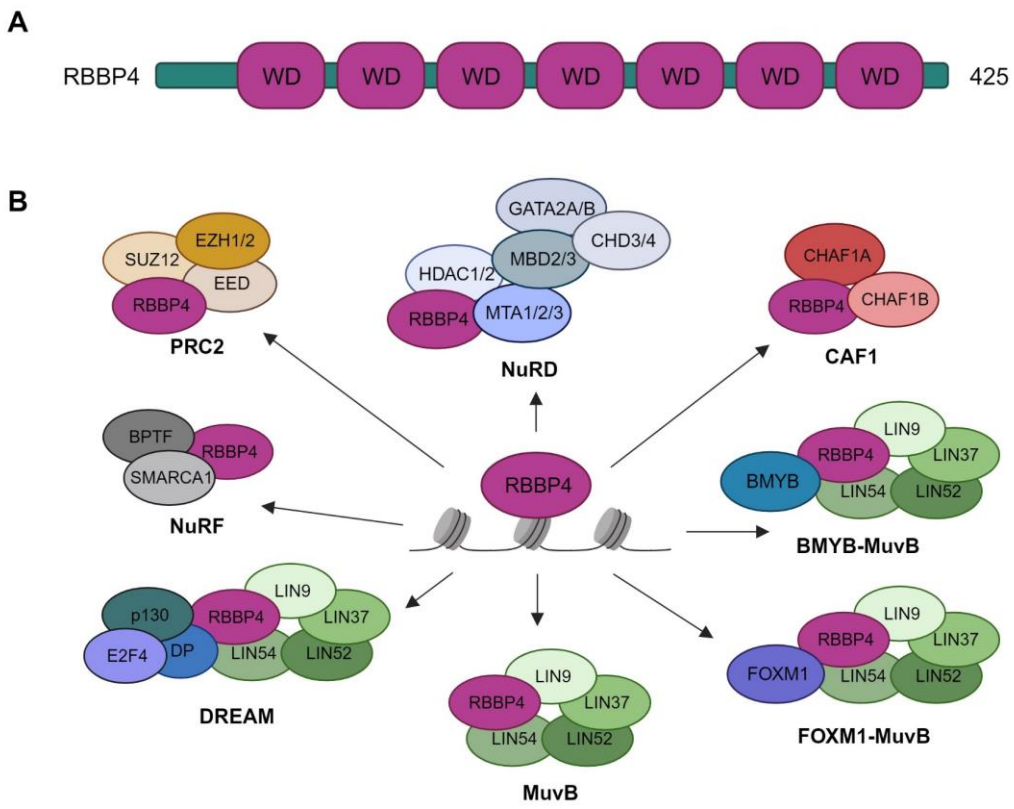

Figure 1.6: RBBP4 and associated complexes. A. Structure and domains of RBBP4. (WD: WD repeat domains) **B.** Complexes RBBP4 interact with including PRC2, NuRD, CAF1, NuRF. MuvB is part of DREAM complex, and associates with BMYM and FOXM1. Figure created in Biorender.com.

CAF1 is a histone chaperone with three subunits: CHAF1A (p150), CHAF1B (p60) and RBBP4 (p48) (Sykaras et al., 2021). Main function of CAF1 complex is to deposit H3-H4 histones onto DNA during DNA replication. CAF1 binds to PCNA during DNA synthesis and mediates nucleosome assembly via another histone chaperone ASF1 during the S-phase (Verreault et al., 1996). Another important role of CAF1 is in DNA damage response where the complex is recruited to the damaged area and reassembles the nucleosomes (Z. Yu et al., 2015).

PRC2 is involved in H3K27 methylations throughout the genome via its core components EZH1/2, EED, SUZ12 and RBBP4/7 (Glancy et al., 2021). EZH1/2 is responsible for the deposition of methyl groups to H3K27 position via its HMT activity. EED is a WD-repeat protein and like RBBP4, it has β-propeller structure. Folding of EED is essential for EZH2 to exert its function since EZH2 binding to EED is essential for HMT activity of PCR2 (Kouznetsova et al., 2019). SUZ12 acts as a stabilizer for H3K27 methylation. The role of RBBP4 in PRC2 complex is involved in H3 and H4 histone binding, acting as histone chaperones. Binding of RBBP4 to H3-H4 histone dimers is essential for the recruitment of PRC2 complex to the chromatin (Shi et al., 2017). Besides its four components, three other proteins, JARID2, AEBP2 and PCLs are associated with PRC2 complex for its function (Margueron & Reinberg, 2011).

NuRD complex is a corepressor with HDACs and ATPases being the major players. NuRD complex is associated with many functions involving DNA repair, genomic stability, chromatin organization and gene expression with its components HDAC1/2, RBBP4/7, CHD3/4, GATAD2a/2b, MTA1/2/3 and MBD2/3 (Torchy et al., 2015). HDAC1, RBBP4 and MTA1 form the deacetylase module, in which HDAC1 deacetylase lysine residues form a scaffold with the help of MTA1 while RBBP4 is responsible for binding on nucleosomes (Zhang et al., 2016). Experiments show that RBBP4 cannot bind to both MTA1 and histones at the same time, allowing other proteins to bind to NuRD complex. One such example is the FOG1 interaction of RBBP4 (Lejon et al., 2011). CHD4, MBD3 and GATAD2a form the chromatin remodeler module; MBD3 recruits GATA2Da and CHD4 to methylated CpGs where CDH4 can exert its effect as ATPase (Millard et al., 2020).

NuRF complex is part of the ISWI family of chromatin remodelers (Y. Li et al., 2021). Core components of NuRF include BPTF, SNF2L and RBBP4/7 (Alkhatib & Landry, 2011). This complex is associated with nucleosome sliding (Hamiche et al., 1999).

DREAM (dimerization partner, RB-like, E2F and multi-vulval class B (MuvB)) complex is associated with expression of various cell cycle genes during cell cycle phases (Sadasivam & Decaprio, 2013). MuvB is the core component of DREAM complex and is composed of 5 proteins, RBBP4, LIN9, LIN37, LIN52 and LIN54 (Fischer & Müller, 2017). Main function of MuvB is to repress the transcription of genes involved in G1/S and G2/M during quiescence (Litovchick et al., 2007). However, MuvB is also responsible for transcriptional activation through S-to-G2/M phases via interaction with BMYB and FOXM1 proteins (Sadasivam et al., 2012). Although the exact function of RBBP4 in MuvB is not clear, it is thought to be an assembly factor for repressor complexes, due to its involvement in many other chromatin remodeler complexes (Iness & Litovchick, 2018).

1.10 RBBP4 and Cancer

RBBP4 is implicated in many cancer types. Studies conducted with 240 breast cancer patients showed that RBBP4 along with HDAC1 is upregulated in tumors, where high RBBP4 expression is associated with poor survival (Guo et al., 2020). More recently, Zheng et al demonstrated that downregulation of RBBP4 resulted in decreased epithelial-to-mesenchymal transition (EMT) in triple negative breast cancer (TNBC) (Zheng et al., 2022).

RBBP4 is highly expressed in Acute Myeloid Leukemia (AML) (Casas et al., 2003). Khateb et al showed that RNF5, a ubiquitin ligase, ubiquitinates RBBP4 and induces its localization to promoters of AML-related genes. The authors observed that downregulation of RBBP4 results in increased sensitivity towards HDAC inhibitors, therefore concluded that RNF5/RBBP4 axis could be a potential marker (Khateb et al., 2021).

Recent studies showed that RBBP4 is an important protein for glioblastoma. In 2016, Kitange at al found that RBBP4 mediates the expression of many genes involved in DNA repair upon TMZ administration, especially *MGMT* and *RAD51* (Kitange et al., 2016). The same group later showed that this modulation is achieved via RBBP4/p300 interaction, that downregulation of RBBP4 or p300 resulted in TMZ sensitization *in vitro* and *in vivo* (Mladek et al., 2022). An MGMT-independent mechanism for TMZ resistance was demonstrated by Li et al, via induction of DSB repair by regulation of MRN complex. Not only TMZ but also radiotherapy sensitization was observed upon RBBP4 silencing in MGMT-negative GBM cells (J. Li et al., 2023). Shou et al showed HOXA-AS2 and RBBP4 to be upregulated in glioblastoma tissues, and GBM progression can be involved with HOXA-AS2/miR-885-5p/RBBP4 axis (Shou et al., 2021).

1.11 Aim of the Study

Glioblastoma remains to be one of the most aggressive tumors with low survival rate. Therapeutic options are quite limited, and response to treatments are poor. Epigenetic alterations are known to play important roles in the regulation of drug response in cancers. Glioblastoma, on the other hand, is a puzzle with only a few pieces put together. Our aim is to find the missing pieces that would allow us to understand the drug resistance mechanism of glioblastoma along with cell fitness in the context of epigenetics. Identifying important epigenetic regulators would grant us the opportunity to overcome therapy resistance and open a new door for new therapeutic options.

The first aim of this thesis is to identify chromatin modifiers that are essential for glioblastoma. For this purpose, we performed drop-out screens using EPIKOL in 2 different cell lines (U87MG and U373). We also performed EPIKOL screen in human astrocytes as the non-malignant control.

Temozolomide resistance is an important issue for glioblastoma treatment. To study what is behind the therapy resistance, we established an *in vivo* compatible TMZ resistant cell line using the dose escalation method. The newly generated cell line is called U87MG-R. Characterization of the resistant cell line is done via different viability assays and transcriptome analysis.

The final aim of this thesis is to understand and overcome drug resistance. Drug resistance in glioblastoma is primarily caused by MGMT; however, there are many potential mechanisms and therapy strategies that are not known. For this purpose, we conducted EPIKOL screens using our TMZ-resistant cell lines, with or without drug administration. We validated our findings with functional assays.

2 MATERIALS AND METHODS

2.1 Cell Culture

Human GBM cell lines U87MG, T98G and U373 along with Human Embryonic Kidney 293T cells, were purchased from American Tissue Type Culture Collection (ATCC). Human Astrocytes (HA) were purchased from ScienCell. U87MG, U373, HA and HEK293T, as well as the TMZ-resistant cell lines, U87MG-R and TMZRT were cultured in DMEM, supplemented with 1% Penicillin/Streptomycin and 10% Fetal Bovine Serum. Astrocytes were seeded over culture dishes coated with 0.01 w/v Poly-l-lysine. Cells were maintained in humidifier incubators with 5%CO2 and 37˚C.

Mutation status of p53, RB1 and CDKN2A of GBM cell lines used in this study was listed in **Table 2.1**. This was listed based on ATCC cell lines by gene mutation guideline (Cell Lines by Gene Mutation), and literature (García-Claver, n.d.; Y.-J. Lee et al., 2020; Wiedemeyer et al., 2010). TMZ response was also listed, based on Lee et al (S. Y. Lee, 2016).

Table 2.1: Mutation and TMZ response status of GBM cell lines.

Cell Line	p53 Status	RB Pathway Status	TMZ Response
U87MG	WT	RB1 WT CDKN2A del	Sensitive
U373	Mut	RB1 WT CDKN2A del	Sensitive
T98G	Mut	RB1 WT CDKN2A del	Resistant

2.2 Viral Packaging and Titering

For lentivirus packaging, HEK293T cells were seeded to 10 cm culture dishes as 2.5x106 cells. Next day, Fugene mixture containing 15 µl Fugene 6 (Roche) + 185 µl serum free DMEM and DNA mixture containing 225 ng VSVG + 2250 ng psPAX2 + 2500 ng Vector in 200 µl with serum free DMEM was prepared. DNA mixture was mixed

with Fugene mixture and incubated 30 minutes at RT. Mixture was added onto the seeded cells drop by drop and placed in the viral incubator. 16 hours later, the medium was changed. The supernatant was collected 48 and 72 hours after transfection. To concentrate the virus, collected supernatant was passed through 45 μM filter over 5X PEG8000, with final concentration of PEG8000 being 1X, and kept at 4˚C for 1-4 days. Viruses were centrifugated at 2500 rpm for 20 minutes. In laminar flow, supernatant was removed, and tubes were centrifuged again at 1200 rpm for 5 minutes. The remaining supernatant was removed, and the virus pellet was resuspended in PBS as 100X.

For viral titer determination, cells were seeded as 100,000 cells/well in 6well plates. Viral transduction at concentrations 1 μl, 10-1 μl, 10-2 μl and 10-3 μl was given along with 8 μg/ml protamine sulphate. Following antibiotic selection, uninfected cells and remaining cells in transduced wells were counted by hemocytometer. The number of cells were compared with uninfected cells, and viral titers were determined.

2.3 Cas9 Activity

To determine the Cas9 activity of U87MG, Flow Cytometry was used. U87MG was transduced with pLentiCas9-blast and Hygro-GFP lentiviruses in this order with low MOI (0.4). Non-transduced cells were selected with Blasticidin (10 μg/ml) and Hygromycin (200 μg/ml) respectively. U87MG-Cas9-GFP cells were later transduced with either non-targeting control vector (NT1) or GFP targeting vector (T1) and selected with puromycin (2 μg/ml). %GFP was measured with flow cytometry every 3 days.

2.4 EPIKOL Screens

To uncover the chromatin modifiers that regulate cell fitness along and drug resistance, EPIKOL screens were conducted. For this purpose, Cas9 expressing U87MG, U87MG-R, U373 and TMZRT cells were transduced with EPIKOL lentivirus with MOI:0.4 and as 1000X coverage. HA-Cas9 cells were transduced with 125X coverage due to difficulty of maintaining the cells. Experiments were performed as triplicates, except for NHA screen which was done as a single replicate. Following transduction, Puromycin selection (1-2 μg/ml) was performed for 3-4 days to eliminate the non-

transduced cells. First samples are collected after puromycin selection as 8x106 cells, this served as initial point. Cells were passaged until they completed Cas9 activity, 19-20 days for U87MG and U87MG-R, and 17-18 days for U373 and TMZRT cells. Following Cas9 activity, U87MG, U87MG-R and TMZRT cells were separated into two groups as Treatment and Control. U373 cells continued to be passaged until doubling time is completed (15-16) and NHA cells were passaged around 40 days post transduction. U87MG cells are treated with either 50 μM of TMZ or DMSO. Due to cytostatic effect of TMZ, while DMSO group reached 20 doublings, TMZ group only reached 4 doublings, therefore TMZ and DMSO was removed, and cells were kept in culture until treatment group reached 14 doublings. The samples taken from treatment and control groups at PDL 4 and 20, respectively were named as TMZ and DMSO. Once the treatment group reached 14 doublings and control to 34 doublings, the screen was finished and these samples were named as After TMZ and After DMSO, respectively. For U87MG-R and TMZRT screens, 200 μM and 250 μM of TMZ was used, respectively. When both DMSO and TMZ group reached 14-15 doubling, the screen was finished.

2.5 Genomic DNA Isolation, Nested PCR and Next Generation Sequencing (NGS)

Genomic DNA isolation was performed using MN Nucleospin Tissue kit according to the manual. Tissue isolation protocol was used due to the high number of cells within the pellet (8x106). Isolated gDNA served as the template for the amplification of gRNAs within the population and the addition of Illumina compatible adaptors. For this purpose, Nested PCR was performed. The first round of PCR was used to amplify the gRNAs within the genome with 250x coverage, equal to 13.2 μg DNA. For initial (or external PCR) 4 reactions were prepared as, 3.3 μg DNA, 2 μL dNTP mix, 20 μL 5X GC Buffer, 5 μL of external forward and 5 μL reverse primer (10 μM each) and 1 μL Phusion DNA polymerase with dH2O to complete 100 μl. Reactions were collected and in the second round of PCR (internal PCR), 5 μl of external PCR product was used as template. Instead of external forward and reverse primers, Illumina adapters which are the staggers (forward primer, 10 μM) and index sequences (reverse primer, 10 μM) were used as primers. Detailed protocol and primer information can be found in EPIKOL paper (Yedier-Bayram et al., 2022).Thermal cycler conditions for PCRs were as follows: 95C

for 3 minutes, 95ºC for 25 seconds, 65ºC for 20 seconds and 72ºC for 15 seconds (17X for external PCR and 23X for internal PCR),72ºC for 3 minutes and infinite hold at 4ºC. PCR products were loaded on 2% Agarose gel and isolated using MN Nucleospin Gel and PCR Cleanup kit. Samples were sent to Genewiz Company in NJ, USA for Next Generation Sequencing (NGS). Analysis of the NGS data was performed in-house by using MAGeCK(W. Li et al., 2014) by Dr. Ali Cenk Aksu and by Dr. Ayşe Derya Cavga. Detailed explanation of MAGeCK analysis for CRISPR screens can be found in Yedier-Bayram et al study (Yedier-Bayram et al., 2022).

2.6 Generation of Temozolomide Resistant Cell Line

To generate TMZ resistant cell line, dose escalation method was used. For this purpose, U87MG cells were exposed to TMZ starting from 5 μM. Dosage was increased every two to three weeks or when cells show resistance. Upon treatment with 200 μM, morphological changes were visible in U87MG cells therefore cell viability assays were used for the determination of resistance. The newly generated cell line was called U87MG-R. Parental U87MG cells were aged and treated with DMSO.

2.7 Cell Viability Assays

For long-term viability assessment, colony formation assay was used. Cells were seeded to 6 well plates as 750-800 cells/well as triplicates. Treatment was made one day after seeding and TMZ was removed after 72 hours. 250-300 cells/well were seeded to 12 well plates as triplicates and TMZ treatment was done 48 hours after seeding. Cells were kept in culture for 10-14 days until visible colonies were observed. Later, cells were fixed with cold 100% Methanol for 5 minutes, followed by Crystal Violet Staining for 30-40 minutes. Plates were scanned and quantification was performed in ImageJ program with ColonyArea plugin (Bagga et al., 2014).

For MTT assay, 3 mg/ml MTT reagent was dissolved sterile PBS and added to the wells as 1:4 of the initial medium. Plates were incubated for 1-4 hours in cell culture incubator. Next, medium was discarded and 100 μL of DMSO was added to each well.

Plate shaker was used to dissolve the formazan crystals and absorbance measurement at 570 nm was performed using Synergy H1 Reader (Biotech, USA).

2.8 RNA sequencing

For RNA sequencing, Parental U87MG and TMZ resistant U87MG-R cells were seeded in 10 cm culture plates as triplicates without TMZ or DMSO. Once cells reached ~80% confluency, cells were trypsinized and collected. High quality RNA was isolated with MN Nucleospin RNA isolation kit. Isolated RNA samples were shipped to BGI in Hong Kong, China. Library preparation and sequencing was performed by BGI. Analysis of the data was performed by the Bioinformatics Core in KUTTAM. For RBBP4 knock-out RNA sequencing, cells were seeded to 6well plates as triplicates and infected with RBBP4 g1, g2 and NT1 viruses the next day. Following puromycin selection, cells were transferred to 10cm plates and at post transduction day9, cells were collected, and RNA was isolated as explained. Sequencing was performed at Oxford University and analysis was performed by Ebru Yılmaz. Detailed analysis of transcriptome analysis can be found in Yedier-Bayram et al study (Yedier-Bayram et al., 2022).

2.9 Dual Color Competition Assay

Competition assay was performed as shown in **Figure 2.1**. For competition assay, U373-Cas9 and U87-Cas9 cell lines were transduced with PGK-H2B-mCherry (Addgene) or PGK-H2B-eGFP lentiviruses with high MOI. Cells labelled with H2B-mCherry were transduced with NT1 lentiviruses and cells labelled with H2B-eGFP was transduced with lentiviruses containing gRNAs. Following Puromycin selection, cells with NT1 and gRNAs were mixed 50%-50% and seeded as triplicates to 24well plates. Day0 imaging was taken the next day with Cytation5 Cell Imaging Reader (BioTek) with 4X objective. Images were taken once every 5 days. mCherry+ and eGFP+ cells were counted by Gen5 software (BioTek) and percentage of eGFP+ cells were determined. Measurement was normalized to Day0.

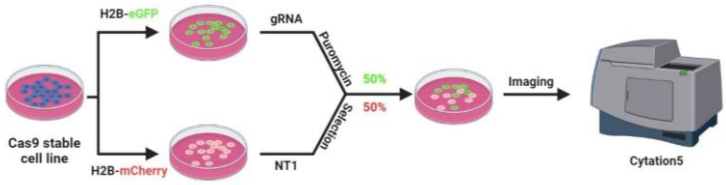

Figure 2.1: Dual Color Competition Assay Schematics. H2B-GFP labeled gRNAs and H2B-mCherry labelled NT1 mixed 50-50% and image-based readouts were taken by Cytation5 Reader.

2.10 Western Blot

For western blot, cells were collected via trypsinization and pellet was stored at -80 until isolation. For whole cell lysates, NP-40 lysis buffer containing 1% NP-40, 50 mM Tris, 250 mM NaCl, 1X EDTA, 0.02% NaN3, 1 nM PMSF and 1X protease inhibitor cocktail was used. The pellet was resuspended in NP-40 lysis buffer followed by incubation on ice for 30 minutes. The sample was centrifuged at maximum speed for 10 minutes at 4ºC. Supernatant was transferred to clean tube and protein quantification was performed using BCA protein assay kit (Thermo Scientific, 23225).

20 µg of protein was mixed with 4X loading dye (4X Laemni buffer (Bio-rad, 1610747) with 1:10 beta-mercaptoethanol) and boiled at 95ºC for 10 minutes. Samples were loaded to precast 4-12% Mini Protean TGX Precast Gel (Bio-rad, 456-1044). Following gel run, gel was transferred onto PVDF membrane using Bio-RadTrans-Blot® Turbo™ Transfer System (Bio-Rad, USA). Transfer of gel to the membrane, Ponceau staining (EcoTech, Turkey) was performed. To prevent non-specific binding, the membrane was blocked in 5% blocking grade blocker prepared in 1X TBS-T for 1 hour. Membrane was incubated with primary antibody overnight at 4ºC. Next day, the membrane was washed 3 times with 1X TBS-T and incubated with secondary antibody at RT. Visualization of bands was performed using Li-Cor Odyssey® FC Imaging System. Primary and secondary antibodies used in the experiments were listed in **Table 2.2.**

Table 2.2: Antibody list.

MGMT	Cell Signaling Technologies	2739S	rabbit
GAPDH	Cell Signaling Technologies	D4C6R	mouse
RBBP4 (RBAP48)	Proteitech	20364-1-AP	rabbit
Alpha-Tubulin	Abcam	ab15246	rabbit

2.11 Real Time Quantitative PCR (qPCR)

For detection of expression changes, real time quantitative PCR was used. First, RNA isolation was performed using MN Nucleospin RNA isolation kit. Isolated RNA was kept at -80. For cDNA synthesis, 500-1000 ng of RNA was used as starting material. RNA, random hexamers (1 µl), 2 mM dNTP (2.5 µl) was mixed and completed to 16.5 µL using nuclease free dH2O. Mixture was placed in the thermal cycler for RNA melting and incubated for 5 minutes at 65ºC, samples were placed on ice afterwards. 5X first strand buffer (5 µl), 0.1M DTT (2 µL) and RNAsin (0.5 µL) was added to the samples and incubated at RT for 10 minutes. For the reverse transcriptase reaction, MMLV-RT enzyme (1 µL) was added to each sample and RT reaction was initiated using thermal cycler as 37ºC for 1 hour followed by 70ºC for 15 minutes for heat inactivation. Before qPCR, 75 µL of NF dH2O was added to each sample and stored at -20ºC.

qPCR reactions were performed as triplicates per sample. 2 µL of diluted cDNA, 10X SyberGreen (10µL), 10 µM primer mix (1 µl) and dH2O (7 µL) was added to each well of qPCR plate. qPCR reaction was performed using LightCycler 480 Instrument II (Roche). Thermal Cycler reaction conditions were as follows: 95ºC for 5 minutes as pre-heating step, 95ºC for 10 seconds, 60ºC for 30 seconds, 72ºC for 30 seconds as 45 cycles followed by melting curve and cooldown. GAPDH was used as housekeeping gene and calculations were done by $2^{-DeltaCT}$ method. Primers used for the qPCR reactions were listed in **Table 2.3**.

Table 2.3: qPCR primers.

Name	Forwar Primer	Reverse Primer
GAPDH	AGCCACATCGCTCAGACAC	GCCCAATACGACCAAATCC
MGMT	GTG ATT TCT TAC CAG CAA TTA GCA	CTG CTG CAG ACC ACT CTG TG
RBBP4	ATGACCCATGCTCTGGAGTG	GGACAAGTCGATGAATGCTGAAA
RAD50	GGAAGAGCAGTTGTCCAGTTACG	GAGTAAACTGCTGTGGCTCCAG
MRE11	ATGCAGTCAGAGGAAATGATACG	CAGGCCGATCACCCATACAAT
NBN	GACTGGCGTTGAGTACGTTGT	TGATTTCGGCTGATCGACTGA
ROBO2	GTTTGTGTTGCGAGGAACTATCT	GTTTTGTCGGAAGTCATCTCGTA
TMEM132D	AGGAGCGCACGGATTATACTG	ATCTGCATGACCTCGTAGGAG
KLHL4	ATACCATTGAAAGTTTGCTGGCT	GCATCTCCAAATGATCGAATCCC
TUBA3C	AGGAGTCCAGATCGGCAATG	GTCCCCACCACCAATGGTTT
SEMA6D	AGGCAATATCCGGTTTTTAGAGG	CCCTGCCAGCAATATAAAGTGT
CES1	ACCCCTGAGGTTTACTCCACC	TGCACATAGGAGGGTACGAGG
ESM1	ACAGCAGTGAGTGCAAAAGCA	GCGGTAGCAAGTTTCTCCCC
COLEC10	GCTCGGCTCAAGACATCTATG	TGAACACCCGAAAGAAGCCAC
PASD1	GTCGAACATGGTGATAGTTCTGC	AGCCACTAAAGACCACAGGAA
RNF43	CATCAGCATCGTCAAGCTGGA	TTACCCCAGATCAACACCACT
CSMD1	TGGAGGAGATTCCAGTCGCT	GCATAGTTCGGATACCCGTGA
SLC14A1	ACTATGGTTAGAGTGGACAGCC	ACGGGTTTGTCTTTAAGCTGG
MUTS1	TTGACAAATTGAAGCGTTTCCAG	CTGCCTTGAGATTGCCATGTG
CELF2	GCGTTCAGCGGCATTCAAC	AGAGAGAGGGTTTGCATTGGT
MGMT-Exon2-1	GAAGCTGGAGCTGTCTGGTT	CAGGATCACGTGGGCTCATA
MGMT-Exon2-2	ACGACCAGCCTCTTACCTAT	TCCAGTGTGGTGCGTTTCAT

2.12 Bisulfite Conversion and Methylation Specific Nested PCR

For bisulfite conversion, genomic DNA from samples were isolated as explained previously. EZ DNA methylation-gold kit (Zymo, USA) was used for bisulfite conversion of gDNA according to the manufacturer's instructions. Briefly, 500 ng of high quality gDNA is mixed with CT conversion reagent and placed in thermal cycler as 98ºC for 10 minutes, 64ºC for 2.5 hours and 4ºC hold. Samples are loaded to IC column with M-binding buffer added previously, mixed by inverting the tube and centrifuged at 11.000xg for 30 seconds. M-Wash buffer was added to the column and centrifuged again. M-Desulphonation buffer was added over the columns and incubated at RT for 17 minutes followed by centrifugation as explained. Later, M-wash buffer was added to column and centrifuged, and these steps repeated one more time. Finaly, M-elution buffer was added directly to the column, placed in Eppendorf tube and centrifuged. DNA is stored in -20ºC.

Methylation specific PCR primers and conditions were taken and adjusted from previously published articles (Belinsky et al., 2007) (Anel et al., 2000) (Vlassenbroeck et al., 2008). PyroMark PCR Kit (978703, Qiagen) was used for PCR reactions. For first

round, 1 µL of bisulfite converted DNA was used as template and reaction was setup as 12.5 µl 2x master mix, 2.5 µl coral load, 1 µl mgmt. reverse primer (5 µM), 1 ul mgmt. forward primer (5 µM), completed to 25 µl with dH2O. Reaction steps were as follows: 95ºC for 15 minutes, 94ºC for 30 seconds-56ºC for 30 seconds-72ºC for 30 seconds for 45 cycles, 72ºC for 10 minutes and 4ºC hold. For the second round PCR, PCR product was diluted 1:50 with dH2O. Each product was placed in reaction with either methylated MGMT primers or unmethylated MGMT primers. 5 µL of diluted PCR product, 12.5 µl of 2x PCR master mix, 2.5 µL coral load, 1 µl of methylated/unmethylated-forward primer (5 µM), 1 µl of methylated/unmethylated-reverse primer (5 µM) and 3 µL of dH2O was mixed. Reaction steps were as follows: 95ºC for 15 minutes, 94ºC for 15 seconds-62ºC for 15 seconds-72ºC for 15 seconds for 40 cycles, 72ºC for 10 minutes and 4ºC hold. 15 µL of PCR product was run on 3% agarose gel and visualized.

Table 2.4: Primers for MGMT methylation specific nested PCR.

Name	Forwar Primer	Reverse Primer
MGMT-MSP	GGATATGTTG GGATAGTT	CCAAAAACCCCAAACCC
Unmethylated-MGMT	TTTGTGTTTTGATGTTTGTAGGTTTTTGT	AACTCCACACTCTTCCAAAAACAAAACA
Methylated-MGMT	TTTCGACGTTCGTAGGTTTTCGC	GCACTCTTCCGAAAACGAAACG

2.13 gRNA Cloning

Guide RNAs were chosen among the good gRNAs from EPIKOL (**Table 2.5**). Oligonucleotides were annealed using T4 Polynucleotide Kinase (NEB). Backbone plentiGuide-Puro (Addgene) vector was digested using BsmI (NEB) followed by agarose gel electrophoresis and digested plasmid was isolated from the gel using Gel and PCR clean-up kit (MN). Annealed insert and digested backbone were ligated using T4 DNA Ligase (NEB). Next, ligated product and competent bacteria were used for transformation. Following plasmid isolation, samples were sequenced by Macrogen.

Table 2.5: Cloned gRNAs for EPIKOL validations.

Epikol Rank	Name	Sequence
4973	PRPF31-g1-F	CACCGCGTTGCTCCAGGATCTGCGG
	PRPF31-g1-R	AAACCCGCAGATCCTGGAGCAACGC

4976	PRPF31-g2-F	CACCGGACACAGCTGGATCTTTCCG
	PRPF31-g2-R	AAACCGGAAAGATCCAGCTGTGTCC
4978	PRPF31-g3-F	CACCGGGCCCAGCGCAAGACGCTGT
	PRPF31-g3-R	AAACACAGCGTCTTGCGCTGGGCCC
426	ASH2L-g2-F	CACCGGAAGCAGACTCCCCATAGTG
	ASH2L-g2-R	AAACCACTATGGGGAGTCTGCTTCC
6811	UHRF1-g1-F	CACCGACACCCGACTCGCTGACCTG
	UHRF1-g1-R	AAACCAGGTCAGCGAGTCGGGTGTC
6816	UHRF1-g2-F	CACCGGAGCTCTCCGACACCGACTCC
	UHRF1-g2-R	AAACGAGTCGGTGTCGGAGAGCTCC
1936	ELP3-g1-F	CACCGGATGCCTGACCTGCCAAACG
	ELP3-g1-R	AAACCGTTTGGCAGGTCAGGCATCC
7129	YEATS4-g3-F	CACCGTCAGACACCAATGCAATGCT
	YEATS4-g3-R	AAACAGCATTGCATTGGTGTCTGAC
3152	KDM2A-g1-F	CACCGAATGTAGAGTATATTCAGCG
	KDM2A-g1-R	AAACCGCTGAATATACTCTACATTC
3160	KDM2A-g3-F	CACCGTTAATGTAGAGTATATTCAG
	KDM2A-g3-R	AAACCTGAATATACTCTACATTAAC
6995	VPS72-g1-F	CACCGCCTGCCTCTCCTGTACCCGA
	VPS72-g1-R	AAACTCGGGTACAGGAGAGGCAGGC
7000	VPS72-g2-F	CACCGTTCTACCAGACGACTTATGG
	VPS72-g2-R	AAACCCATAAGTCGTCTGGTAGAAC
1763	DOT1L-g1-F	CACCGCTGAGCCCGCCGTCTACCCG
	DOT1L-g1-R	AAACCGGGTAGACGGCGGGCTCAGC
1766	DOT1L-g2-F	CACCGGCTGAGACTGAAGTCGCCCG
	DOT1L-g2-R	AAACCGGGCGACTTCAGTCTCAGCC
4902	PRMT1-g1-F	CACCGACCTTGTGATCCGCCCGCCT
	PRMT1-g1-R	AAACAGGCGGGCGGATCACAAGGTC
4928	PRMT5-g2-F	CACCGGGTACTGAGAGTATTTGATG
	PRMT5-g2-R	AAACCATCAAATACTCTCAGTACCC
811	BRD8-g1-F	CACCGAAGAGGAGGCTGAAGTAAAG
	BRD8-g1-R	AAACCTTTACTTCAGCCTCCTCTTC
818	BRD8-g2-F	CACCGGGCTACAGATGCTGCATACC
	BRD8-g2-R	AAACGGTATGCAGCATCTGTAGCCC
821	BRD9-g1-F	CACCGACTCCAGTTACTATGATGAC
	BRD9-g1-R	AAACGTCATCATAGTAACTGGAGTC
826	BRD9-g2-F	CACCGCTTCGCCAACTTGTAGTACA
	BRD9-g2-R	AAACTGTACTACAAGTTGGCGAAGC
827	BRD9-g3-F	CACCGCTTGACGGACAGTACCGCAG
	BRD9-g3-R	AAACCTGCGGTACTGTCCGTCAAGC
5845	SMARCE1-g1-F	CACCGAGTGGGTTACCTGTCTCCAT
	SMARCE1-g1-R	AAACATGGAGACAGGTAACCCACTC

5820	SMARCD1-g2-F	CACCGTTTGTCCAGTTCAATCACCA
	SMARCD1-g2-R	AAACTGGTGATTGAACTGGACAAAC
1982	EP300-g1-F	CACCGATGCTCACAAGTGCCAGCGC
	EP300-g1-R	AAACGCGCTGGCACTTGTGAGCATC
1988	EP300-g2-F	CACCGGGTACGACTAGGTACAGGCG
	EP300-g2-R	AAACCGCCTGTACCTAGTCGTACCC
1443	CREBBP-g1-F	CACCGATTTGGGTTACTTAAAGAAG
	CREBBP-g1-R	AAACCTTCTTTAAGTAACCCAAATC
1445	CREBBP-g2-F	CACCGCAGGACGGTACTTACGTCTG
	CREBBP-g2-R	AAACCAGACGTAAGTACCGTCCTGC
7721	RLP11-g1-F	CACCGCATGCGCTGGTTCCAGCAGA
	RLP11-g1-R	AAACTCTGCTGGAACCAGCGCATGC
7724	RLP11-g2-F	CACCGGCATCGCAGACAAGAAGCGC
	RLP11-g2-R	AAACGCGCTTCTTGTCTGCGATGCC
5611	SFPQ-g1-F	CACCGAGTACGAATATTCTCAGCGA
	SFPQ-g1-R	AAACTCGCTGAGAATATTCGTACTC
5614	SFPQ-g2-F	CACCGCGAAGCTGTCTACCTCTCAT
	SFPQ-g2-R	AAACATGAGAGGTAGACAGCTTCGC
4308	PAXIP1-g1-F	CACCGTCTTCATAAATAATCAGACG
	PAXIP1-g1-R	AAACCGTCTGATTATTTATGAAGAC
6743	UBE2N-g1-F	CACCGATATTAGATACCTGTTTCTA
	UBE2N-g1-R	AAACTAGAAACAGGTATCTAATATC
6748	UBE2N-g2-F	CACCGCTGTTGCCTTCATAGATAAG
	UBE2N-g2-R	AAACCTTATCTATGAAGGCAACAGC
5116	RBBP5-g1-F	CACCGCGAATAATCAGAGTTTATGA
	RBBP5-g1-R	AAACTCATAAACTCTGATTATTCGC
5119	RBBP5-g2-F	CACCGTGAACCTATGCAGAAATTGC
	RBBP5-g2-R	AAACGCAATTTCTGCATAGGTTCAC
3675	MGMT-g1-F	CACCGGGTACTTGGAAAAATGGACA
	MGMT-g1-R	AAACTGTCCATTTTTCCAAGTACCC
3680	MGMT-g2-F	CACCGTGAAATGAAACGCACCACAC
	MGMT-g2-R	AAACGTGTGGTGCGTTTCATTTCAC
6046	SUDS3-g1-F	CACCGGTTAACAAATAGTTTAGCTG
	SUDS3-g1-R	AAACCAGCTAAACTATTTGTTAACC
6047	SUDS3-g2-F	CACCGTAGATCAGCAGTACAAAGAG
	SUDS3-g2-R	AAACCTCTTTGTACTGCTGATCTAC
3314	KDM8-g1-F	CACCGGAACTCGTTGACCGTCATGA
	KDM8-g1-R	AAACTCATGACGGTCAACGAGTTCC
872	BRPF1-g1-F	CACCGAGGGTGACTGCAGGCAACGG
	BRPF1-g1-R	AAACCCGTTGCCTGCAGTCACCCTC
878	BRPF1-g2-F	CACCGTACTGCTGTGGCCCACGCCG
	BRPF1-g2-R	AAACCGGCGTGGGCCACAGCAGTAC

6278	TAF5L-g1-F	CACCGTAAGGTGAGGACTTTGCACA
	TAF5L-g1-R	AAACTGTGCAAAGTCCTCACCTTAC
6280	TAF5L-g2-F	CACCGTTGATCGGACGTACCCGCTG
	TAF5L-g2-R	AAACCAGCGGGTACGTCCGATCAAC
6292	TAF6L-g1-F	CACCGAGATCCTGGCAGATCCTGTG
	TAF6L-g1-R	AAACCACAGGATCTGCCAGGATCTC
6298	TAF6L-g2-F	CACCGGCAGACGAACTCCAAGATTG
	TAF6L-g2-R	AAACCAATCTTGGAGTTCGTCTGCC
1985	EP300-g3-F	CACCGCTGTAATAAGTGGCATCACG
	EP300-g3-R	AAACCGTGATGCCACTTATTACAGC
3102	KAT6B-g1-F	CACCGGTTGTCTGGGTCCTTATAGG
	KAT6B-g1-R	AAACCCTATAAGGACCCAGACAACC
3104	KAT6B-g2-F	CACCGTGAAAGACGGACCGCAGTAC
	KAT6B-g2-R	AAACGTACTGCGGTCCGTCTTTCAC
4052	NEK6-g1-F	CACCGACGTACCTCGGTGCATCACC
	NEK6-g1-R	AAACGGTGATGCACCGAGGTACGTC
4055	NEK6-g2-F	CACCGGCAGCGAAAAGACAGCGTGT
	NEK6-g2-R	AAACACACGCTGTCTTTTCGCTGCC
6154	TADA1-g1-F	CACCGACTGGGCTAACCTAAAGCTG
	TADA1-g1-R	AAACCAGCTTTAGGTTAGCCCAGTC
6174	TADA2B-g1-F	CACCGCATGACATGAACTGGTACAG
	TADA2B-g1-R	AAACCTGTACCAGTTCATGTCATGC
6180	TADA2B-g2-F	CACCGTTACGAGATCGAGTATGACC
	TADA2B-g2-R	AAACGGTCATACTCGATCTCGTAAC
2902	INO80-g1-F	CACCGACTCTGAGAATCAGCCTCGC
	INO80-g1-R	AAACGCGAGGCTGATTCTCAGAGTC
2904	INO80-g2-F	CACCGCAGAGACAAATCGATATAGG
	INO80-g2-R	AAACCCTATATCGATTTGTCTCTGC
2909	INO80-g3-F	CACCGTACAGAATCAAAATGTGATA
	INO80-g3-R	AAACTATCACATTTTGATTCTGTAC
2910	INO80-g4-F	CACCGTTGCACCAGACTATATCCAA
	INO80-g4-R	AAACTTGGATATAGTCTGGTGCAAC
7038	WDR77-g1-F	CACCGGTGGTACTGAGTTCATACCG
	WDR77-g1-R	AAACCGGTATGAACTCAGTACCACC
7039	WDR77-g2-F	CACCGTAGTGACTCACCTGAATCGG
	WDR77-g2-R	AAACCCGATTCAGGTGAGTCACTAC
5191	RMI1-g1-F	CACCGAAAATGCCATCGGGTAAAAG
	RMI1-g1-R	AAACCTTTTACCCGATGGCATTTTC
5196	RMI1-g2-F	CACCGGATGGAATCGTACAAATACA
	RMI1-g2-R	AAACTGTATTTGTACGATTCCATCC
4672	PRDM11-g1-F	CACCGATTCATCCACGAAGTACTCC
	PRDM11-g1-R	AAACGGAGTACTTCGTGGATGAATC

4680	PRDM11-g2-F	CACCGTGTGTCAGACACAAACACCG
	PRDM11-g2-R	AAACCGGTGTTTGTGTCTGACACAC
801	BRD7-g1-F	CACCGAACTGATGAGACAATTGCAG
	BRD7-g1-R	AAACCTGCAATTGTCTCATCAGTTC
803	BRD7-g2-F	CACCGAGGAACCATGCTTTAGTATC
	BRD7-g2-R	AAACGATACTAAAGCATGGTTCCTC
6448	TFPT-g1-F	CACCGGCGCTGCCGGGAGATCGAGC
	TFPT-g1-R	AAACGCTCGATCTCCCGGCAGCGCC
6449	TFPT-g2-F	CACCGGGCCCGGTAGTCATCCCCGT
	TFPT-g2-R	AAACACGGGGATGACTACCGGGCCC
3723	MORF4L1-g1-F	CACCGACCTTTGCTTCATAAAGAAG
	MORF4L1-g1-R	AAACCTTCTTTATGAAGCAAAGGTC
3728	MORF4L1-g2-F	CACCGTGTACTGAGGGAGCTCCTTC
	MORF4L1-g2-R	AAACGAAGGAGCTCCCTCAGTACAC
4371	PCGF6-g1-F	CACCGAATCAGGCGCTGCAAATAAA
	PCGF6-g1-R	AAACTTTATTTGCAGCGCCTGATTC
4377	PCGF6-g2-F	CACCGGGGAGGCCGGCAGGACTCGG
	PCGF6-g2-R	AAACCCGAGTCCTGCCGGCCTCCCC
5145	RCOR1-g1-F	CACCGCCGCAGGTGGCGGTGGCATG
	RCOR1-g1-R	AAACCATGCCACCGCCACCTGCGGC
5146	RCOR1-g2-F	CACCGCGGACCCCAGTACCAGGCGG
	RCOR1-g2-R	AAACCCGCCTGGTACTGGGGTCCGC
5446	SENP3-g1-F	CACCGGCTTCCGAGTGGCTTATAAG
	SENP3-g1-R	AAACCTTATAAGCCACTCGGAAGCC
5448	SENP3-g2-F	CACCGGGGGGAGTCAAAACGACAAC
	SENP3-g2-R	AAACGTTGTCGTTTTGACTCCCCCC
5453	SET-g1-F	CACCGAGATTTCCATTTGATTTCGG
	SET-g1-R	AAACCCGAAATCAAATGGAAATCTC
5455	SET-g2-F	CACCGCCGGCCGCACCATGTGGCGG
	SET-g2-R	AAACCCGCCACATGGTGCGGCCGGC
5555	SETDB2-g1-F	CACCGTAGGCGATGCAAAAACTTTC
	SETDB2-g1-R	AAACGAAAGTTTTTGCATCGCCTAC
5558	SETDB2-g2-F	CACCGTGGAAGGAGTCTACGAAACG
	SETDB2-g2-R	AAACCGTTTCGTAGACTCCTTCCAC
4784	PRDM9-g1-F	CACCGCAGAAGATTCTGATGAAGAA
	PRDM9-g1-R	AAACTTCTTCATCAGAATCTTCTGC
4786	PRDM9-g2-F	CACCGGAGCCCTGAAAAGTCCCAAG
	PRDM9-g2-R	AAACCTTGGGACTTTTCAGGGCTCC
2974	JADE3-g1-F	CACCGCCCGCCAGAAGAACGCGCGG
	JADE3-g1-R	AAACCCGCGCGTTCTTCTGGCGGGC
2977	JADE3-g2-F	CACCGCGCGCGTTCTTCTGGCGGGC
	JADE3-g2-R	AAACGCCCGCCAGAAGAACGCGCGC

216	APEX1-g1-F	CACCGCCAAGAGCAGATCTTGAGTG
	APEX1-g1-R	AAACCACTCAAGATCTGCTCTTGGC
219	APEX1-g2-F	CACCGTCAGCTCCTTCGGACAAGGA
	APEX1-g2-R	AAACTCCTTGTCCGAAGGAGCTGAC
628	BAP1-g1-F	CACCGTCAAATGGATCGAAGAGCGC
	BAP1-g1-R	AAACGCGCTCTTCGATCCATTTGAC
629	BAP1-g2-F	CACCGTCTACCCCATTGACCATGGT
	BAP1-g2-R	AAACACCATGGTCAATGGGGTAGAC
2062	EXOSC2-g1-F	CACCGCAGCAAGACCGAATCCAGCC
	EXOSC2-g1-R	AAACGGCTGGATTCGGTCTTGCTGC
2064	EXOSC2-g2-F	CACCGCGACACTAAGAAACATCTAG
	EXOSC2-g2-R	AAACCTAGATGTTTCTTAGTGTCGC
5109	RBBP4_g1_F	CACCGTCTTGGAACCCAAATCTCAG
	RBBP4_g1_R	AAACCTGAGATTTGGGTTCCAAGAC
5110	RBBP4_g2_F	CACCGTCTTTGTTGCGATGATACAA
	RBBP4_g2_R	AAACTTGTATCATCGCAACAAAGAC

2.14 Annexin V/Dead Cell Assay

Muse Annexin V/Dead Cell Assay was used to determine apoptosis according to the manufacturer's instructions. Trypsin was used to detach cells and cells were washed with PBS containing 1%FBS. 75 µl of PBS containing 1%FBS were mixed with 75 µl of reagent and incubated for 20 minutes at dark, at RT. Following incubation, measurements were taken with Muse Cell Analyzer.

2.15 Cell Cycle Analysis

For the assessment of cell cycle, Muse Cell Cycle Assay kit was used (Millipore) according to the instructions. Briefly, cells were detached via trypsin and washed 2X with PBS. 70% ethanol was used as a fixative as 1x106 cells per 1 ml of ethanol for minimum 3 hours at -20ºC. Following fixation, cells were centrifuged at 300xg for 5 minutes and washed once with PBS to remove ethanol. 150 µL of reagent was added over the fixed cells and incubated at dark for 30 minutes at RT. Reads were taken with Muse Cell Analyzer.

2.16 *In Vivo* Experiments and Immunohistochemistry

All animal experiments were approved by the institutional ethical committee of Koç University (2016-15). *In vivo* experiments were performed by Dr. Ahmet Cingöz. Parental U87MG and resistant U87MG-R cells were infected with firefly luciferase-mCherry (FLUC-mCherry) viruses. Tumor cells (100,000 cells/mice) were implanted to 6-8-week-old non-obese diabetic/severe combined immunodeficiency (NOD/SCID) mice stereotactically as n=5 (from bregma, AP: -2 mm, ML:1.5 mm, V (from dura):2 mm). TMZ or DMSO was administrated as 2 mg/kg in PBS, as explained in Senbabaoglu et al (Senbabaoglu et al., 2020).Visualization of tumors were performed with IVIS Lumina III (Perkin Elmer, USA) under the isoflurane anesthesia via intraperitoneal injection of D-Luciferin (150 µg/g body weight) at different time points.

On day 23, brain samples were collected from mice and fixed in 10% neutral buffered formalin (NBF). Sectioning, H&E and Ki-67 staining were performed by Dr. İbrahim Kulaç and Ayşe Hümeyra Dur Karasayar at Koç University Hospital, Pathology Department. Mice brains were sectioned in coronal slices from anterior to posterior and each slide was placed in plastic cassettes for processing. Tissue processing using tissue processor (Tissue-Tek CIP 6 AI, Sakura, Japan) was initiated with dehydration by sequential immersion of the tissues in graded ethanol solutions as 70%, 95% and 100%. Following dehydration, the tissues were treated with xylene and embedded in paraffin. Paraffin-embedded tissues were then sectioned into 5 µ thick slices using microtome. Sections were transferred onto glass slides and let to dry for staining.

For hematoxylin and eosin (H&E) staining, deparaffinization of tissue sections were achieved through sequential xylene and rehydration via graded alcohol washes. Sections were stained with H&E staining using Leica protocol (Leica Biosystems, n.d.).

Ki-67 staining was performed on Ventana XT Autostainer using Ki67 antibody (Rabbit monoclonal, Clone: SP6, dilution 1:100, Biocare Medical, CA, USA). Slides were scanned with Philips Ultra-Fast scanner (UFS). Evaluation of the images was formed using Philips Image Management System. Five areas containing the highest

concentration of Ki-67 on the image were selected and evaluated separately using QuPath. After calibrating the cell size, pixel height, and width in microns, five areas of equal size from the image were annotated, and the built-in positive cell detection algorithm was run. The algorithm outputs underwent assessment by a pathologist, who reviewed the detected cells to incorporate false negatives into the calculations while excluding false positives. The percentages of positive Ki-67 from these 5 areas are then averaged as the final Ki-67 count of the tumor in that slide.

2.17 Statistical Analysis

Statistical analysis of the experiments was performed using GraphPad Prism 10.0. Two groups were compared using student's t-test, more than two groups were compared using two-way ANOVA. * $p<0.05$, ** $p<0.01$, *** $p<0.001$.

3 RESULTS

3.1 Epigenetic Knock-Out Screen in GBM Cell lines

3.2.1. gRNA representation of EPIKOL

To first ensure the EPIKOL gRNAs were normally distributed after cells were transduced with EPIKOL lentivirus, representation analysis via NGS was conducted as shown in **Figure 3.1.A**. For this purpose, U87MG cells were infected with library lentivirus with low MOI (0.4) as 1000X. Following Puromycin selection, pellet was collected. Genomic DNA was isolated from the pellet and library preparation was done via Nested PCR. Size of PCR product was analyzed via Fragment Analyzer, and it showed peak around 360 basepairs, as expected (**Figure 3.1.B**). Later, samples were sent to NGS. Results of NGS indicate normal distribution of gRNAs in **Figure 3.1.C**.

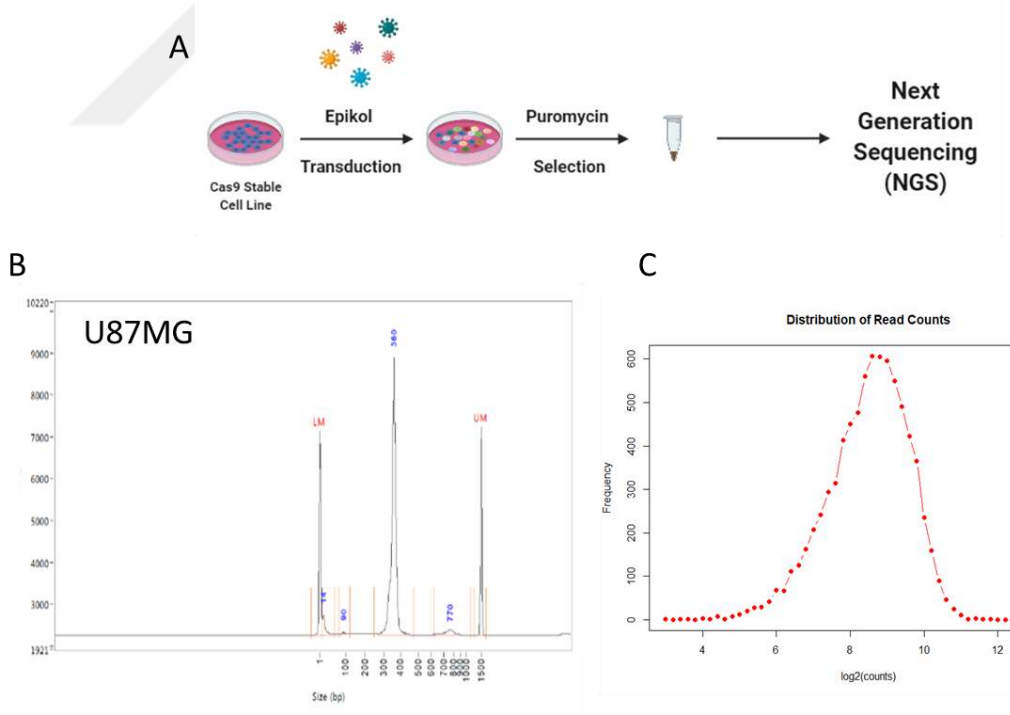

Figure 3.1: EPIKOL gRNA representation. A. Schematics of the representation analysis with U87MG cell line. **B.** Fragment Analyzer results showing single peak at 360 bp. **C.** NGS result showing normal distribution of the gRNAs.

3.2.2. Cas9 Activity Assay

For large scale genetic screens, it is very important to understand how efficient the CRISPR/Cas9 system would work in each cancer cell line. To determine the Cas9 activity in U87MG cells, cells were transduced with GFP-Hygro and selected the with Hygromycin. Later, selected cells were infected with the Cas9 lentivirus which contains Blasticidin antibiotic selection marker. Once the cells were selected with Blasticidin, GFP targeting (T1) and non-targeting (NT1) lentiviruses were introduced to the cells. Following Puro selection, measurements with Flow Cytometer were taken every 3 days. Results show that even after 21 days, 50% Cas9 activity was observed (**Figure 3.2**). Since the highest efficiency was reached at around 20 days and plateaued, 20 days were selected as the number of days for Cas9 activity to be completed. U87MG cells did not show superior Cas9 efficiency, yet we wanted to use this cell line as it is compatible with mouse models, that would serve as to validate our findings *in vitro* and *in vivo*. However, we added another cell line U373 to our screens as well (High Cas9 efficiency was previously demonstrated by other members of the lab).

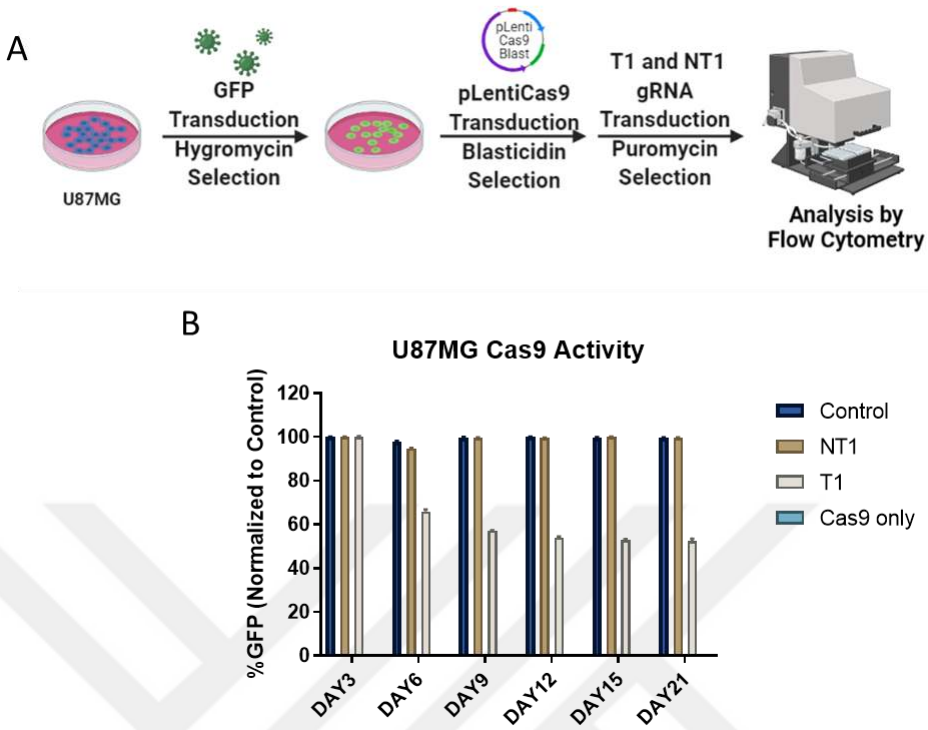

Figure 3.2: Cas9 Activity. A. Diagram showing the flow of Cas9 activity experiment. **B.** %GFP levels of U87MG. Control is GFP only cells, Cas9 only is GFP negative group, therefore no GFP levels were detected.

3.2.3. Essentiality Screens with U373, U87MG and NHA

To investigate the essential chromatin modifiers that regulate GBM cell fitness, drop-out screens using U87MG and U373 cell lines were conducted **(Figure 3.3)**. Normal Human Astrocytes were included as control, as non-malignant cells. For the essentiality screens low MOI (0.4) with 1000X coverage was used. 125x coverage was used for the astrocyte screen due to difficulty of the maintenance of the cell line and growth capabilities. U373 cells were passaged until they reached around 14 doublings and U87MG cells were passaged until 34 doublings, as essentiality comparison. NHA cells were passaged for up to 40 days post transduction. Following NGS, Endpoint samples were compared with After puro samples. Results show the Principal Component Analysis (PCA) plots and log2 fold change (LFC) graphs in **Figure 3.4**. PCA plots show that replicates are clustered together in both U373 and U87MG cell lines. LFC graphs show

the distribution of the genes according to their LFCs. As expected, non-targeting gene (a compilation of nontargeting gRNAs) is located near the X-axis as its LFC is close to 0. Ribosomal genes, as essentiality controls, are mostly distributed on the negative side of the graph. Chosen chromatin regulators are shown in red and have negative LFC values.

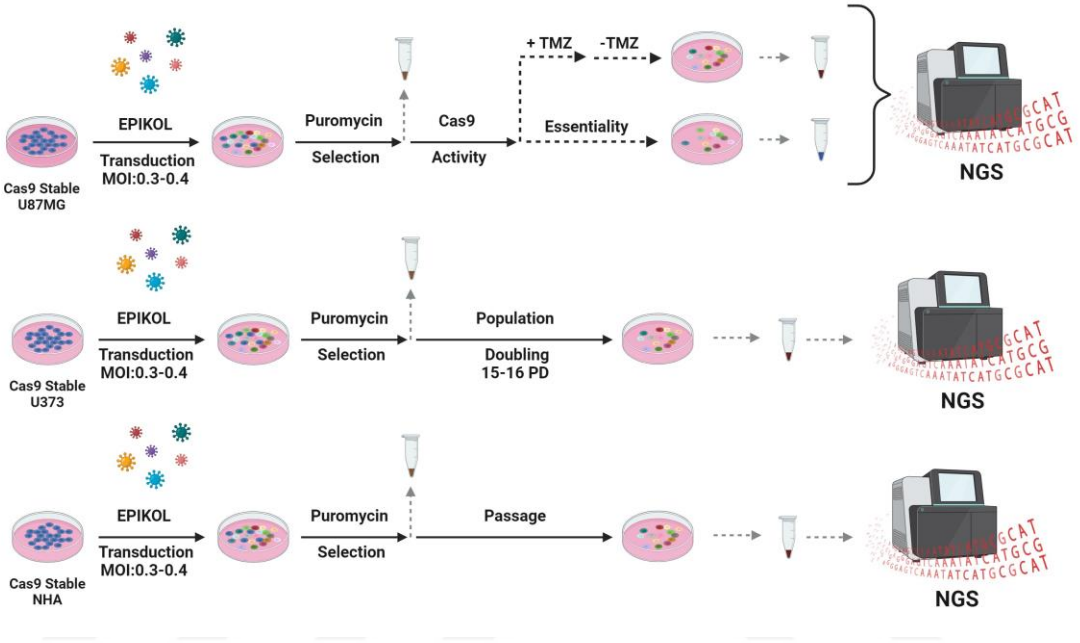

Figure 3.3: Schematics for screening strategies. U87MG cells were separated into two groups following Cas9 activity, one group was treated with 50 uM of TMZ for 4 doublings then TMZ was removed until 14 doubling was reached. Essentiality comparison was used to determine cell fitness regulatory genes. U373 and NHA cell lines were screened as shown.

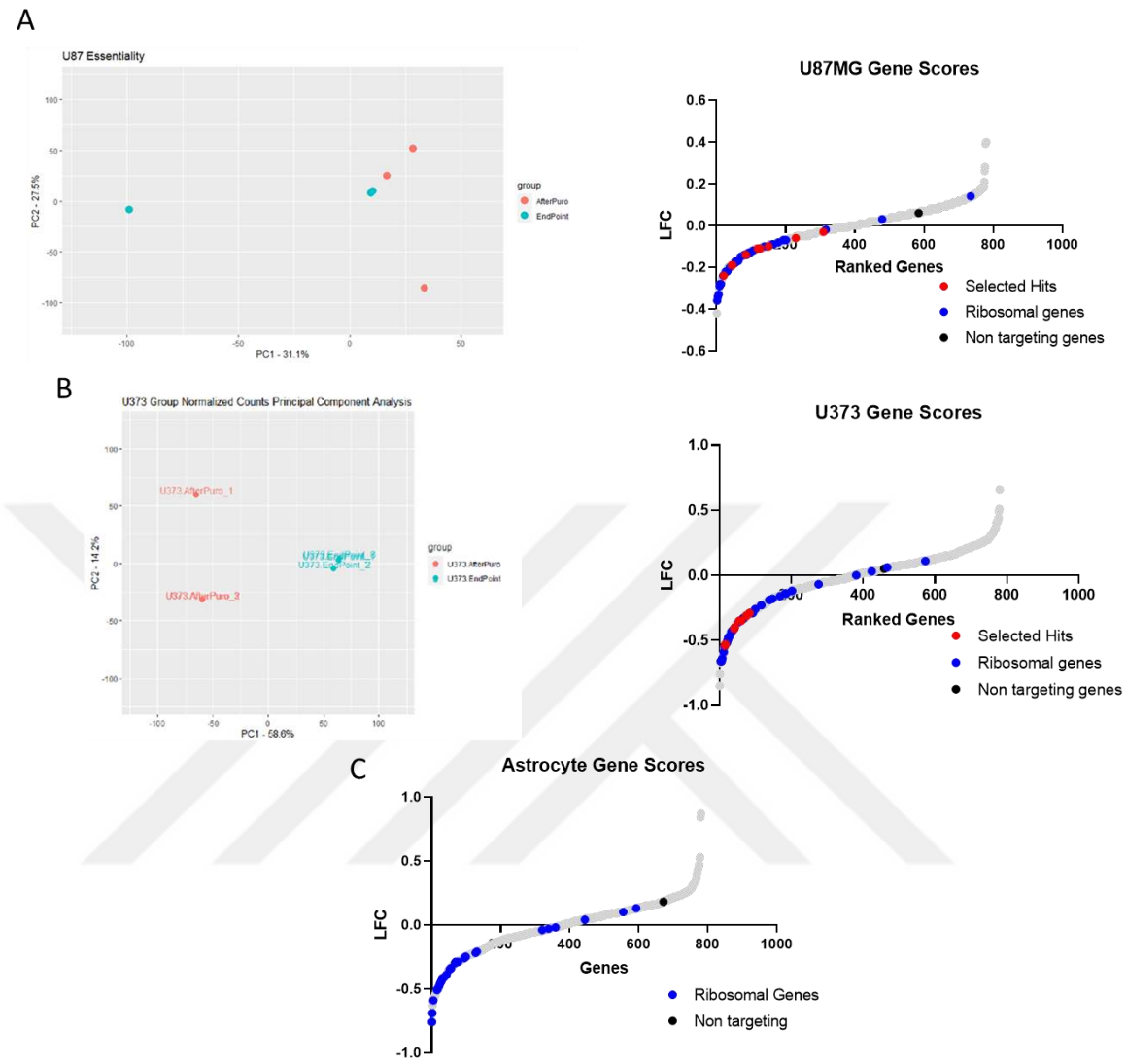

Figure 3.4: Essentiality screen results. A. PCA plot and LFC graph for U87MG cell line. **B.** PCA plot and LFC graph of U373 cell line. **C.** LFC graph of Astrocytes. Selected hits identified in U373 and U87MG screens were not identified in Astrocyte screen, therefore not shown on LFC graph.

Cancer specific regulators were determined by eliminating ribosomal genes and hits from Astrocytes, **Figure 3.5.A**. LFC<0 and p<0.05 cutoff was used. Based on the cutoffs and eliminations, 14 epigenetic regulators, namely *PRPF31, UHRF1, YEATS4, KDM2A, SFPQ, DOT1L, PRMT1, ASH2L, ELP3, VPS72, PRMT5, PAXIP1, UBE2N* and

RBBP4 shown in **Figure 3.5.B** were selected from either common from both cell lines and from only one cell line.

A

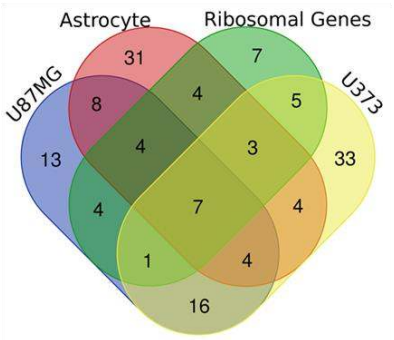

B

Selected Genes		
PRPF31	DOT1L	PRMT5
UHRF1	PRMT1	PAXIP1
YEATS4	ASH2L	UBE2N
KDM2A	ELP3	RBBP5
SFPQ	VPS72	

Figure 3.5: Chromatin regulator selection and validation. A. Venn diagram showing number of hits, common and separated from different groups. **B.** Selected hits from U373 and U87MG cell lines.

3.2.4. Essentiality Screen Validations

To validate the findings of our screen results, hit genes were determined and individual gRNAs against these genes (2/gene) were designed, cloned, and verified by sequencing. Then these gRNAs were employed for packaging and lentiviral transduction and further assays. Competition assay for the validation of these hits were conducted using Cytation5 image-based quantification, where fluorescently labeled cells can be visualized over time. U87MG and U373 cell lines were labelled with PGK-H2B-mCherry or PGK-H2B-eGFP and later transduced with NT1 for mCherry+ cells and gRNAs for eGFP+ cells. Images were taken once every 5 days. Heatmap shows the depletion of gRNAs based on %eGFP (**Figure 3.6**). Depletion starts at Day10 for U373 cells, whereas for U87MG cells it starts after Day14. For both cell lines, NT1 shows no depletion and positive control RPL11 gRNAs show clear depletion.

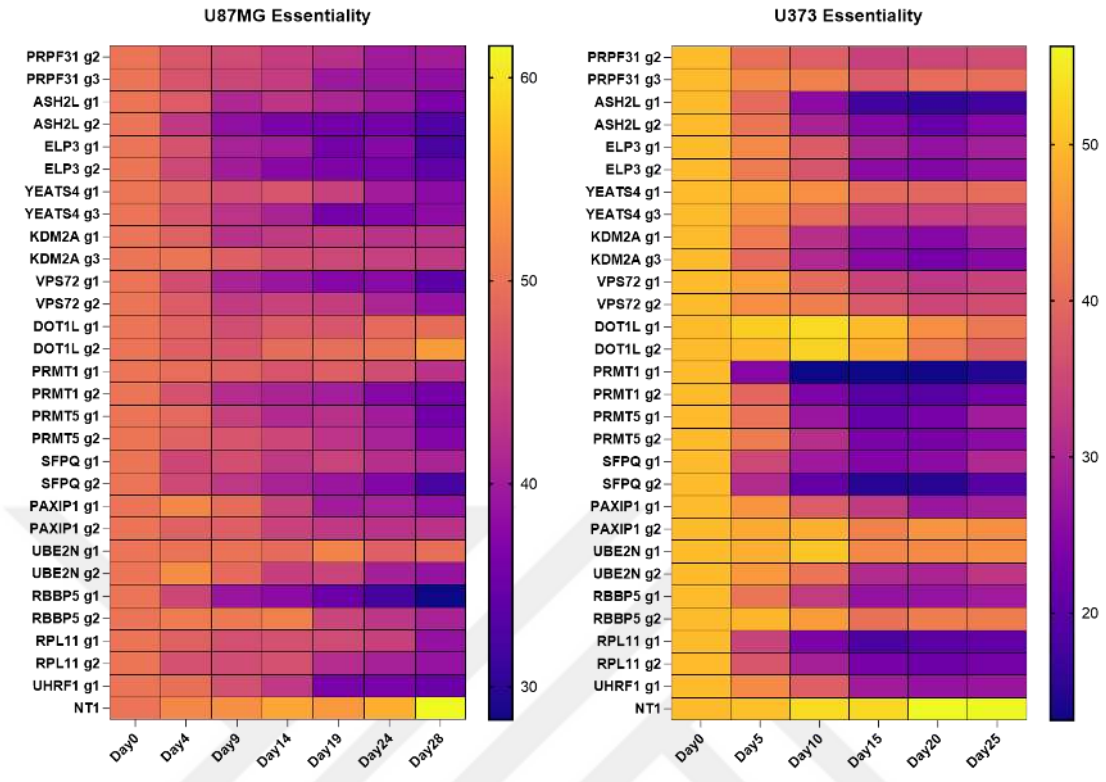

Figure 3.6: Heatmap of Competition Assay. Heatmap of gRNA depletions at each time point, colors scales indicate the %GFP measured during the assay.

Cutoff was determined as 30% for U373 and 40% for U87MG cell lines. Detailed graphs and images are shown in **Figure 3.7** for U87MG and **Figure 3.8** for U373. Graphs show the depleted gRNAs with determined cutoff for each cell line. ASH2L g1 and g2, ELP3 g1 and g2, PRMT1 g1, PRMT5 g1 and g2, SFPQ g2, PAXIP1 g1, RBBP5 g1 and UHRF1 g1 were common in both cell lines. Initial time point and final time point images of commonly depleted gRNAs were also shown in the figures.

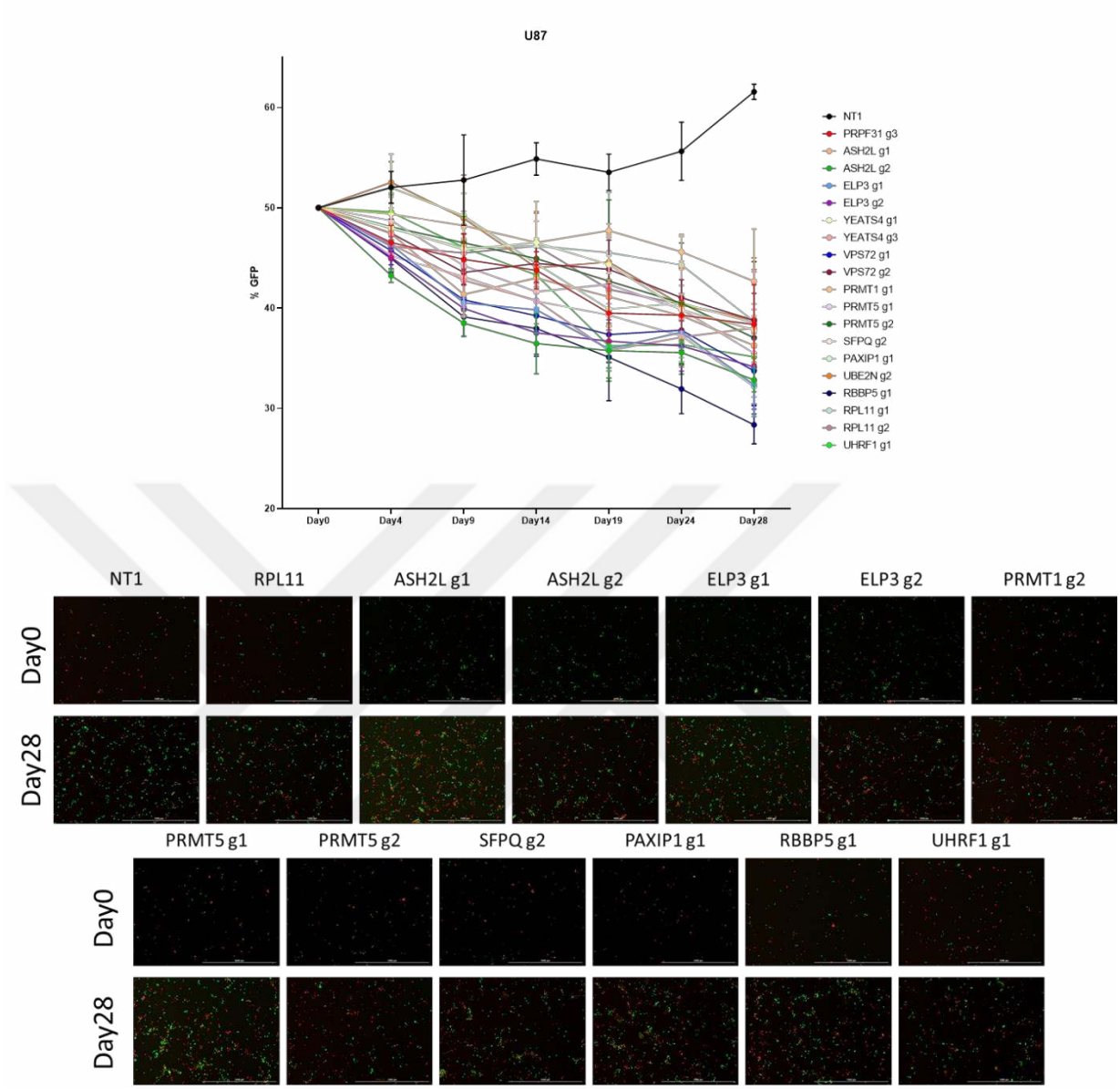

Figure 3.7: Competition Assay results for U87MG cells. Graph showing the %GFP levels of each gRNA, starting from Day0 to Day28. Representative images of Day0 vs Day28 were shown for the most depleted gRNAs. Green cells indicate the gRNA population, red cells indicate the NT1 population. Scale bar 1000 µm.

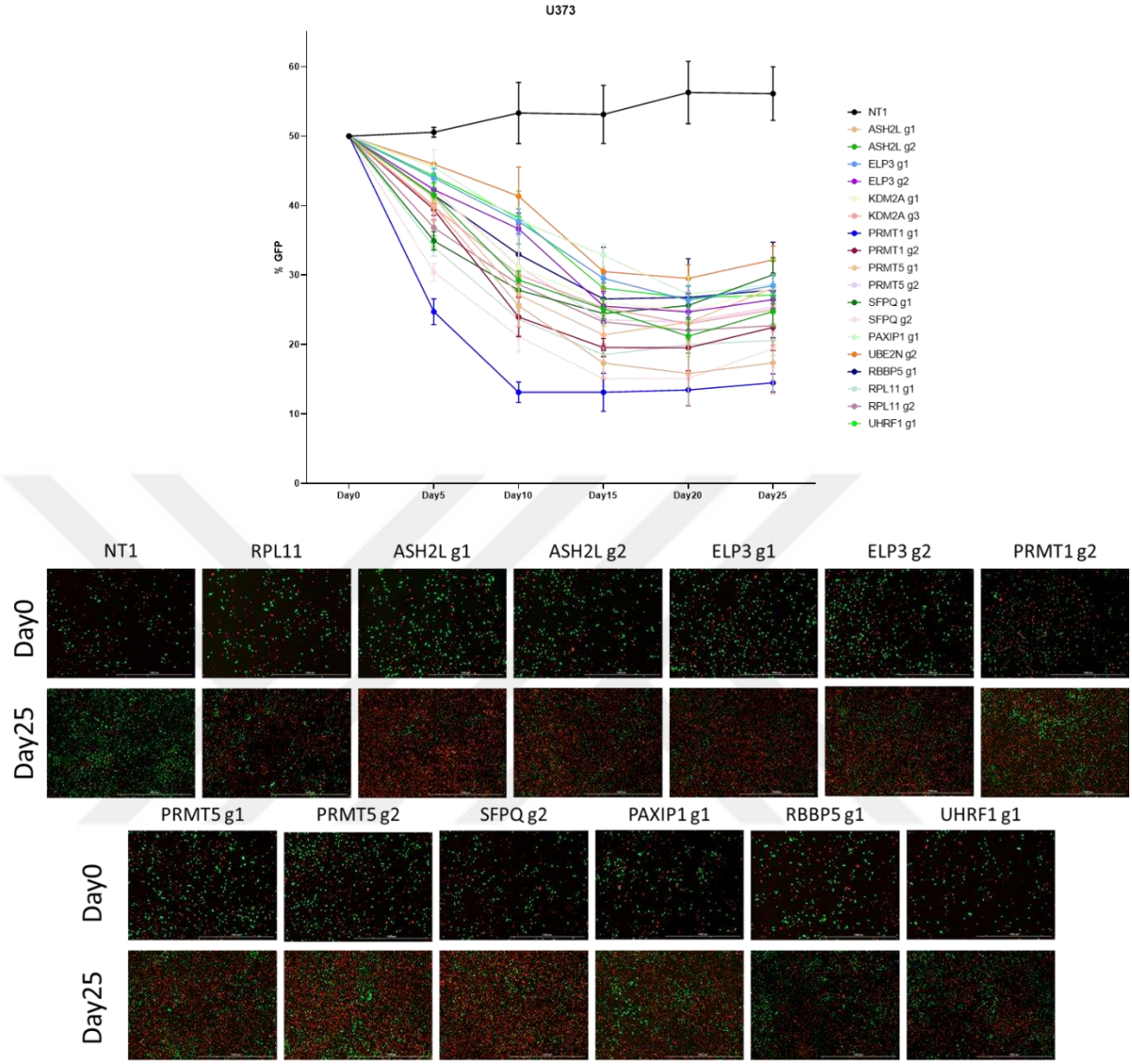

Figure 3.8: Competition assay results for U373. Graph showing the %GFP levels of each gRNA, starting from Day0 to Day25. Representative images of Day0 vs Day28 were shown for the most depleted gRNAs. Green cells indicate the gRNA population, red cells indicate the NT1 population. Scale bar 1000 µm.

During the competition assay, GFP+ cells infected with different gRNAs were used to perform the clonogenic assay, which measures long term growth ability of a given cell line. Cells were seeded to 6 well plates as triplicates as explained previously and left to grow for 14-15 days, after which they were fixed and stained. **Figure 3.9** shows the

effect of gRNAs commonly depleted in competition assay for both cell lines. Graph shows the quantification of clonogenic assay, normalized to NT1. U87MG cells transduced with gRNAs show decreased colony forming ability whereas for some gRNAs, such as RBBP5 g1, ELP3 g1-g2 and UHRF1 g1, we do not see the same phenotype in U373 cells.

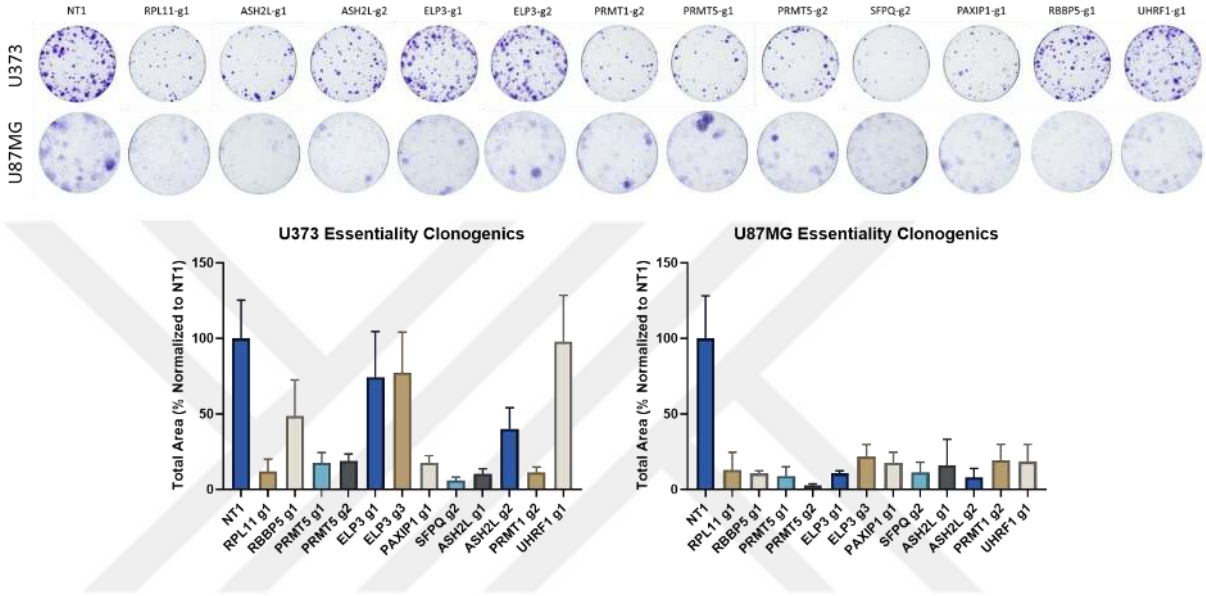

Figure 3.9: Clonogenic assay for essentiality validation and analysis. Colony formation assay following gRNA infection in both cell lines show essential genes. Validation of the colony formation assay show that most gRNAs were essential for U87MG while some, such as ELP3 and UHRF1 was not essential for U373 cell line.

ASH2L knock-out was studied further. For this purpose, U87MG and U373 cells were infected with NT1 or ASH2L viruses, and colony formation assay, along with MTT assay was conducted. As in previous results. ASH2L decreased cell viability significantly in both colony formation assay (**Figure 3.10.A**) and MTT assay at day5 (**Figure 3.10.B**). ASH2L as a potential GBM fitness gene was studied extensively in our laboratory and it was shown that effect of ASH2L knock-out leads to cell cycle alterations and cell death (Ozyerli-Goknar et al., 2023).

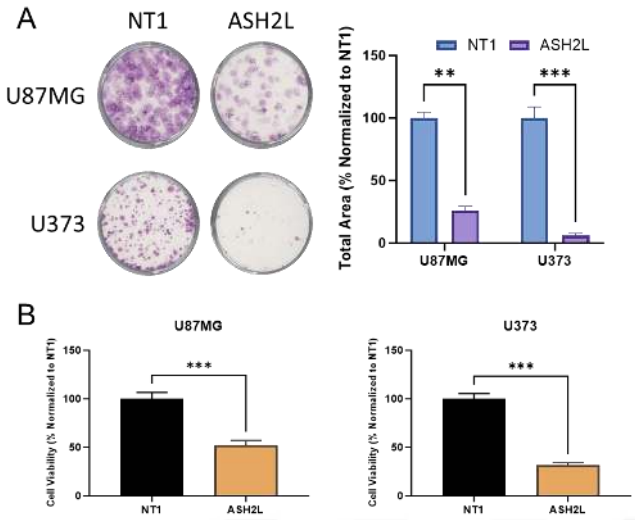

Figure 3.10: Cell viability upon ASH2L knock-out. A. Colony formation assay and quantification with U87MG and U373. **B.** MTT results at Day5. Student's t-test, * $p<0.05$, ** $p<0.01$, *** $p<0.001$.

3.2.5. TMZ Sensitization Screen

To find epigenetic modulators of TMZ sensitivity in naïve glioblastoma cells, we administered TMZ to U87MG cells after Cas9 activity during EPIKOL screen. This sensitization screen with U87MG cell line was proceeded according to the schematics in **Figure 3.3**. A low dose of TMZ (50 µM) and an equivalent volume of DMSO was given. Due to the effect of TMZ on population doubling, TMZ was removed after 4 doublings (called TMZ) and cells were passaged without TMZ (called After TMZ) until they reached 14 doublings **(Figure 3.11.A).** Venn diagram in **Figure 3.11.B** shows the common epigenetic regulators when TMZ and After TMZ points were analyzed compared to DMSO. BRD9, BRD8, EP300, CREBBP, SMARCD1 and SMARCE1 were selected to study their inhibition as potential TMZ-sensitizers. The LFC graph in **Figure 3.11.C** shows the distribution of these genes.

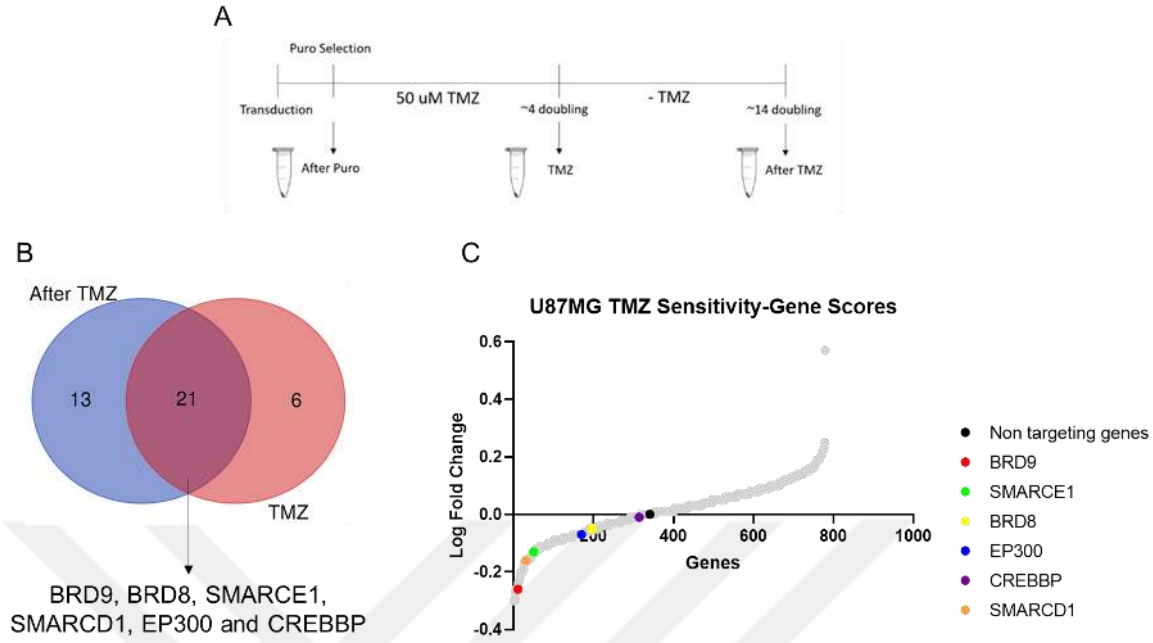

Figure 3.11: TMZ sensitization screen with U87MG. A. Schematics of TMZ administration during screening and doubling times. **B.** Venn diagram showing the common genes in both time points and selected genes. **C.** LFC graph with labelled genes.

To validate these genes, gRNAs designated for the genes were cloned in pLentiGuide vector. Following cloning, lentiviruses were produced and U87MG cells were transduced. Cells were seeded for colony formation assay following puromycin selection. One day after seeding, cells were treated with 5 µM of TMZ. Since 50 µM TMZ used in the screen was decreasing the doubling, dosage was reduced for further experiments. **Figure 3.12** shows the results of colony formation assay for potential sensitizers. Based on quantification, only SMARCD1 g1 was shown to sensitize U87MG cells to TMZ significantly.

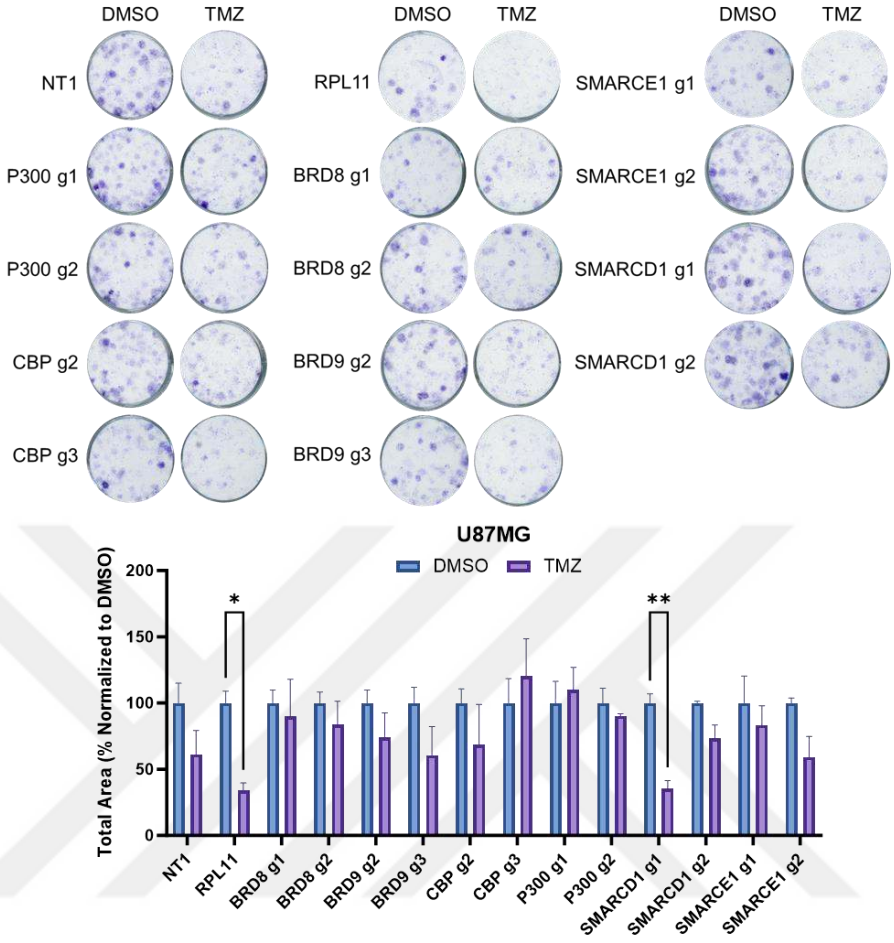

Figure 3.12: Validation of Sensitization Screen. Colony formation assay results with 5 μM of TMZ. Analysis shows only one gRNA was inducing sensitization. Student's t-test, * $p<0.05$, ** $p<0.01$.

Later, the effect of SMARCE1 on TMZ sensitization was investigated with both U87MG and U373 cells along with TMZ-resistant versions, U87MG-R and TMZRT, respectively. Colony formation assay and the quantification is shown in **Figure 3.13**. TMZ concentration for parental cells is 10 μM, 200 μM for U87MG-R and 250 μM for TMZRT. Results show that there was significant sensitization to TMZ in parental cell lines, but not on resistant cells. The sensitization effect was the same with NT1 ko as well as SMARCE1 ko with two gRNAs. MTT assay was conducted 5 days after seeding with the same TMZ dosages in colony formation assay shows no sensitization in a 96well plate format (**Figure 3.14**).

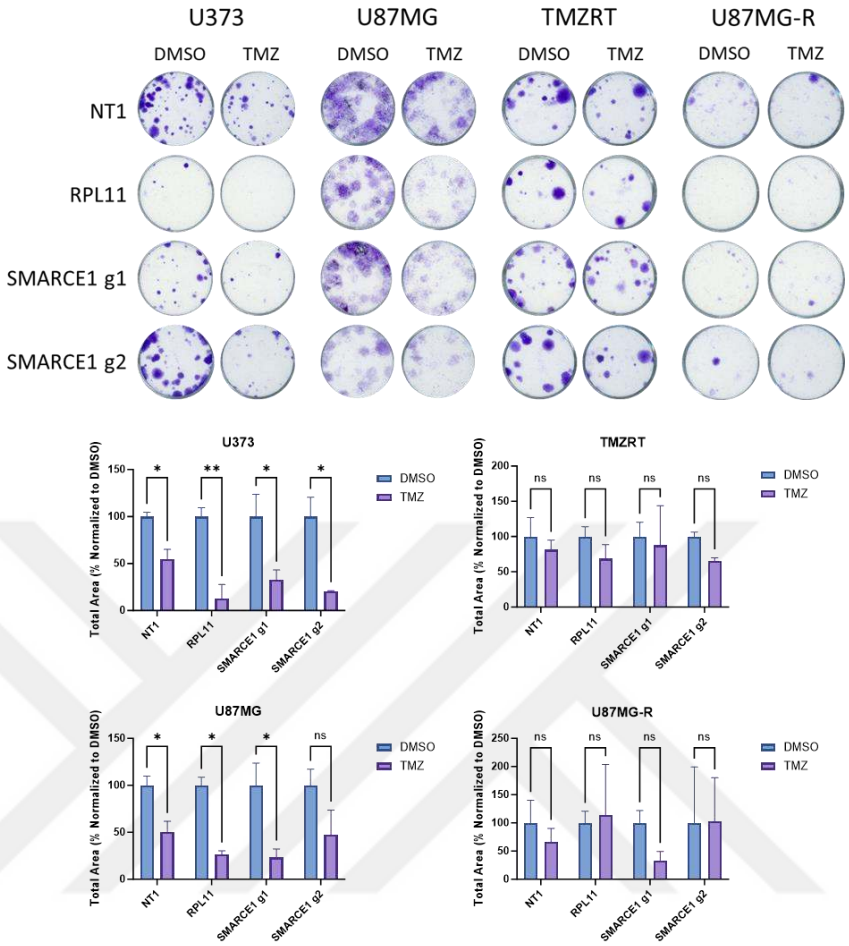

Figure 3.13: Colony formation assay with parental and resistant pairs after SMARCE1 KO. Sensitization experiment performed with naïve and resistant cell lines demonstrate that no sensitization is induced in resistant cells while slight sensitization is present for naïve cell lines. Student's t-test, * $p<0.05$, ** $p<0.01$.

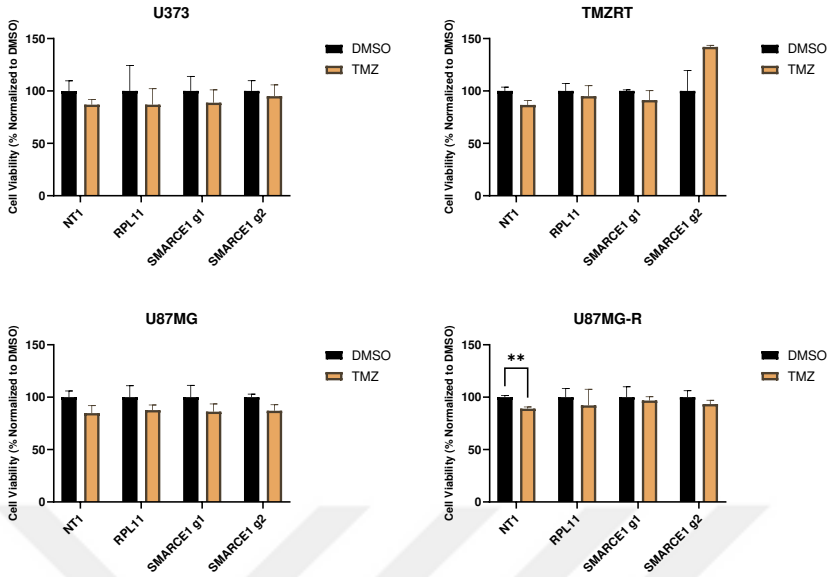

Figure 3.14: MTT results for SMARCE1 KO. 5 days MTT results with TMZ or DMSO were shown. Student's t-test, ** p<0.01.

Due to failed validations, we did not continue to investigate the potential sensitizers from this screen.

3.2 Generation of Temozolomide Resistant Cell Line

3.2.1. TMZ Response for U87MG

TMZ dose response was established with colony formation assay in U87MG cell line (**Figure 3.15**). For this assay, 5, 7.5, 10, 15, and 20 µM of TMZ dosages were used. Based on these findings, 5 µM of TMZ was selected for the start of resistant cell line generation.

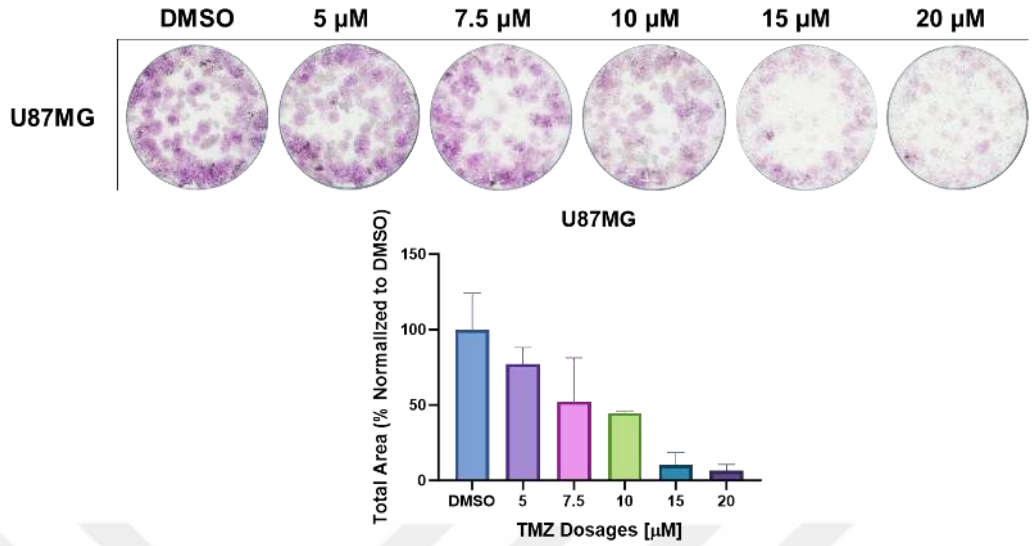

Figure 3.15: Dose response colony formation assay for U87MG. Escalating dosages of TMZ were administered to U87MG cells for colony formation assay. Quantification shows the decrease in total area with increasing dosages.

3.2.2. Generation of TMZ resistant cell line

For the establishment of TMZ resistant cell line, dose escalation method was used (**Figure 3.16**). U87MG cells were exposed to increasing dosages of TMZ, starting from 5 µM. Once the cells start to adjust to TMZ dosage, the dosage was doubled.

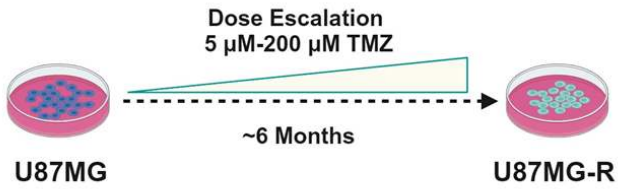

Figure 3.16: Scheme for resistant cell line generation. U87MG cell line was treated with increasing dosages of TMZ for a period of 6 months and new cell line was named U87MG-R.

After 6 months, morphological changes that were different from U87MG parental cells were observed (**Figure 3.17.A**). At this point, the cells were treated with 200 µM of

TMZ. MTT and colony formation assays were performed to show resistance (**Figure 3.17.B**). Increased IC50 value and colony forming ability was observed in resistant cell line which was named as U87MG-R. No colonies were formed after 10 µM for parental cell line meanwhile colonies were present even at 400 µM of TMZ in U87MG-R cell line (**Figure 3.17.C**). Cell viability assays have shown that TMZ resistant cell line was established.

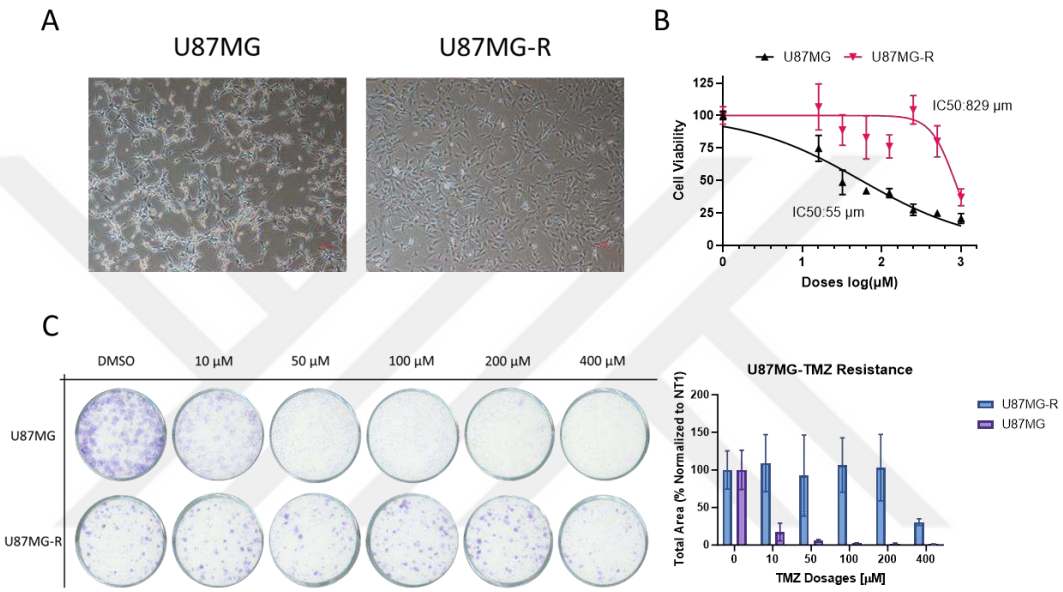

Figure 3.17: Characterization of U87MG-R. A. Morphology of U87MG and U87MG-R cell line, taken with light microscope at 4X. **B.** MTT results showing IC50 values for both cell lines. **C.** Colony formation assay and quantification.

3.2.3. Cell cycle analysis

Since TMZ induces a cytostatic effect *in vitro*, cell cycle analysis was performed using Muse Cell Analyzer. After 72 hours of TMZ treatment, cells were fixed and stained with cell cycle kit. Results are shown in Figure 3.18 as up to 88 percent of parental cells were in G2/M phase upon TMZ treatment whereas no difference was observed in resistant cell line.

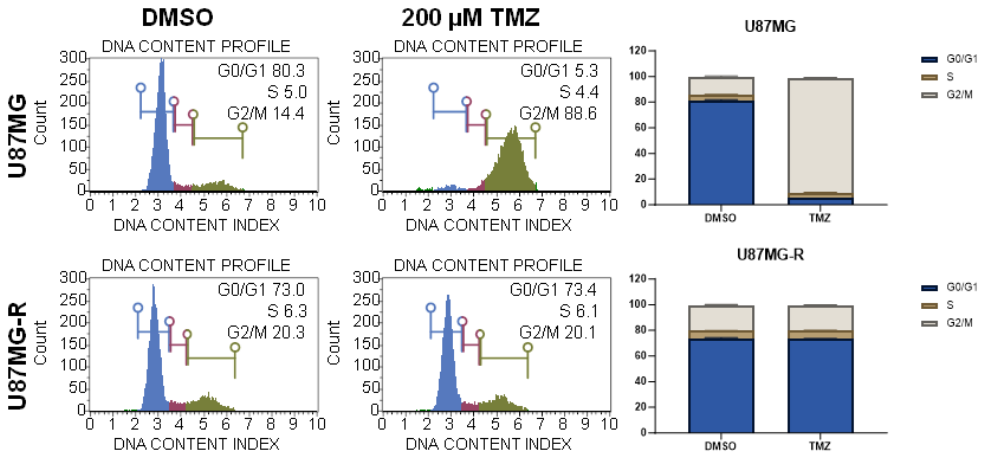

Figure 3.18: Cell cycle analysis of parental and resistant cell lines at 72 hours after TMZ treatment. Shift at G2/M phase was observed in naïve cell line U87MG while no change was present in resistant cell line U87MG-R following 72-hour TMZ treatment.

3.2.4. *In vivo* characterization of U87MG-R

To test the resistance phenotype *in vivo*, implantation of tumor cells was performed by Dr. Ahmet Cingöz as explained in **Figure 3.19.A**. Fluc-mCherry labelled U87MG cells were implanted to NOD-SCID mice intracranially, and luciferin measurements were taken at different time points. From Day8 to Day12, TMZ (2 mg/kg) was administered to the animals for 5 consecutive days. Representative images of animals at Day0 and Day24 from each group was shown after luciferin injection (**Figure 3.19.B**). Analysis of each measurement was demonstrated in **Figure 3.19.C**. These results indicate that both U87MG and U87MG-R cells could form tumors, and TMZ administration diminishes the tumor formed by U87MG cell line. However, TMZ does not affect tumor formed by U87MG-R cell line, proving the resistant capability of the generated model.

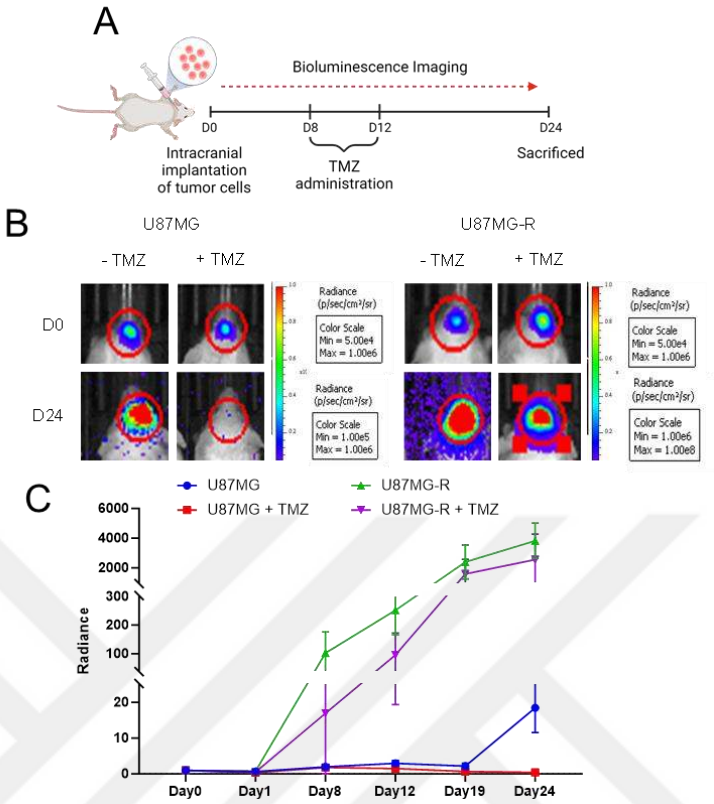

Figure 3.19: ***In vivo* characterization of resistant cells. A.** Schematic explanation of *in vivo* experimental setup. **B.** Representative images of tumors at initial and final time points. **C.** Radiance graph of tumors at each time point. (n=5 for each group)

On Day24, animals were sacrificed, and the brains of each animal were collected in formalin. Cross sections of the brains were performed by Koç University Hospital Pathology Department, by Dr. İbrahim Kulaç and Ayşe Hümeyra Dur Karasayar. Cross sections indicate that the tumor formed using U87MG cell line was completely gone after TMZ treatment, leaving some apoptotic cells. Whereas in tumors formed by resistant cells, it is observed that a highly invasive and aggressive tumor was formed which spread outside of injected area. The tumor size was not reduced following TMZ treatment. To see the proliferating cells in the tumor area, Ki-67 staining was performed as well. 5 areas within the section were used to calculate the number of Ki-67 positive cells, except for U87MG + TMZ samples, only one small part was stained. Quantification shows that over 70% Ki-67 positive cells were present in -/+ TMZ U87MG-R samples whereas only 40%

of cells were positive in U87MG -TMZ group. Less than 20% of cells were Ki-67 positive in U87MG +TMZ group **(Figure 3.20).**

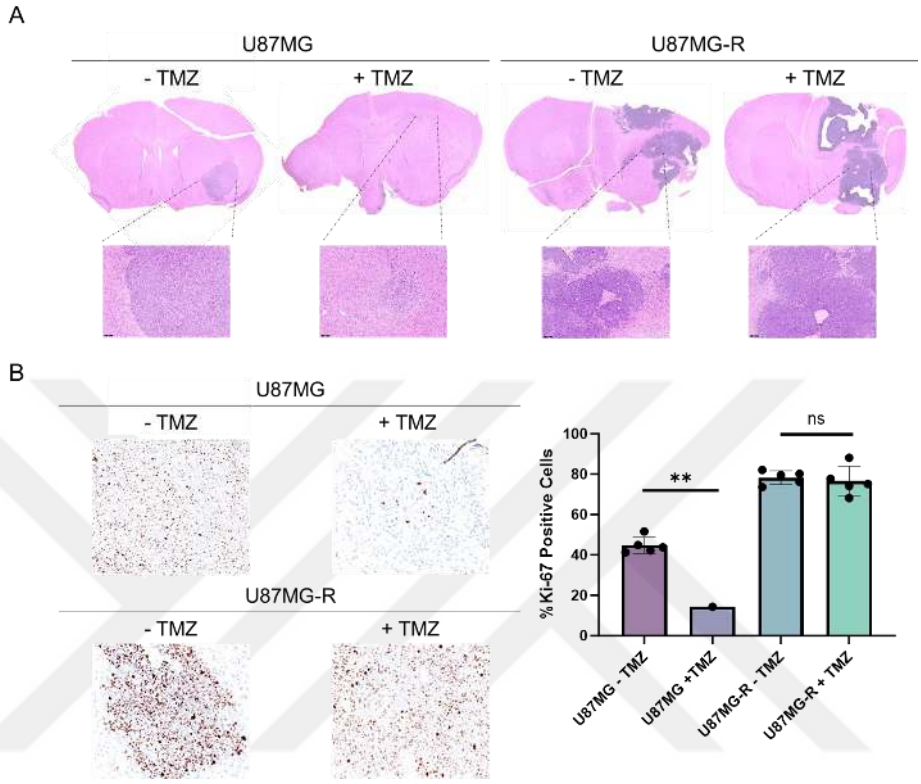

Figure 3.20: H&E and Ki-67 staining of cross sections for tumors. A. Cross section and closeup images of H&E-stained brain sections. Scale bar 100 µm. **B.** Ki-67 staining showing the proliferative cells in tumor sections (20X) and quantification of staining. Student's t-test, ** $p<0.01$.

3.2.5. U373-derived TMZ resistant cell line characteristics

Another TMZ resistant GBM cell line was established in the laboratory by a former PhD student Dr. Filiz Senbabaoglu. This model was generated by high dose selection method, explained in **Figure 3.21.A**. U373 cell line was treated with 250 µM of TMZ for 15 consecutive days followed by recovery. Later, the cell line was treated again with the same TMZ dosages for 2 months and the generated cell line was named TMZRT. Resistant phenotype was observed with both colony formation assay and MTT assays (**Figure 3.21.B** and **Figure 3.21.C**). Increased G2/M phase accumulation was also

observed in parental cells after 72h of TMZ treatment with no change in resistant cell (**Figure 3.21.D**). This cell line was also used in the following experiments.

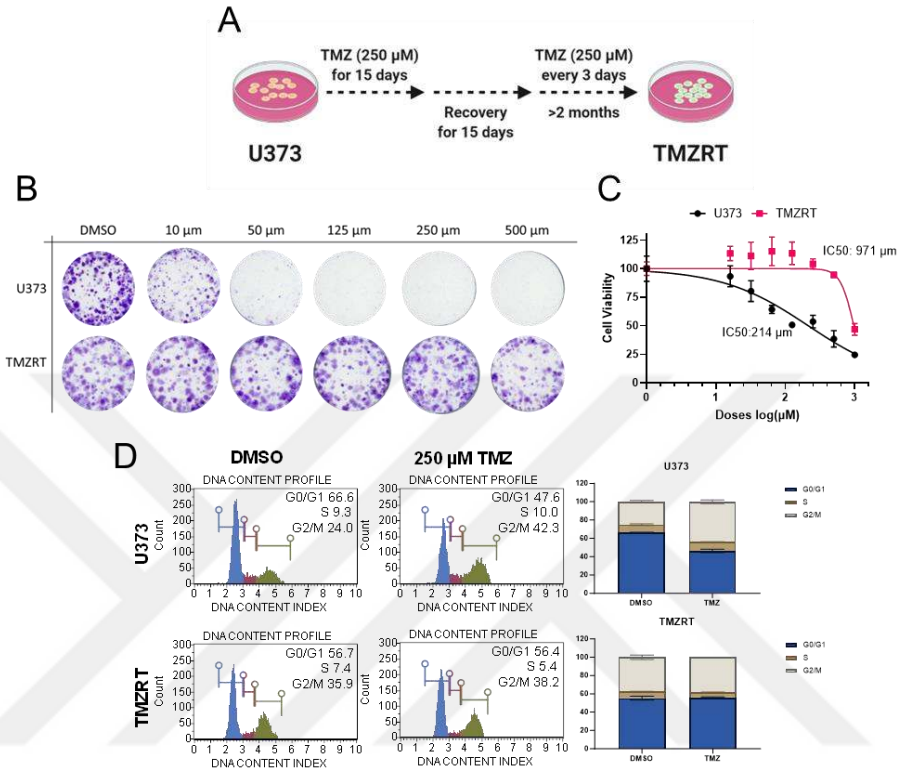

Figure 3.21: Generation and characterization of TMZRT cell line. A. High dose selection method for resistant cell line generation. **B.** Colony formation assay with different dosages of TMZ. **C.** MTT assay demonstrating increased IC50. **D.** Cell cycle analysis of resistant and parental cell lines after 72h of TMZ treatment.

3.2.6. Transcriptome analysis of resistant and parental cell pairs

Transcriptome analysis of U87MG-R cells compared to U87MG was conducted to understand the difference in gene expression patterns during resistance. For this purpose, cells were passaged without TMZ or DMSO for 3-4 days then collected as pellets. High quality RNA was isolated. Samples were sent for analysis as triplicates. PCA plots show that U87MG samples were clustered together, U87MG-R cells have low variance even though they do not cluster together (**Figure 3.22.A**). Volcano plot shows the significantly upregulated and downregulated genes based on their LFC values (**Figure**

3.22.B). There are over 1100 upregulated and around 1000 downregulated differentially expressed genes.

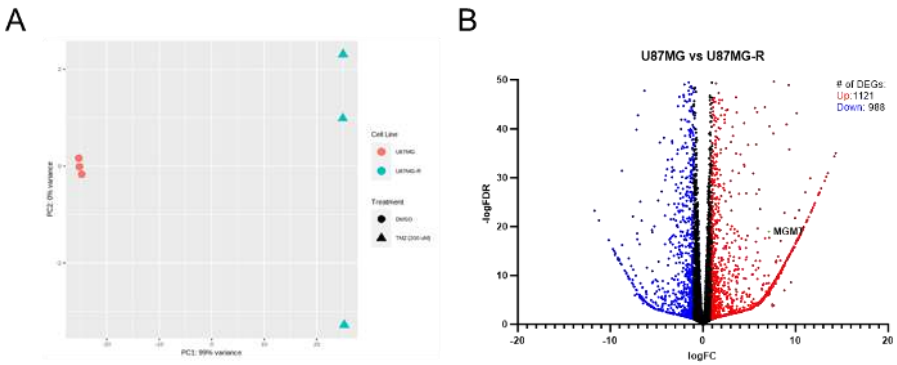

Figure 3.22: Transcriptome analysis of U87MG-R. A. Principal component analysis (PCA) plots for resistant and parental cell lines. **B.** Volcano plot with LFC<-1, LFC>1 cutoffs. MGMT was highlighted as an upregulated gene.

Gene set enrichment analysis was performed with the whole transcriptome. GSEA plot was shown in **Figure 3.23.A** with one upregulated and one downregulated pathway highlighted. Enrichment plots for EMT and Hypoxia pathways were listed in **Figure 3.23.B** with Negative Enrichment Scores (NES), NOM p values and FDR q values. The top 10 upregulated and downregulated Hallmark pathways according to GSEA have been shown in **Figure 3.23.C.** Besides EMT, several other pathways involved in cell polarity, cell-to-cell interaction and signaling pathways were upregulated.

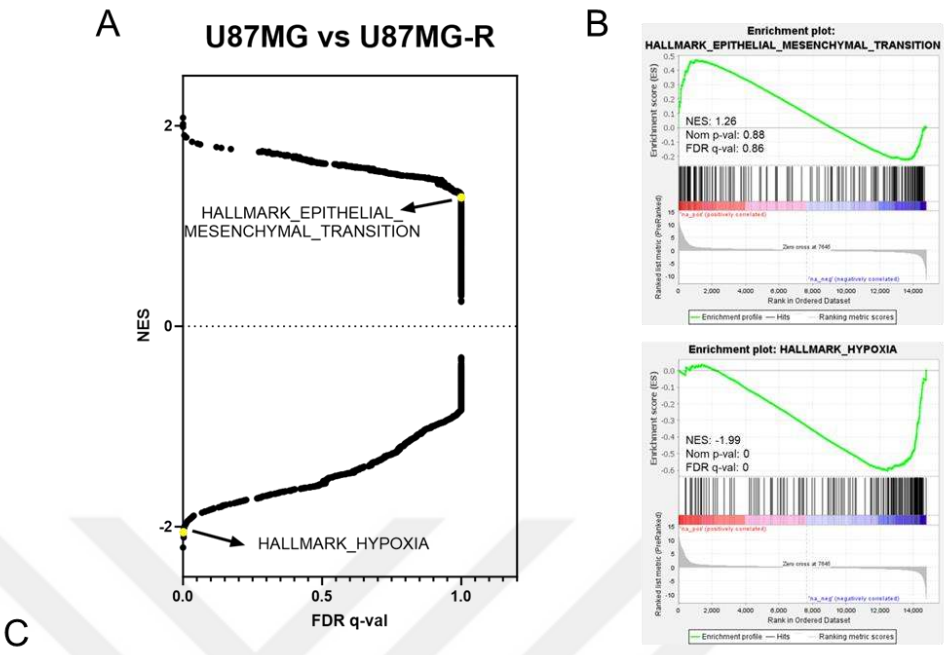

U87MG Vs U87MG-R	GeneSet	Negative Enrichment Score (NES)	Nominal p-value	FDR q-value
Upregulated	HALLMARK_APICAL_SURFACE	1.754569	0	0.003930843
	HALLMARK_APICAL_JUNCTION	1.422065	0.01599016	0.54139274
	HALLMARK_ESTROGEN_RESPONSE_EARLY	1.3110131	0.050887574	0.9918494
	HALLMARK_KRAS_SIGNALING_DN	1.2790737	0.114775725	0.9601756
	HALLMARK_EPITHELIAL_MESENCHYMAL_TRANSITION	1.2612833	0.08809524	0.86911035
	HALLMARK_KRAS_SIGNALING_UP	1.2477622	0.10552147	0.7988231
	HALLMARK_ANDROGEN_RESPONSE	1.245128	0.13189772	0.6996293
	HALLMARK_IL6_JAK_STAT3_SIGNALING	1.2065084	0.1966759	0.79255825
	HALLMARK_ESTROGEN_RESPONSE_LATE	1.1903917	0.17344497	0.7820309
	HALLMARK_TNFA_SIGNALING_VIA_NFKB	1.1847813	0.16923077	0.72546005
Downregulated	HALLMARK_HYPOXIA	-1.9928442	0	0
	HALLMARK_GLYCOLYSIS	-1.7631978	0	0.005417346
	HALLMARK_MTORC1_SIGNALING	-1.4671098	0	0.10857896
	HALLMARK_REACTIVE_OXYGEN_SPECIES_PATHWAY	-1.260385	0.1331058	0.33382306
	HALLMARK_UNFOLDED_PROTEIN_RESPONSE	-1.243408	0.116935484	0.2971536
	HALLMARK_ALLOGRAFT_REJECTION	-1.1650627	0.1273585	0.39454785
	HALLMARK_MYOGENESIS	-1.1049607	0.22777778	0.4758786
	HALLMARK_DNA_REPAIR	-0.97877085	0.50537634	0.8150475
	HALLMARK_ADIPOGENESIS	-0.86621326	0.83125	1
	HALLMARK_PEROXISOME	-0.7869004	0.90612245	1

Figure 3.23: GSEA plots for U87MGvsU87MG-R RNAseq. A. GSEA plot with highlighted pathways. **B.** Enrichment plots for EMT and Hypoxia Hallmark pathways. **C.** List of top 10 upregulated and downregulated Hallmark pathways including NES, nominal p-value and FDR q-values.

Transcriptome analysis for U373vsTMZRT was also performed previously. Volcano plot with LCF<-1, >1 cutoffs and number of DEGs were shown in Figure **3.24.A**. GSEA plot with the same pathways identified in U87MGvsU87MG-R were highlighted

in **Figure 3.24.B**. The top 10 upregulated and top 8 downregulated hallmark pathways were listed in **Figure 3.34.C**. although there are several common differentially regulated pathways in both cell lines, there are also many different pathways as well. EMT was not one of the top 10 upregulated pathways for U373vsTMZRT RNA sequencing. There were only 8 downregulated hallmark pathways identified by GSEA.

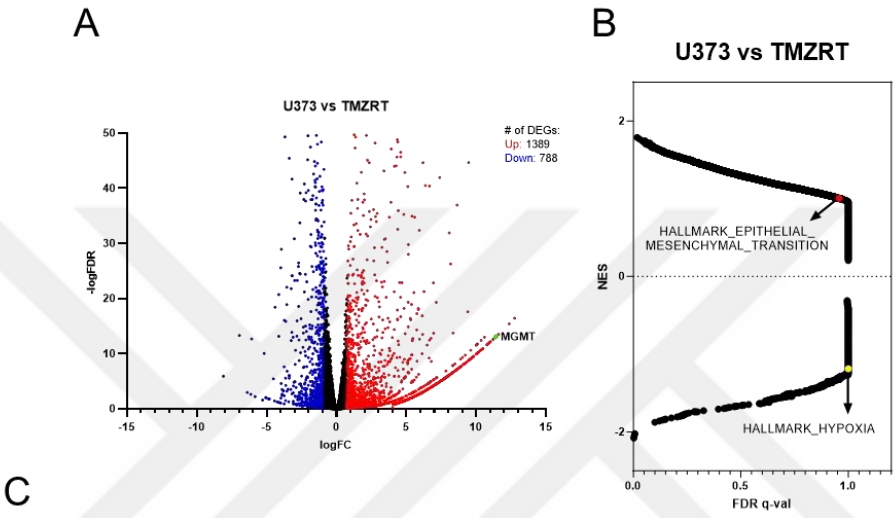

C

U373 vs TMZRT	GeneSet	Negative Enrichment Score (NES)	Nominal p-value	FDR q-value
Upregulated	HALLMARK_KRAS_SIGNALING_UP	1.5701233	0	0.03652633
	HALLMARK_INFLAMMATORY_RESPONSE	1.4604363	0.003089598	0.13815263
	HALLMARK_UV_RESPONSE_DN	1.3961135	0.01525941	0.2477734
	HALLMARK_ANGIOGENESIS	1.3372171	0.100367196	0.40040463
	HALLMARK_SPERMATOGENESIS	1.3318819	0.051391862	0.3389929
	HALLMARK_WNT_BETA_CATENIN_SIGNALING	1.3037916	0.119277105	0.39550945
	HALLMARK_ALLOGRAFT_REJECTION	1.2993993	0.06638567	0.35523543
	HALLMARK_IL2_STAT5_SIGNALING	1.2901994	0.039473683	0.3438162
	HALLMARK_APICAL_JUNCTION	1.2722781	0.041624367	0.36847618
	HALLMARK_MYC_TARGETS_V2	1.2504371	0.14915255	0.41182256
Downregulated	HALLMARK_HYPOXIA	-1.1935587	0	1
	HALLMARK_PEROXISOME	-1.0157627	0.35	1
	HALLMARK_FATTY_ACID_METABOLISM	-0.995353	0.36	1
	HALLMARK_UV_RESPONSE_UP	-0.96415263	0.56666666	1
	HALLMARK_MTORC1_SIGNALING	-0.9432109	0.61538464	0.94843465
	HALLMARK_REACTIVE_OXYGEN_SPECIES_PATHWAY	-0.7084898	0.95555556	1
	HALLMARK_MITOTIC_SPINDLE	-0.6007772	1	1
	HALLMARK_OXIDATIVE_PHOSPHORYLATION	-0.5068188	1	0.9965761

Figure 3.24: RNAseq of U373vsTMZRT. A. Volcano plot for DEGs. **B.** GSEA plot with highlighted pathways. **C.** The top 10 upregulated and and top 8 downregulated hallmark pathways with NES, nominal p-value and FDR q-values.

To understand the resistance mechanism, commonly upregulated genes were investigated among the cell lines. MGMT was one of the drivers for TMZ resistance and was among the upregulated gene sets in both cell lines. Among the upregulated DEGs, 182 were common in both cell lines. The top 15 genes were identified and listed in **Figure 3.25.A**. These genes were *TUBA3C, ROBO2, RNF43, MTUS1, COLEC10, SEMA6D, MGMT, PASD1, CES1, CSMD1, TMEM132D, CELF2, SLC14A1, KLHL4* and *ESM1*. These genes were named as signature resistance genes. Next, qPCR was used to validate these genes. qPCR results in Figure **3.25.B** shows that all 15 genes were indeed upregulated in U87MG-R cell line compared to U87MG. qPCR experiment was also performed with U373 and TMZRT with most of the genes and again, the results were validated showing the upregulation of these genes in resistant cell line (**Figure 3.25.C**).

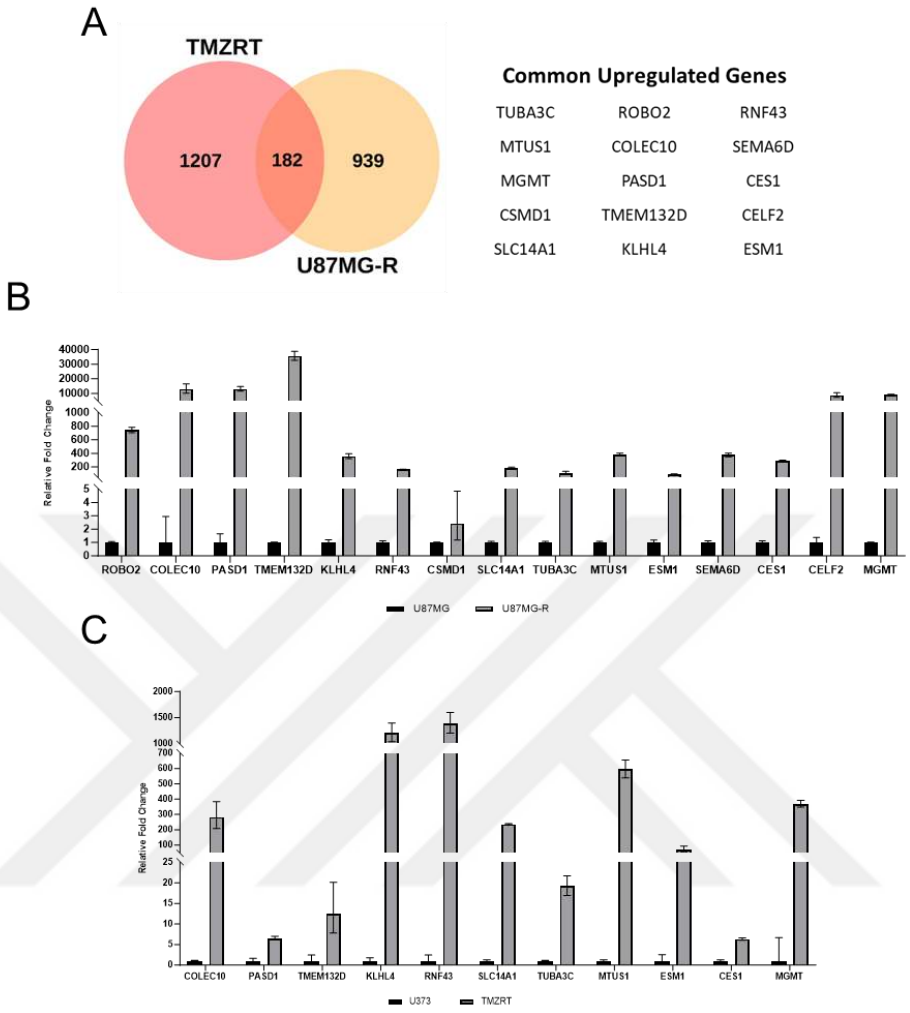

Figure 3.25: Identification of signature resistance genes. A. Venn diagram showing the common upregulated genes and names of top 15 genes. **B-C.** qPCR results for signature genes.

3.2.7. TCGA Analysis for Signature Genes

To investigate the expression profiles and effect of these genes on survival, TCGA (the cancer genome atlas) analysis was formed with Low Grade Glioma (LGGs) and Glioblastoma (GBM) datasets by Prof. Mehmet Gönen. **Figure 3.26** focused on subtype analysis of signature genes in LGG and GBM patients. Significant differences in expression of genes between LGG and GBM samples were observed in all genes except *PASD1. CELF2, CSMD1, SLCA14A, MTUS1, TMEM132D* and *RNF43* genes were

expressed less in GBM patients than LGG patients, whereas *CES1, ESM1, KLHL4, MGMT, ROBO2, SEMA6D* and *TUBA3C genes* were expressed more.

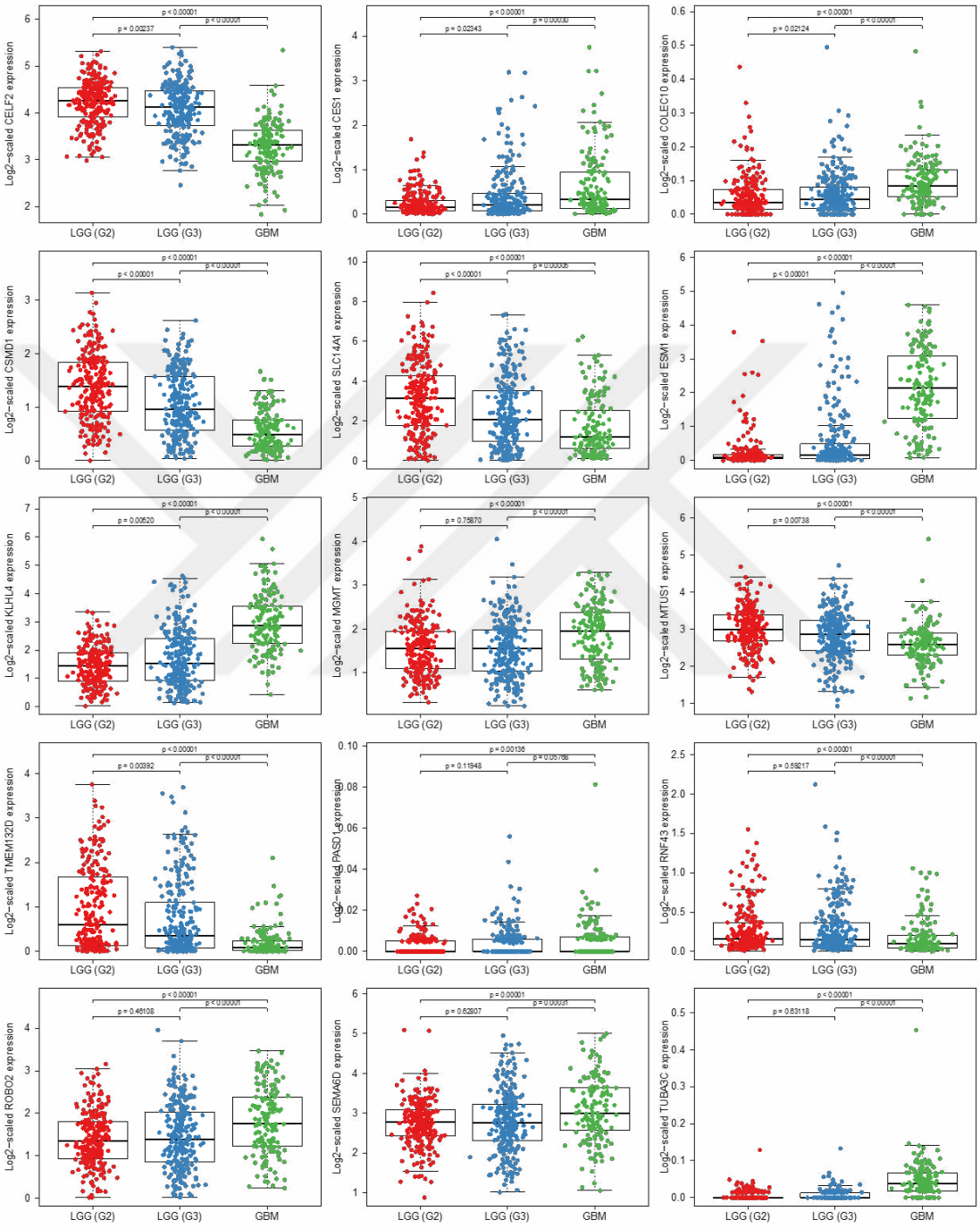

Figure 3.26: Subtype analysis of signature genes with LGG and GBM datasets.

Survival analysis gives information of how the expression of a certain gene affects the lifespan of the patient. **Figure 3.27** shows the survival plots for signature genes with respect to all LGG and GBM patients in the datasets. Only GBM dataset analysis does not provide much significant results due to the limited number of patients and low survival rates. Therefore, exploring survival data with LGG datasets provides better results. These results demonstrate that only 4 of the signature genes are significantly affecting the survival of patients based on p-values. High expression of CELF2 and TMEM132D was associated with prolonged survival whereas high expression of ESM1 and KLHL4 decreases the life expectancy.

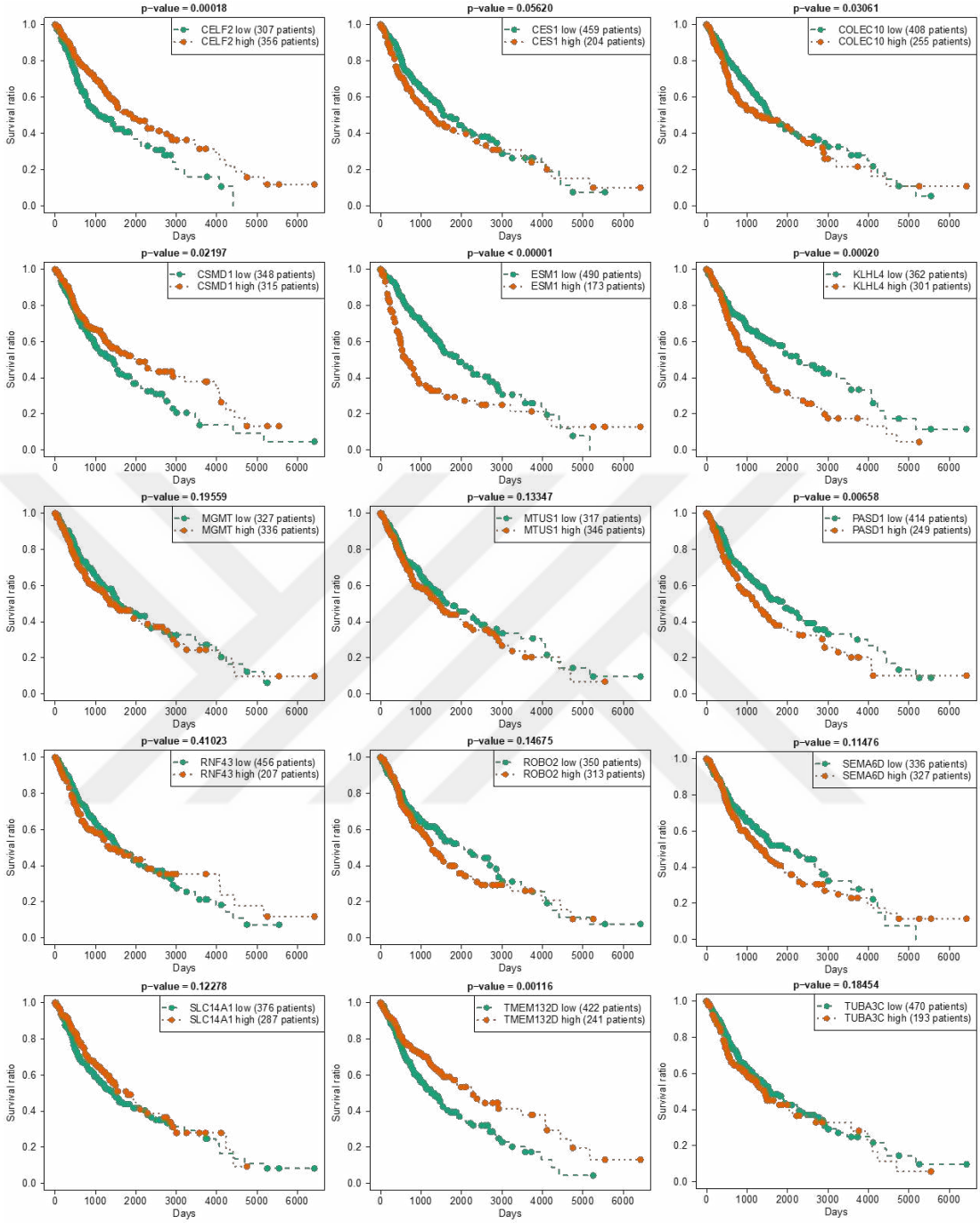

Figure 3.27: Survival analysis of signature genes with LGG and GBM datasets.

3.2.8. MGMT Knock-Out in U87MG-R and TMZRT

Since MGMT was highly upregulated in both resistance models, the effect of knock-out of MGMT was investigated using CRISPR/Cas9. For this purpose, two gRNAs

and NT1 were used to transduce U87MG-R and TMZRT cell lines. First, KO was validated using western blot in **Figure 3.28. A**. In both cell lines, complete KO was observed. Alpha-tubulin was used as a housekeeping control. Next, colony formation assay was conducted with or without TMZ administration. 200 µM of TMZ and 250 µM of TMZ were used for U87MG-R and TMZRT, respectively. Results in **Figure 3.28.B** indicate that cells were sensitized to TMZ upon MGMT knock-out significantly.

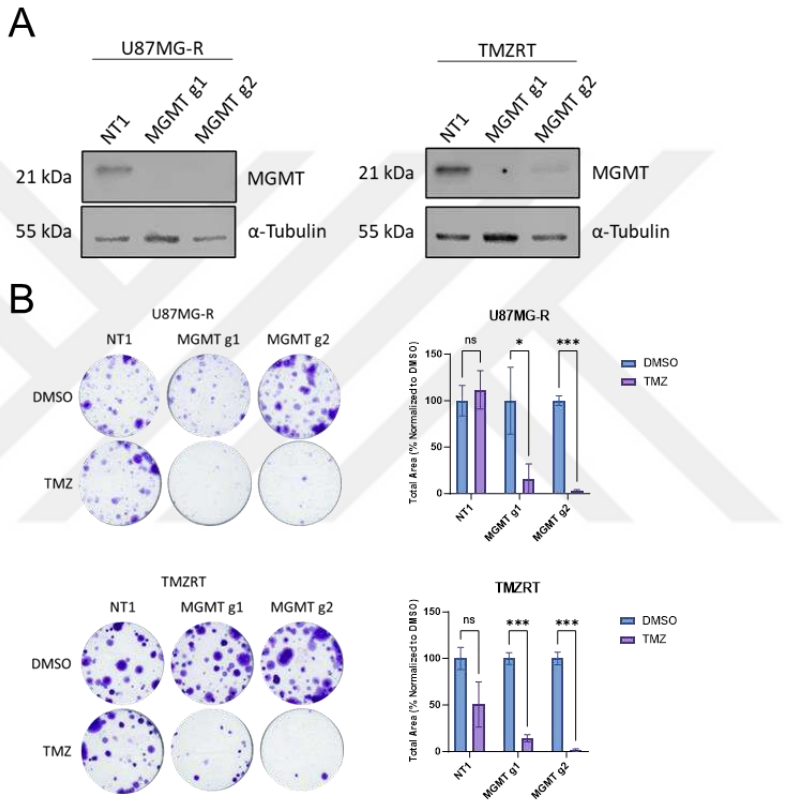

Figure 3.28: MGMT knock-out. A. Western blot images for the knock-out phenotype. **B.** Colony formation assay and quantification of MGMT KO. Student's t-test, * $p<0.05$, *** $p<0.001$.

3.2.9. MGMT Methylation Status and Genomic Amplification Determination

Since methylation status of MGMT is important for GBM, the methylation status of the resistant models was investigated. For this reason, bisulfite conversion followed by

methylation specific nested PCR was performed. In this experiment, naïve 293T cells and innately TMZ resistant T98G cells were used as negative and positive control, respectively. The assay was run on 3% agarose gel. Results in **Figure 3.29** indicate that while U87MG cells do not have unmethylated MGMT, U87MG-R cells have both methylated and unmethylated MGMT. U373 cells have slight unmethylated MGMT which was amplified much further in TMZRT cell line.

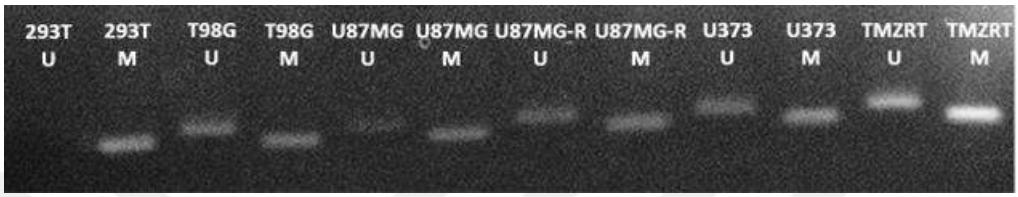

Figure 3.29: Methylated/Unmethylated MGMT assay. U indicates Unmethylated MGMT, M indicates Methylated MGMT**.**

To determine whether there is any change in gene copy number of MGMT in naïve and resistant cell line, genomic amplification qPCR was performed. Induced pluripotent stem cell genomic DNA was used as control. 2 primers, shown in red box, were designed to span both exon 2 and intron boundaries as depicted in **Figure 3.30**. This qPCR was performed using gDNA of iPSC, U87MG and U87MG-R cell lines. Results show that no marked change was observed in resistant cell line compared to naïve cell line.

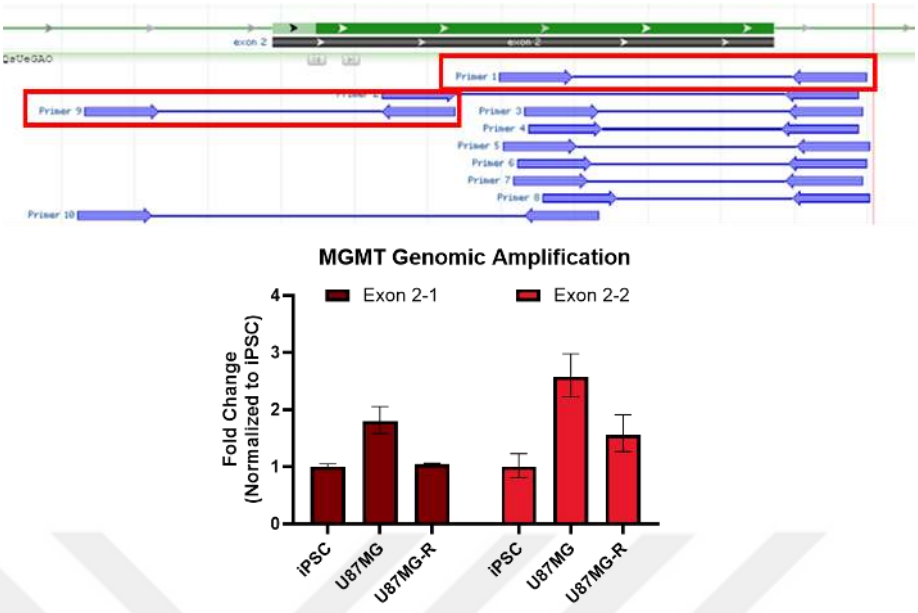

Figure 3.30: MGMT genomic amplification. Selected primers for exon-intron junctions were shown in the upper panel. qPCR results for MGMT genomic amplification, using iPSC as control, were seen in the graph.

3.3 EPIKOL screens with Resistant Cell lines

3.2.1. Screen results and quality check

Understanding mechanisms that can overcome therapy resistance was the main goal. For this purpose, EPIKOL screens using resistant cell lines were conducted as explained in **Figure 3.31**. EPIKOL screens were performed as 1000X and in triplicates. Following infection and puro selection, cells were passaged until Cas9 activity was completed (15-18days). Later, cells were divided into TMZ and DMSO groups. 250 µM of TMZ was given for TMZRT and 200 µM TMZ was given for U87MGR. Groups were passaged until they reached 14 doublings. Genomic DNA was isolated and library preparation was performed via Nested PCR, as previously described.

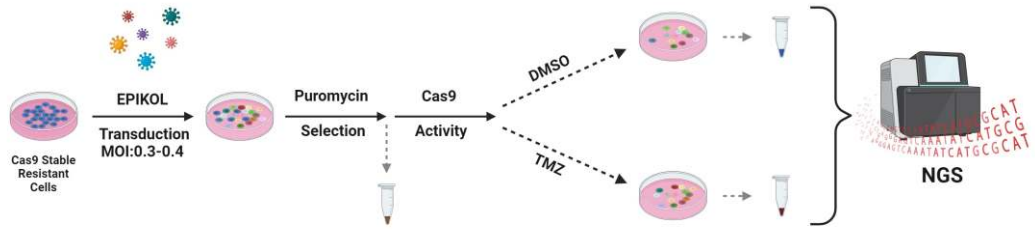

Figure 3.31: Schematics for resistance screens. Cas9 stable resistant cells were infected with EPIKOL viruses with low MOI and subjected to puromycin selection. Following Cas9 activity, cells were separated into two groups as TMZ or DMSO. Maintenance dose of TMZ/DMSO was used. Screens continued until cells reach 14-16 doublings.

Following screens, quality control assays were conducted. PCA plot shows the clustering of AP (after puro), D (DMSO) and T (TMZ) groups (**Figure 3.32**). Each replicate for TMZ group for U87MG-R cell line was separated from each other, whereas DMSO and after puro replicates were clustered together. For TMZRT cell line 2 out of 3 replicates showed low variance but one replicate from after puro and TMZ group was separated from the rest of the replicates.

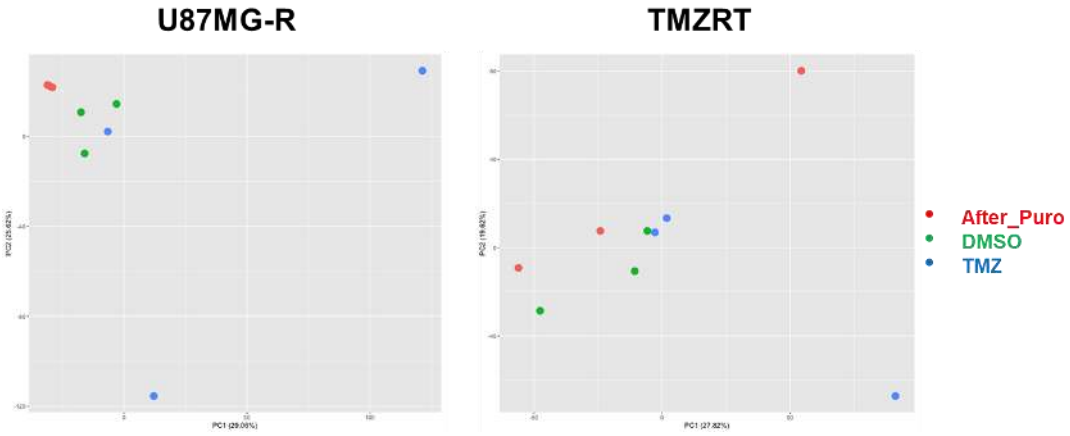

Figure 3.32: PCA plots for resistance screens. Red for after-puro samples, yellow for DMSO samples and blue for TMZ samples.

The next quality check for the screen was to plot the gRNA count distribution graphs. gRNA counts were read per million normalized per group and log2 converted.

Graphs on **Figure 3.33** show the gRNAs distributions of each replicate of DMSO or TMZ with respect to after puro for U87MG-R cell line. Non-targeting gRNAs should be on the diagonal axis as they were expected not to be depleted and essential genes should be below the diagonal axis. For U87MG-R DMSO groups, most essential genes were found to be depleted in all three replicates and most non-targeting gRNAs were in the center of the plots. However, for TMZ comparison, non-targeting gRNAs were distributed along the graph rather than accumulating on the diagonal axis. Essential genes were below the diagonal, as expected.

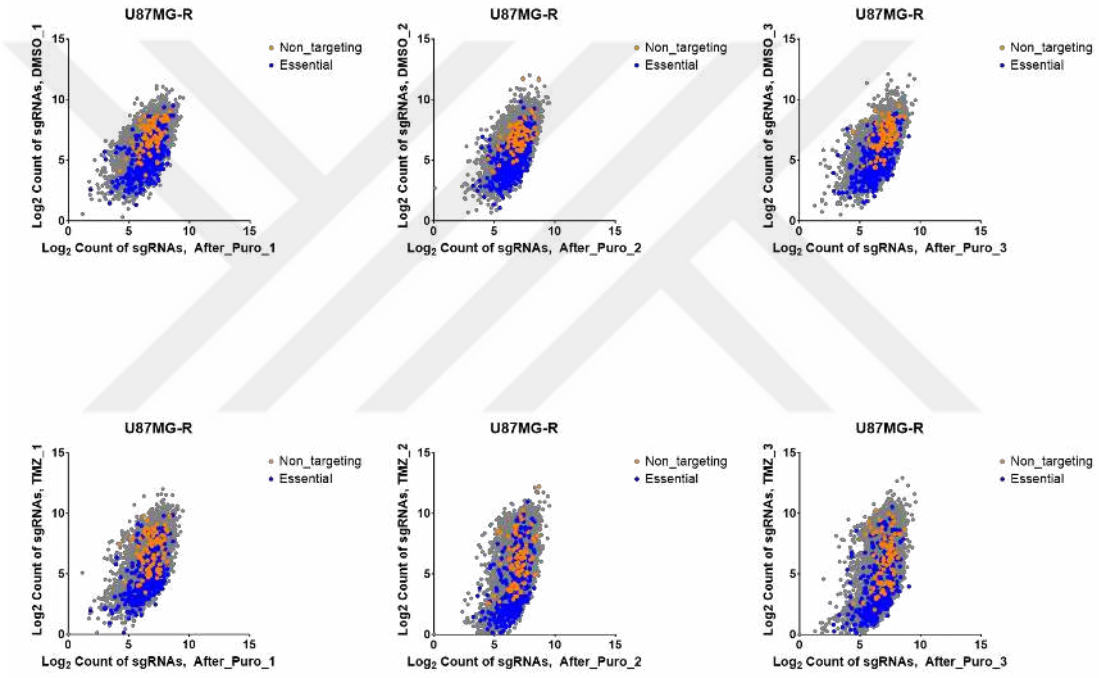

Figure 3.33: gRNA count distribution graphs of U87MG-R cell line for both DMSO-After puro and TMZ-After puro comparisons. Blue dots represent essential gRNAs and orange dots represent non-targeting gRNAs.

Count distribution graphs for TMZRT cell line were generated as explained. For both DMSO and TMZ comparisons, non-targeting gRNAs were on the diagonal axis and essential genes were below the axis, showing good distribution in **Figure 3.34**.

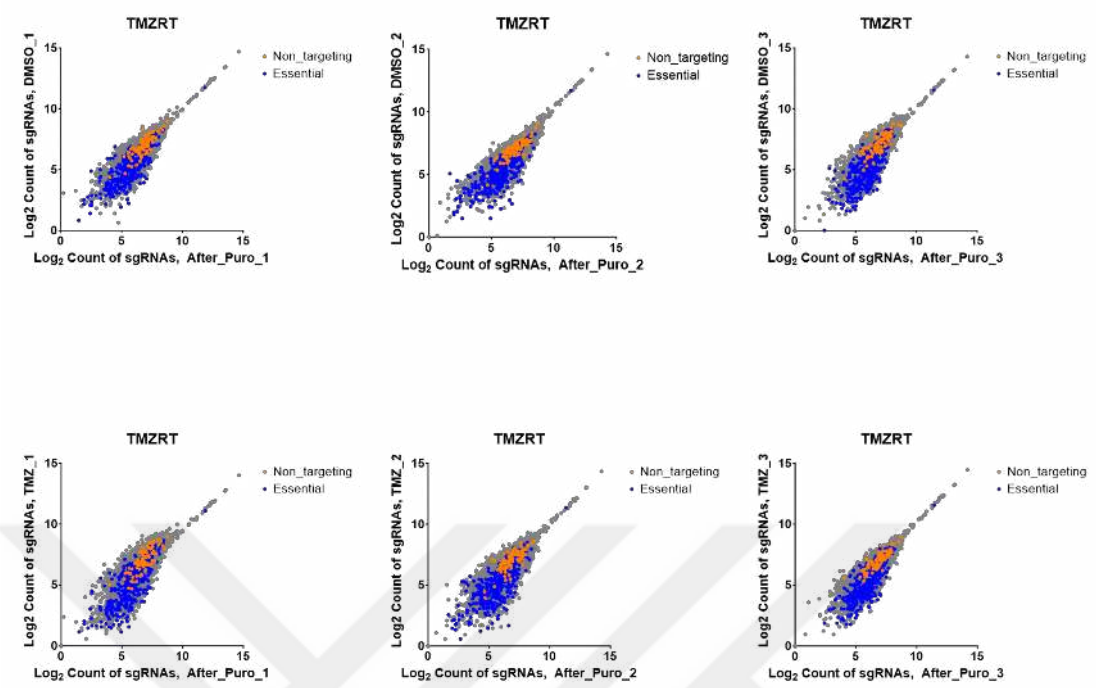

Figure 3.34: gRNA count distribution graphs of TMZRT cell line for both DMSO-After puro and TMZ-After puro comparisons. Blue dots represent essential gRNAs and orange dots represent non-targeting gRNAs.

3.2.2. TMZvsDMSO comparisons

To identify genes related with TMZ resistance, endpoint comparisons were taken into consideration. DMSOvsTMZ groups were analyzed for each cell line and potential sensitizers were identified. These genes were labelled on Log2FoldChange-log10pvalue graphs shown in **Figure 3.35**. LFC <-1 and p-value<0.05 cutoffs were used for the selections followed by literature reviews.

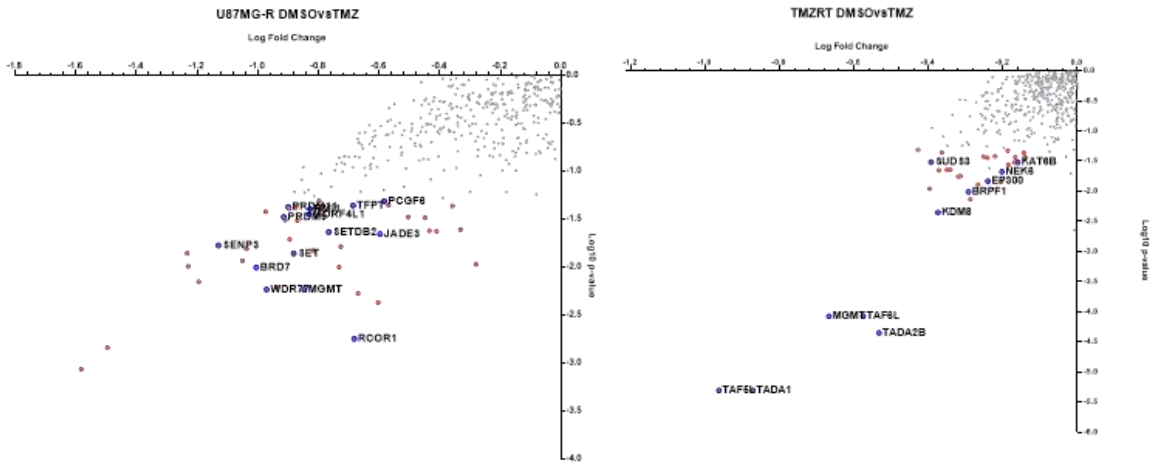

Figure 3.35: LFC graphs for both cell lines demonstrating potential TMZ sensitizer genes. Red and blue dots represent the significantly depleted genes based on LFC and p-value. Selected genes were indicated in blue.

To validate the result of the resistance screens in two different TMZ resistant cell lines, gRNAs of the genes listed in Figure 3.34 were individually cloned. Cloning of the gRNAs were checked via sequencing before producing lentiviruses along with ribosomal control RPL9. For the validation, cells were seeded to 24 well plates and transduced with lentiviruses. First, hits from each cell line were tested with that cell line using colony formation assay with TMZ or DMSO. The assay ended when colonies were formed or after 14 days. The results of TMZRT colony formation assays and quantification for U87MG-R cell line were shown in **Figure 3.36**. Quantification was done by normalizing each gRNA with its DMSO control. No significant TMZ sensitizer was identified. Some gRNAs, such as those targeting RMI1 or WDR77, completely killed the cells.

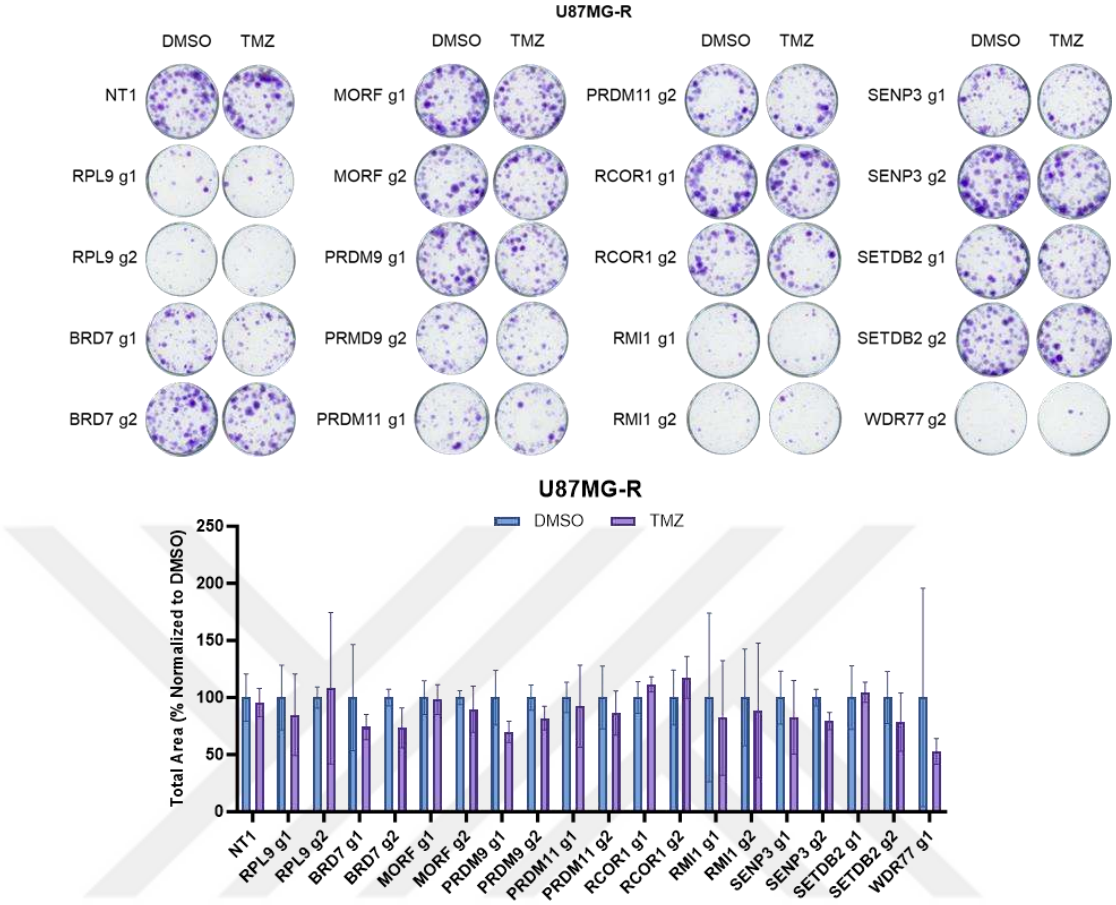

Figure 3.36: Validation of U87MG-R hits with colony formation assay. Colonies with DMSO or TMZ were shown in upper panel. Quantification of the assay was performed with ImageJ and % total area normalized to DMSO was shown in the graph.

TMZRT hits were validated via colony formation assay, shown in **Figure 3.37**. Same with the U87MG-R cell line, some gRNAs killed the cells even in the presence of DMSO. No potential sensitizers were identified in this group either.

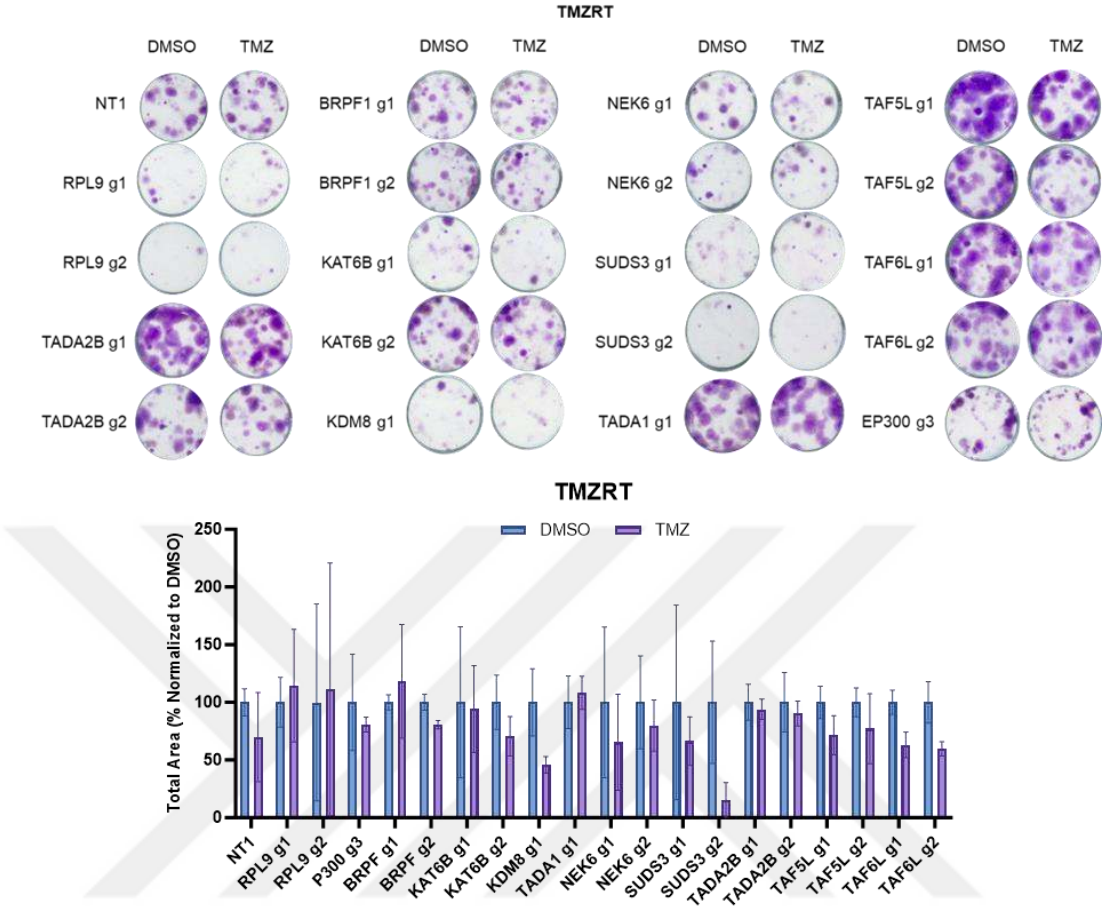

Figure 3.37: Validation of TMZRT hits with colony formation assay. Colonies with DMSO or TMZ were shown in upper panel. Quantification of the assay was performed with ImageJ and % total area normalized to DMSO was shown in the graph.

Next, common genes in two cell lines with endpoint comparisons were studied. Only 4 genes were common in both cell lines as SET, PCGF6, APEX1 and MGMT (**Figure 3.38**).

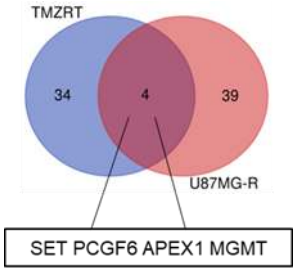

Figure 3.38: Venn diagram for common genes from TMZRT and U87MG-R screens. Number of common genes in DMSOvsTMZ comparison for both cell lines are shown. Names of the 4 common genes are listed.

The result of MGMT knock-out leading to TMZ sensitization was demonstrated in **Figure 3.28**. Out of three genes, SET and PCGF6 were tested for validation in both cell lines (**Figure 3.39**). None of the gRNAs significantly sensitized cells to TMZ in U87MG-R cell line. In TMZRT cell line, SET g1 was shown to significantly sensitize cells to TMZ but in this assay, NT1 also sensitizes cells to TMZ. Therefore, this experiment was not very successful. APEX1 will be studied as well, as future direction.

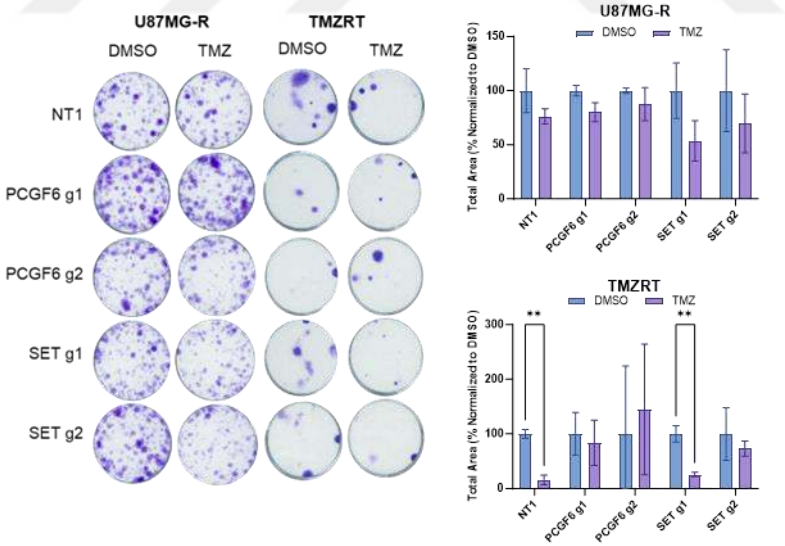

Figure 3.39: SET and PCGF6 validations in U87MG-R and TMZRT cell lines. Colony formation assay and its quantification was performed with SET and PCGF6. Student's t-test, ** $p<0.01$.

3.2.3. APvsDMSO comparisons

Since no potential TMZ sensitizers were identified based on endpoint comparisons, the next step was to study the vulnerability genes. For this purpose, DMSOvsAfter puro comparisons were used and essential genes along with hits from NHA screen was eliminated. Resulting 7 genes were listed in **Figure 3.40.A**. LFC graph in **Figure 3.40.B** shows the location of the selective vulnerability genes.

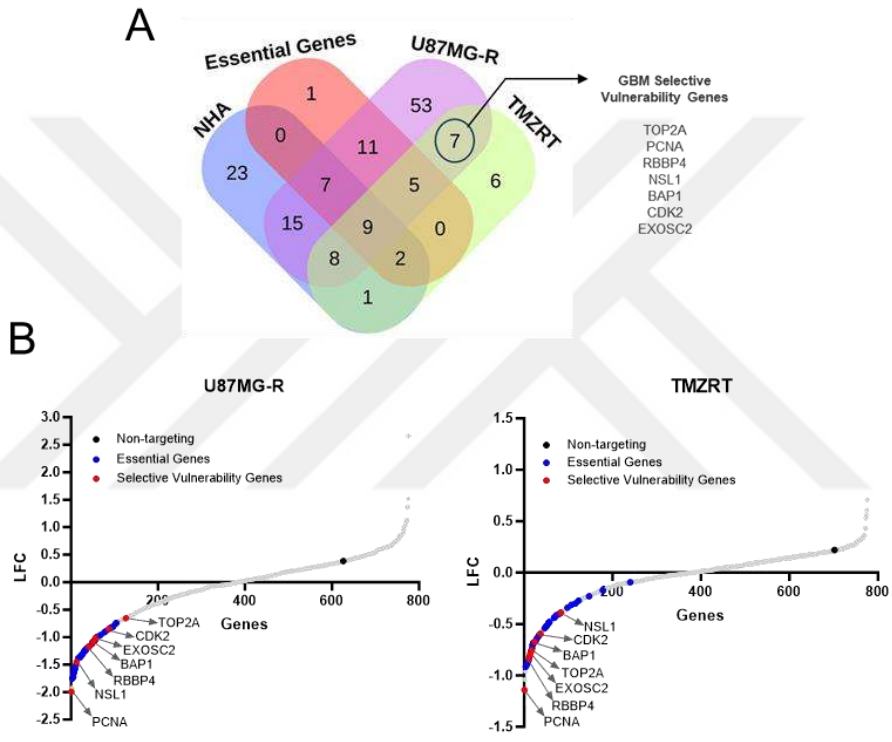

Figure 3.40: GBM selective vulnerability genes. A. Venn diagram with common genes listed. **B.** LFC plots for the selected genes.

For the validations, first the gRNAs that were not present in the laboratory were cloned to PLG vector. Following virus production, U87MG-R cell line was transduced with viruses. RPL9 and MGMT were included as controls in the experiment. Results are shown in **Figure 3.41**. RBBP4 and Cylin Dependent Kinase 2 (CDK2) were shown to be promising hits for selective vulnerability.

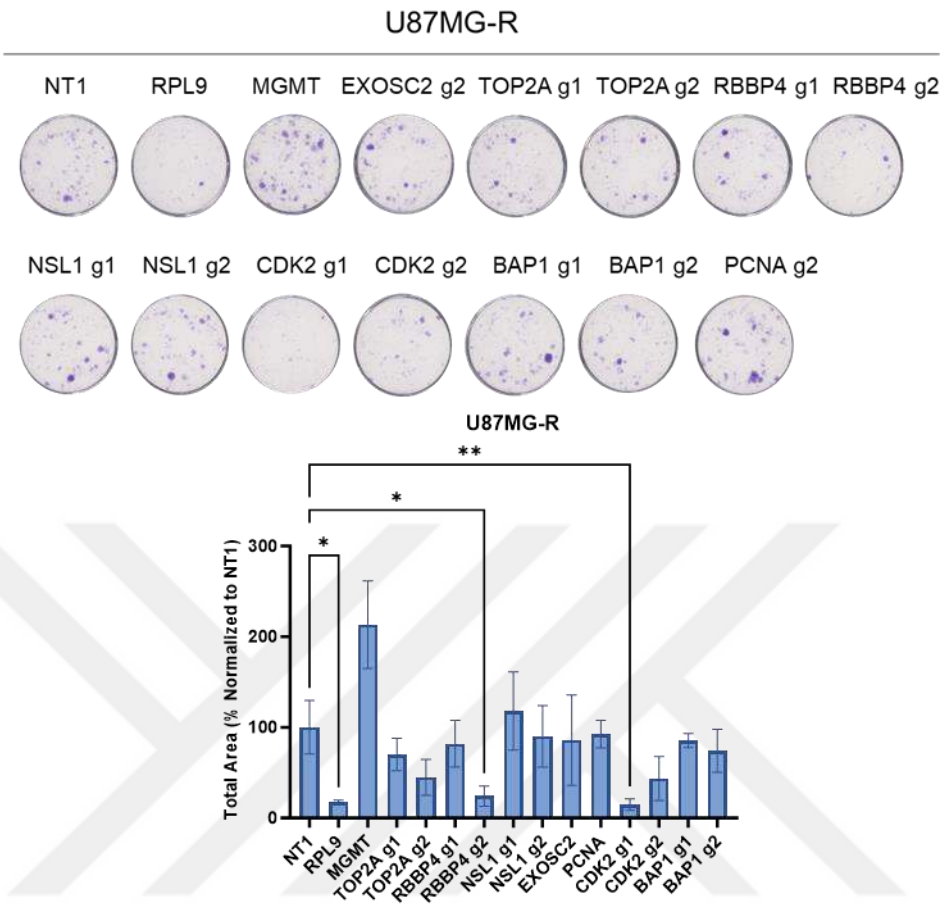

Figure 3.41: Validation of selective vulnerability genes. Colony formation assay with selected genes in U87MG-R cell line. MGMT and RPL9 were used as controls. Quantification was performed by ImageJ and shows that RBBP4 and CDK2 significantly decreased % total area compared to NT1. Ordinary One-Way Anova, * $p<0.05$, ** $p<0.01$.

3.2.4. Effect of RBBP4 Knock-Out on Cell Viability

For the next steps, RBBP4 was followed up as a potential hit. To further characterize its role in resistance models, KO was validated first with western blot from pellets collected at post transduction day9 (PT9). Complete KO was observed with both gRNAs in both cell lines (**Figure 3.42.A**). Next, the colony formation assay was performed again on PT9. Both gRNAs for RBBP4 showed significant reduction in colony formation in both cell lines (**Figure 3.42.B**). Growth curve analysis was done by MTT

assay at days 1, 3, 5, and 7. Results were normalized to day1. Significantly less cell growth was observed (**Figure 3.42.C**).

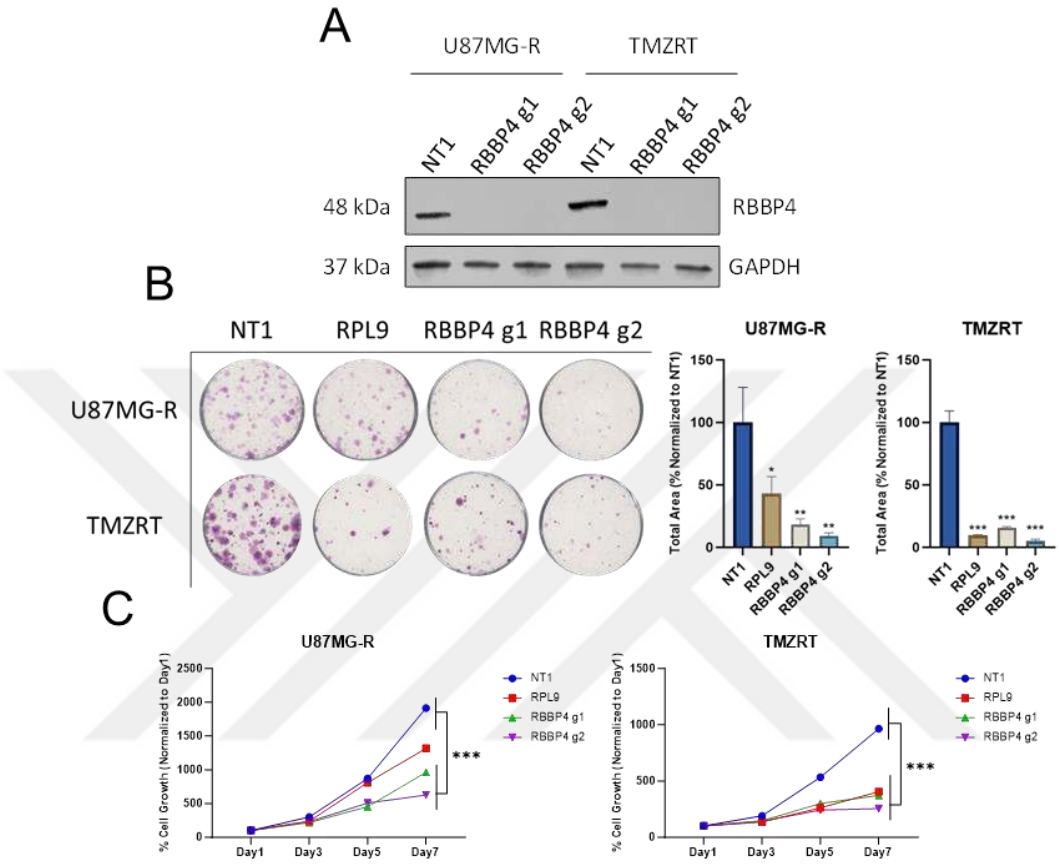

Figure 3.42: Effect of RBBP4 KO on cell growth. A. Western blot for validation of KO. **B.** Colony formation assay and quantification. Student's t-test, * p<0.05, ** p<0.01, *** p<0.001. **C.** Growth curve normalized to day1. Two-way Anova, * p<0.05, ** p<0.01, *** p<0.001.

3.2.5. Cell cycle and apoptosis analysis upon RBBP4 silencing

Since cell growth was slowed and decreased colony forming ability was observed upon KO, Annexin/Dead Cell assay was performed for examination of apoptosis. Cells were seeded on PT9 and collected for measurement at PT13. Results show that both early and late apoptosis was induced in KO cells compared to NT1 in both cell lines. Total

apoptosis was increased significantly (**Figure 3.43**). High apoptosis was also observed in RPL9 as expected since it is an essential gene.

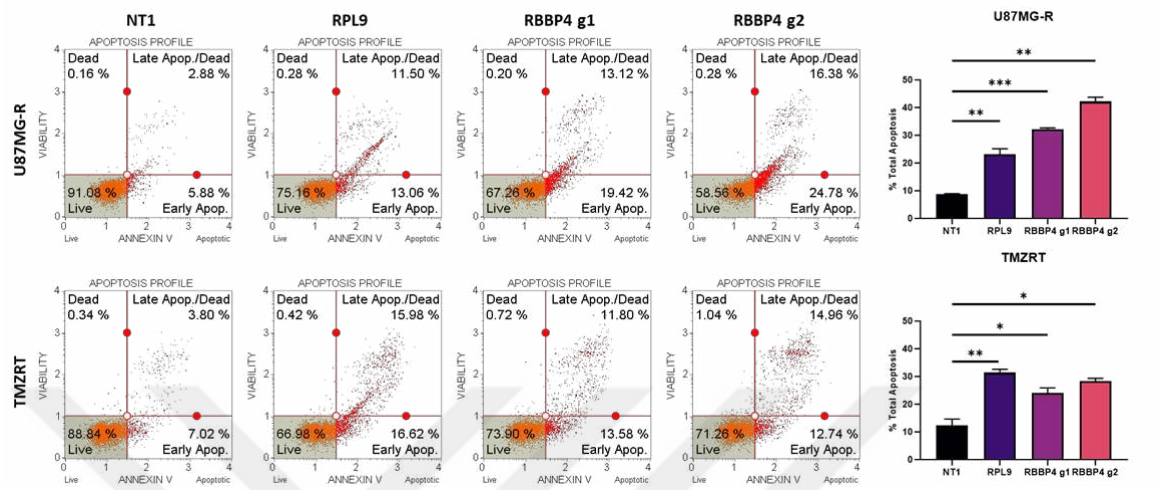

Figure 3.43: Annexin/Cell Death assay for KO cells. Apoptosis at day13 post transduction shows increased total apoptosis. Student's t-test, * $p<0.05$, ** $p<0.01$, *** $p<0.001$.

Cell cycle analysis was performed with the same setup as annexin assay (**Figure 3.44**). Cells were collected and fixed at PT13. With RBBP4 KO, cells were seen to accumulate at G2/M phase in both cell lines. Together with annexin assay results, it was observed that RBBP4 knock-out leads to G2/M arrest and induces apoptosis in U87MG-R and TMZRT cell line.

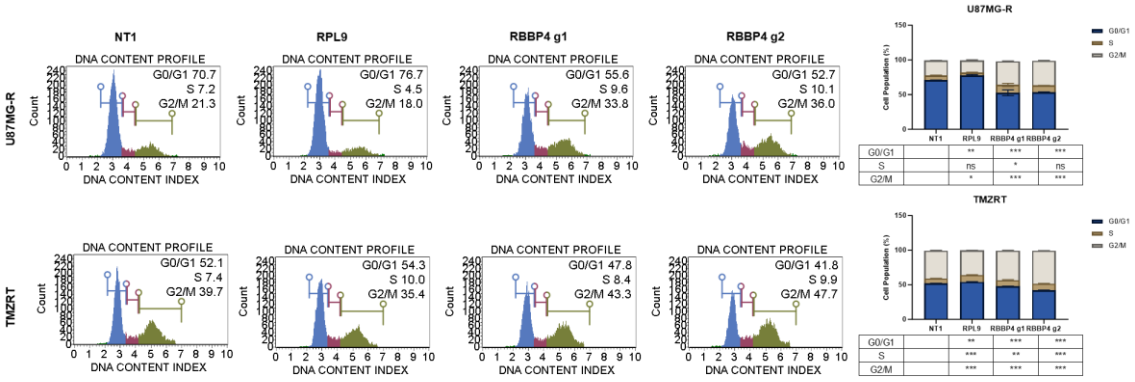

Figure 3.44: Cell cycle analysis for RBBP4 KO. Cell cycle analysis was performed on Day13 following RBBP4 transduction. Cell cycle arrest was observed in both cell lines. Two-way Anova, * p<0.05, ** p<0.01, *** p<0.001.

3.2.6. Possible mechanisms for regulation by RBBP4 in resistant cell lines

To uncover the potential mechanisms for RBBP4 KO phenotype, some known partners were investigated. Literature states that RBBP4 regulates MGMT expression (Kitange et al., 2016)(Mladek et al., 2022). Therefore, MGMT expression was studied upon RBBP4 KO. qPCR results at PT9 of knock-out reveals that no significant change in MGMT expression was observed in both cell models (**Figure 3.45**). This may indicate that regulation of vulnerability was not mediated by MGMT, as opposed to the published knowledge in the literature.

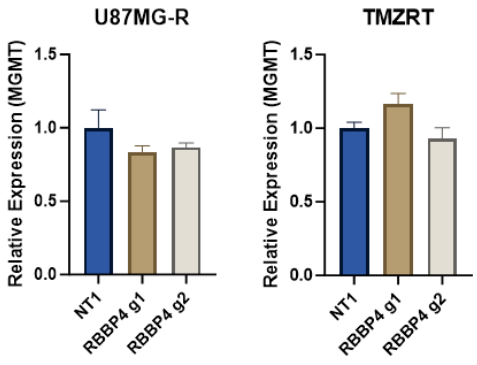

Figure 3.45: qPCR results for MGMT expression. MGMT mRNA expression was measured at PT9 of RBBP4 KO in both cell lines, showing no significant change.

Literature also states that MRN complex was associated with RBBP4 (J. Li et al., 2023). MRN complex members RAD50, MRE11 and NBN expression was analyzed upon RBBP4 KO (**Figure 3.46).** Results do not show any indication that the expression of MRN complex members significantly changes. Phenotype was not associated with this complex.

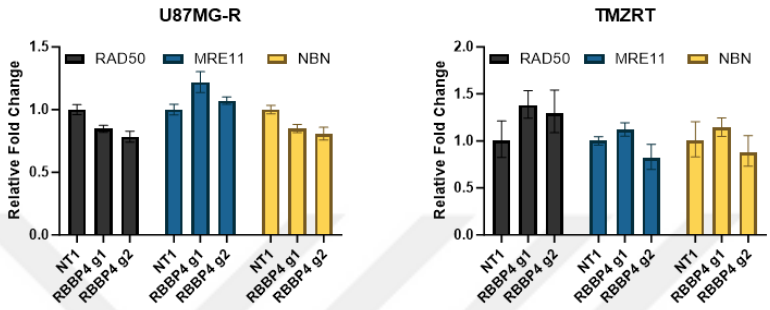

Figure 3.46: qPCR results for MRN complex members' expression. RAD50, MRE11 and NBN expression levels at PT9 of RBBP4 KO in both cell lines.

Next, some of the signature resistance genes were analyzed via qPCR in both cell lines upon KO to examine if there is any change in the expression of these genes. Interestingly, expression profile changes dramatically between cell lines. It was observed that ESM1, KLHL4, TMEM132D, CELF2 and ROBO2 gene expression was increased upon RBBP4 KO in U87MG-R cell line, whereas decreased in TMZRT. The only consistent results were obtained for SLC14A1 gene, which was upregulated in both cell lines. Further analysis on understanding the mechanisms behind RBBP4 phenotype is required.

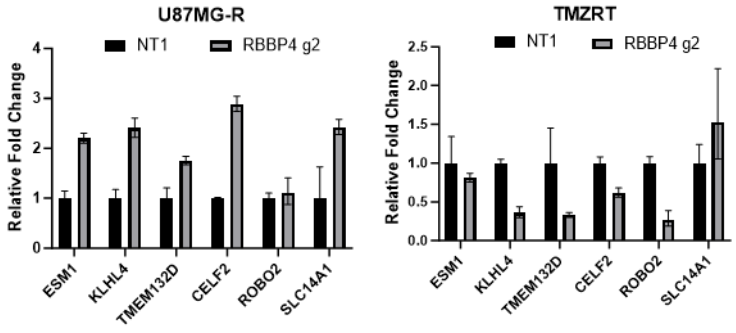

Figure 3.47: qPCR results for signature resistance gene expression. mRNA expression levels of ESM1, KLHL4, TMEM132D, CELF2, ROBO2 and SLC14A1 at PT9 of RBBP4 KO in both cell lines.

3.2.7. Effect of RBBP4 KO on naïve GBM cells and astrocytes

The knock-out of RBBP4 was tested on different GBM cells and non-malignant controls. With this purpose, U87MG and Immortal-NHAs were transduced with RBBP4 viruses. Colony formation assay was performed afterwards, and results are shown in **Figure 3.48.** RBBP4 KO does not affect U87MG cells. In I-NHA, RBBP4 KO decreases colony forming ability of the cells, even though RBBP4 was not an essential gene for NHA in CRISPR screen.

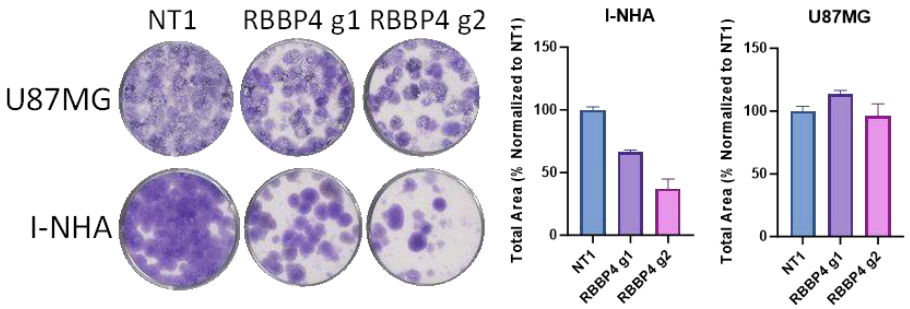

Figure 3.48: Effect of RBBP4 KO on viability for U87MG and I-NHA cell lines. Colony formation assay with two gRNAs targeting RBBP4 and its quantification based on total area calculation with ImageJ.

Innately TMZ resistant cell line T98G was also used to study the effect of RBBP4 KO. TMZ was also administered to the cells during colony formation. No change was observed between TMZ and DMSO groups. A significant decrease in colony formation was seen in T98G cells, especially with gRNA 2. Expression of RBBP4 and MGMT was checked with qPCR following RBBP4 KO. RBBP4 levels were dropped quite significantly. Interestingly, RBBP4 g2 decreased MGMT expression in T98G cells, consistent with the literature (Kitange et al., 2016).

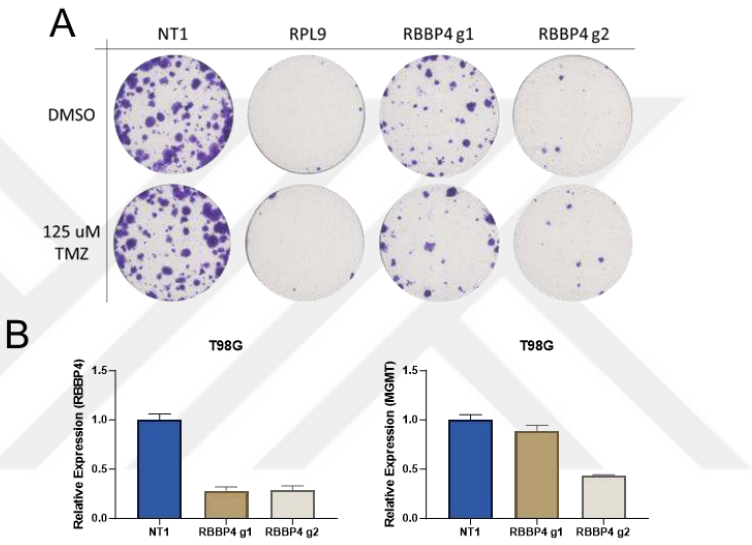

Figure 3.49: RBBP4 KO on T98G cell line. A. Colony formation results with TMZ. **B.** qPCR results for the expression of both RBBP4 and MGMT at PT9.

3.2.8. RNA sequencing results for RBBP4 KO in U87MG-R

To understand the mechanism behind RBBP4 phenotype, RNAseq with g1 and g2 (and NT1 as control) in U87MG-R cell line was performed. Cells were collected at PT9 as triplicates. Volcano plots show the DEGs and number of upregulated and downregulated genes with LFC<-0.5, >0.5 cutoffs. RBBP4 was one of the top downregulated genes, as a testament to the success of our profiling experiment.

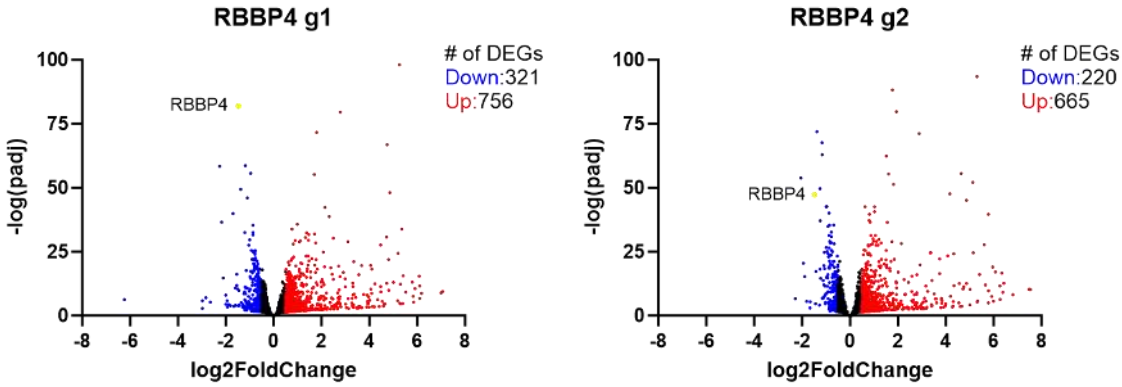

Figure 3.50: Volcano plots for RBBP4 g1vsNT1 and RBBP4 g2vsNT1 with RBBP4 labeled on the downregulated part of the graph. Number of differentially expressed genes were listed on the graph based on LFC<-0.5, >0.5 cutoff.

Next, GSEA was performed with the transcriptome data. Inflammatory response and related pathways were highly overexpressed upon RBBP4 KO. G2/M checkpoint pathway was one of the significantly downregulated pathways. This was exciting since cell cycle arrest at G2/M was observed via cell cycle assay previously.

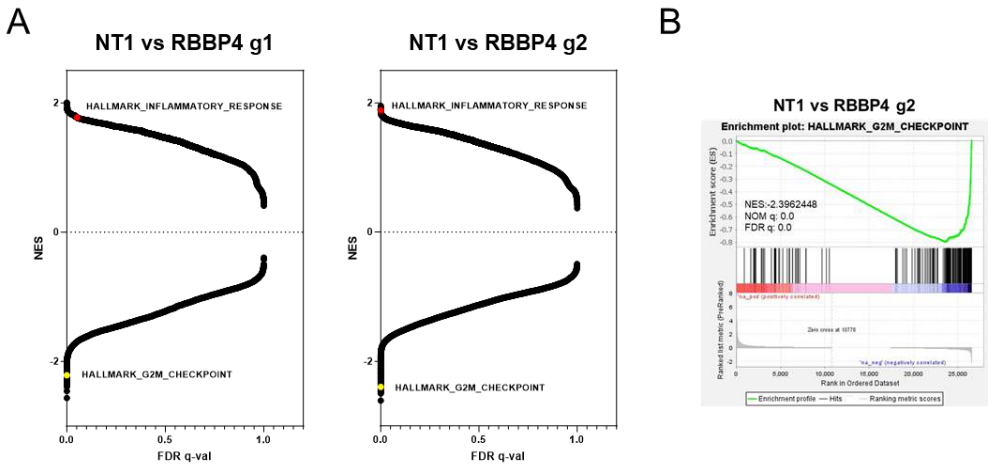

Figure 3.51: GSEA graphs and enrichment plot showing Hallmark_G2M_ Checkpoint as one of the downregulated pathways. A. GSEA plots with upregulated and downregulated representative pathways highlighted based on negative enrichment score and FDR. **B.** Enrichment plot for G2M-Checkpoint from NT1vsRBBP4 g2.

Downregulated gene signatures were studied by overlapping downregulated genes with LFC<-0.5 cutoff. There were 169 genes commonly downregulated in both gRNAs. Overlap analysis by MsigDB for hallmark pathways with the common genes revealed G2M checkpoint, E2F targets and mitotic spindle pathways to be significantly downregulated. These results indicate that phenotype seen upon KO was related with the cell cycle mechanism of TMZ-resistant cells.

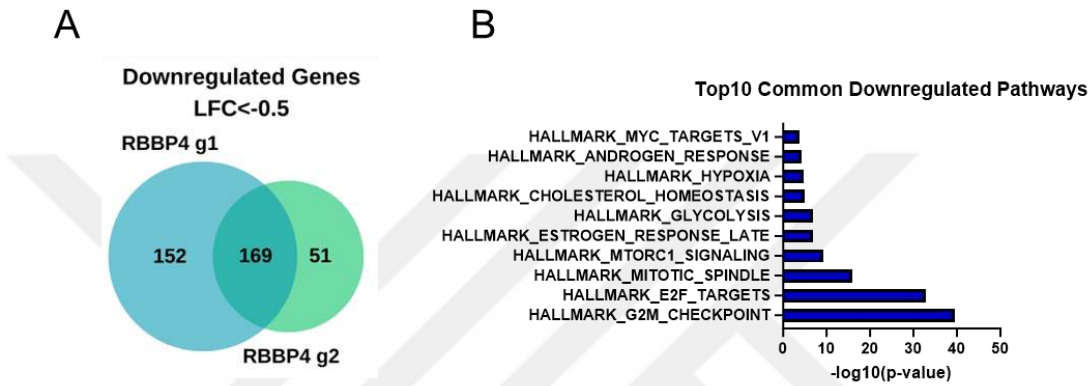

Figure 3.52: Commonly downregulated pathways. A. Venn diagram of common downregulated genes in both gRNAs based on LFC<0.-5 cutoff. **B.** Overlap analysis results for the top 10 pathways.

Using the genes from the top three pathways, a heatmap was generated based on LFC values of each gene in transcriptome analysis data. Some of these genes such as PLK1 were common in all three pathways, whereas some such as NEK2 were common in only two pathways.

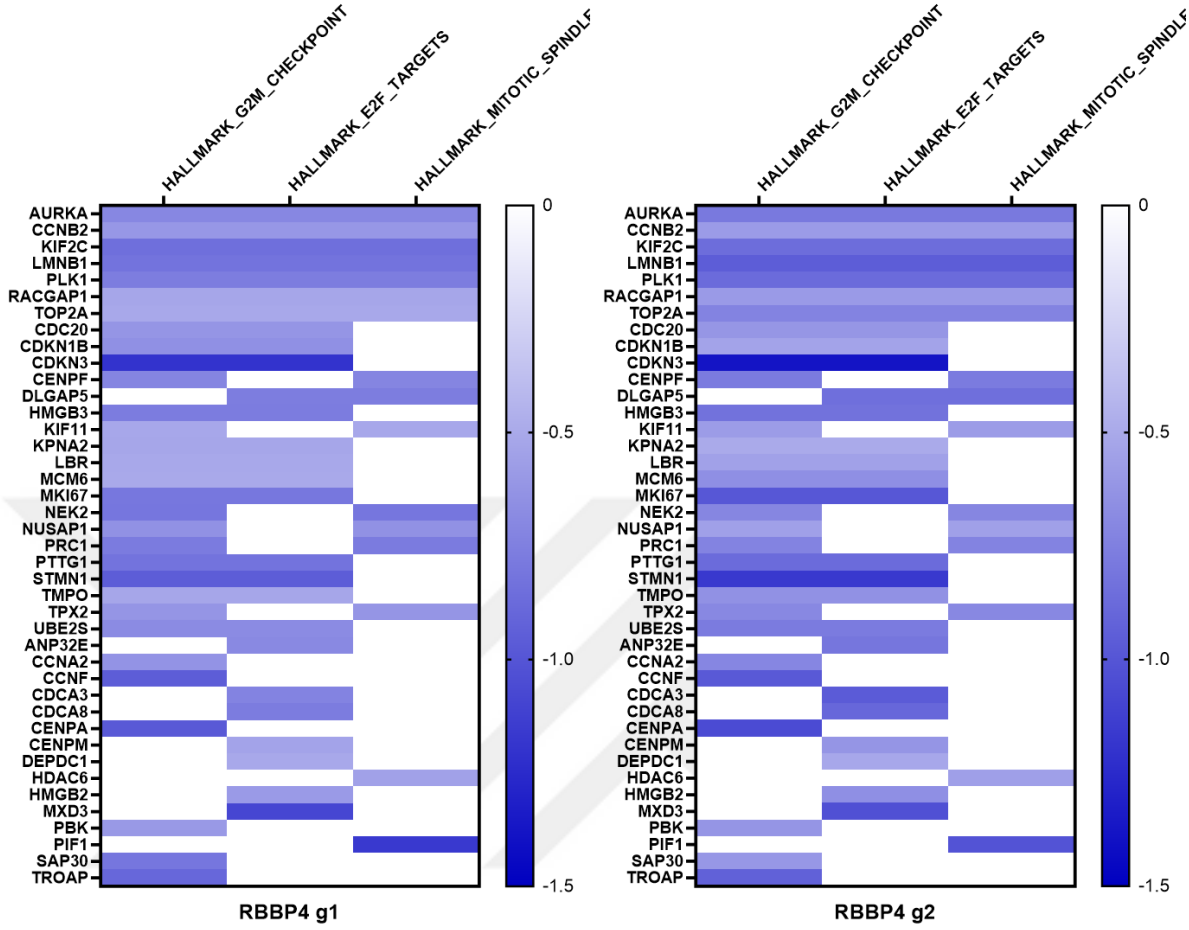

Figure 3.53: Heatmap of genes found in commonly downregulated pathways. A. Genes found in the top three pathways were listed as a heatmap based on their LFC values from RBBP4 g1 and g2 data. The color scale indicates the LFC values.

4 DISCUSSION

Glioblastoma is the most aggressive primary brain tumor with poor survival and high recurrence rate. Glioblastoma is characterized as IDH-wildtype and grade 4 according to 2021 WHO classifications. Therapeutic options for patients include surgical resection of the tumor, radiation therapy and chemotherapy by alkylating agent Temozolomide. Although TMZ is a gold standard for the treatment of glioblastoma, its effectiveness can be hindered by repair enzymes that reverse the DNA damage caused by TMZ. This recovery is mostly associated with MGMT enzyme in which the promoter methylation of MGMT is used as a prognostic marker. Epigenetic alterations play important roles in glioblastoma progression and chemotherapy resistance. New targets and therapeutic options need to be discovered for glioblastoma therapy.

In this thesis, our aim was to identify important epigenetic targets that are required for glioblastoma cell survival and uncover chromatin modifiers that are essential for TMZ response and therapy resistance. For this purpose, we first performed EPIKOL screens in naïve cell lines and uncovered epigenetic targets that are essential for GBM survival. Next, to study TMZ resistance, we generated TMZ resistant cell lines and characterized these cell lines both *in vitro* and *in vivo* and investigated the transcriptomic changes. Finally, we performed EPIKOL screens in TMZ resistant models in the presence and absence of TMZ and identified RBBP4 as a target for therapy resistant cell vulnerability.

EPIKOL screens reveal epigenetic targets required for cell fitness in naïve glioblastoma cells.

To identify fitness genes for glioblastoma survival, we performed EPIKOL screens (Yedier-Bayram et al., 2022). We utilized EPIKOL in U87MG and U373 cell lines and as a non-malignant control, we used NHA cell line. Initially, we checked the library quality by infecting U87MG cell line with EPIKOL lentiviruses and collected samples after puromycin selection. We sent this sample to NGS following library preparation and it passed the quality check. Next, we performed Cas9 activity in U87MG

cell line, however GFP-targeting gRNA (T1) did not deplete more than 50%. EPIKOL screens in U87MG and U373 cell lines were conducted as 1000x representation and in triplicates. Following the screen, we decided to validate several genes that were either common in two cell lines or selective for U87MG or U373. We performed dual color competition assay and colony formation to validation. ASH2L was one of the genes that were depleted in competition assay in both cell lines and showed decreased colony forming ability upon KO. ASH2L is a histone lysine methyltransferase, and it is involved in many complexes including SET1/MLL family (Vedadi et al., 2017). We further validated the ASH2L KO phenotype via viability assays. In our lab, we have generated a different epigenetic based CRISPR/Cas9 library called EpiDoKOL and identified ASH2L as a regulator of glioblastoma cell fitness as well (Ozyerli-Goknar et al., 2023). We demonstrated that ASH2L leads to cell cycle alterations and inhibits glioblastoma growth both *in vitro* and *in vivo*. As a result, we identified ASH2L as a potential target for glioblastoma survival in two different CRISPR/Cas9 library screens.

TMZ sensitizer screen identifies potential hits.

In an effort to find TMZ sensitizers, we administered TMZ to U87MG cells after Cas9 activity during EPIKOL screen. We separated the U87MG cells infected with EPIKOL lentiviruses into two groups and let one of the groups grow as essentiality comparison. 50 μM of TMZ was used during the screen however this was too much for U87MG cells as cells did not double. Because of this, we removed TMZ and allowed cells to reach 14 doublings. At the end, we compared the TMZ and After-TMZ groups and decided to follow up on BRD9, BRD8, EP300, CREBBP, SMARCD1 and SMARCE1 genes. We decided to focus on the role of SMARCE1 on TMZ sensitization and tested U87MG, U373 along with U87MG-R and TMZRT. We used 10 μM of TMZ for naïve cells and maintenance dose for resistant cells. Although we observed significant sensitization in U87MG and U373 cell lines, this sensitization was similar to NT1. MTT assay results did not show any sensitization. Although identification of a potential TMZ sensitizer was an important part of our research, due to lack of validation and inconsistent results, we did not continue this study and moved on to different goals.

Generation and characterization of TMZ resistant cell line.

Chemotherapy resistant cell models are used for mimicking the therapy resistance of various cancer types. Usually there are two types of resistance generation mechanisms as clinically relevant model, where pulsed treatments are utilized, and high-level models with dose escalation method (McDermott et al., 2014). In this thesis, we generated a TMZ resistant cell model via dose escalation method from U87MG cell line. Previous PhD student, Dr. Filiz Senbabaoglu created a clinically relevant TMZ resistant model from U373 cell line, and we also utilized this cell line for further experiments. We examined the drug response of naïve and resistant cell lines and observed increased IC50 value in U87MG-R cell line. We also performed long term colony formation assay and showed that U87MG cells are not capable of forming colonies under moderate-to-high concentrations of TMZ. We examined the cell cycle distribution of the cells upon TMZ treatment and observed that naïve cells are accumulated in G2/M phase while no change is observed in resistant cells upon TMZ administration. These results are consistent with the literature where it was shown that TMZ resistant cells escape the G2/M checkpoint and move forward with replication (Banelli et al., 2015).

To test the TMZ resistant character of U87MG-R *in vivo*, we implanted naïve and resistant cells to NOD-SCID mice and treated with TMZ/DMSO. We showed that although both U87MG and U87MG-R cells formed tumors, TMZ diminished the tumor formed by U87MG while tumor remained the same in U87MG-R group. We removed the brain tissue and sectioned the tumors for histological analysis of the tumors. H&E staining showed that U87MG-R tumors are highly dispersed throughout the brain compared to U87MG tumors which are highly aggregated. No tumor was visible in U87MG + TMZ group, except for a small area with apoptotic cells. Later, we investigated the proliferation capacity of the tumors with Ki-67 staining. Correlated with the H&E staining, most proliferative cells were present in U87MG-R groups, up to 80% of the tumor was positive for Ki-67. This ratio is around 40% for U87MG -TMZ group and less than 20% of the cells in U87MG +TMZ were positive for Ki-67. These results indicate that the generated cell line U87MG-R is highly invasive *in vivo* and can proliferate more than its naïve derivate U87MG. This phenotype can be the result of increased epithelial-to-

mesenchymal transition, as shown in RNA sequencing, leading to aggressive growth and infiltration over the brain tissue. EMT and glioblastoma interaction is complicated since glioblastoma is a non-epithelial cancer (Colella et al., 2019). EMT-like signatures have been observed especially mesenchymal glioma subtypes, which are the most invasive type(Mahabir et al., 2014) (Verhaak et al., 2010). We also observe that several other pathways such as apical junction and apical surface are upregulated in U87MG-R. These pathways are involved in cell polarity, cell-to-cell interactions and linkage to actin cytoskeleton (González-Mariscal et al., 2020). Cadherin-11 (CDH11) is a mesenchymal marker and is known to regulate cell migration in glioblastoma (Kaur et al., 2012). Cadherin-11 is found in both Hallmark_EMT and Hallmark_Apical_Junction pathways and is upregulated in U87MG-R (data not shown). Together with these findings, we can conclude that the invasiveness and increased migration capacity of U87MG-R *in vivo* may be the result of upregulation of members of these pathways. We also observe that different pathways have been differentially regulated in two models, attesting the different characteristics of the two cell lines. Further experiments are required to be certain, such as immunostaining of some markers to validate these findings.

TMZ resistant cell lines exhibit high MGMT levels and transcriptome analysis identifies signature resistance genes.

We performed RNA sequencing to determine transcriptomic changes that occur in resistant models. Results showed that MGMT expression was highly upregulated in U87MG-R cell line as well as TMZRT cell line. Later, we wanted to find out common genes upregulated in both cell lines. We focused on upregulated genes, as MGMT being one of the known targets that is overexpressed in resistant cells or recurrent tumors. Among common upregulated genes, we studied the top 15. First, we validated the upregulation of these genes via qPCR. Next, we checked their expression levels and relations with patient survival via TCGA analysis. Interestingly, although MGMT expression was higher in GBM patients compared to LGG patients, its expression did not change the survival rate significantly. ESM1 and KLHL4 were the only two genes that are highly expressed in GBM and their expression decreases life span of LGG-GBM patients significantly. ESM1 is endothelial cell specific molecule 1 and involved in

angiogenesis (Tsai et al., 2021). It was shown that ESM1 localizes tumor margins in GBM tumors (Maurage et al., 2009). KLHL4 is part of the Kelch family, and a recent study showed that it is a p53 target and involved in cell proliferation (Choi et al., 2020). The molecular function of KLHL4 is understudied but it is associated with glioma prognosis (Wijethilake et al., 2020). A deeper understanding of the biological function of ESM1 and KLHL4 can be important for TMZ resistant models. In the future, we can target these genes and see if any sensitization to TMZ is induced.

We investigated whether the inhibition of MGMT would reverse the resistance phenotype. Indeed, MGMT knock-out with CRISPR/Cas9 sensitized both resistant models to TMZ. Next, we wanted to analyze the methylation status of MGMT in our models. As explained previously, *MGMT* promoter methylation is an important prognostic marker for TMZ response and GBM progression. Methylation status can be explored by methylation specific PCRs (Vlassenbroeck et al., 2008). By combining protocols and primer information about MGMT methylation specific PCRs (Anel et al., 2000) (Belinsky et al., 2007), we analyzed the methylation status of MGMT in our naïve-resistant cell pairs along with positive and negative controls. Bisulfite conversion followed by nested PCR using primers specific to methylated or unmethylated MGMT, we showed that *MGMT* promoter shifts from methylated to unmethylated in resistant cell lines, especially U87MG-R. 293T cell line was used as negative control, and we see that *MGMT* promoter is methylated. As an innately TMZ resistant cell line, T98G cells (S. Y. Lee, 2016) exhibit both methylated and unmethylated *MGMT* promoter status. Based on these findings, it is seen that MGMT expression is highly important for TMZ resistance and therapy response. It is known that MGMT is highly expressed in non-tumorous tissues since it is an important DNA repair enzyme (SHARMA et al., 2009). This expression can be associated with low toxicity of TMZ since DNA adducts created by TMZ can be repaired by MGMT in peripheral tissues.

We also wanted to check whether the MGMT phenotype we observed was from genomic amplification, therefore we performed qPCR using primers designed to span exon-intron junctions. Results showed us that in U87G-R, the MGMT levels were not increased compared to U87MG. Therefore, we concluded that copy number variation of

MGMT was not an issue for the generated resistant cell line. Together these results prove that generated TMZ models are highly dependent on MGMT. This raises the question of whether more epigenetic mechanisms are required for TMZ resistance.

The question whether the resistance is genetic or non-genetic is difficult to answer. Genetic mechanism of resistance relies on the expansion of a cancer cell carrying genetic alterations that allows adaptation to therapy resistance whereas non-genetic mechanism involves transcriptional and/or metabolic reprogramming of the cell to adapt to therapy pressure (Marine et al., 2020). One of the most reliable methods for the determination of genetic and non-genetic resistance is single cell sequencing due to tumor heterogeneity. Our results indicate a leaning towards epigenetic based mechanism of resistance due to change in methylation of MGMT. We do not observe any copy number alteration of MGMT locus. However, we do not know the accompanying mutational changes that occurred during the resistance generation, therefore we cannot speculate the source of mechanism without further analysis and experiments.

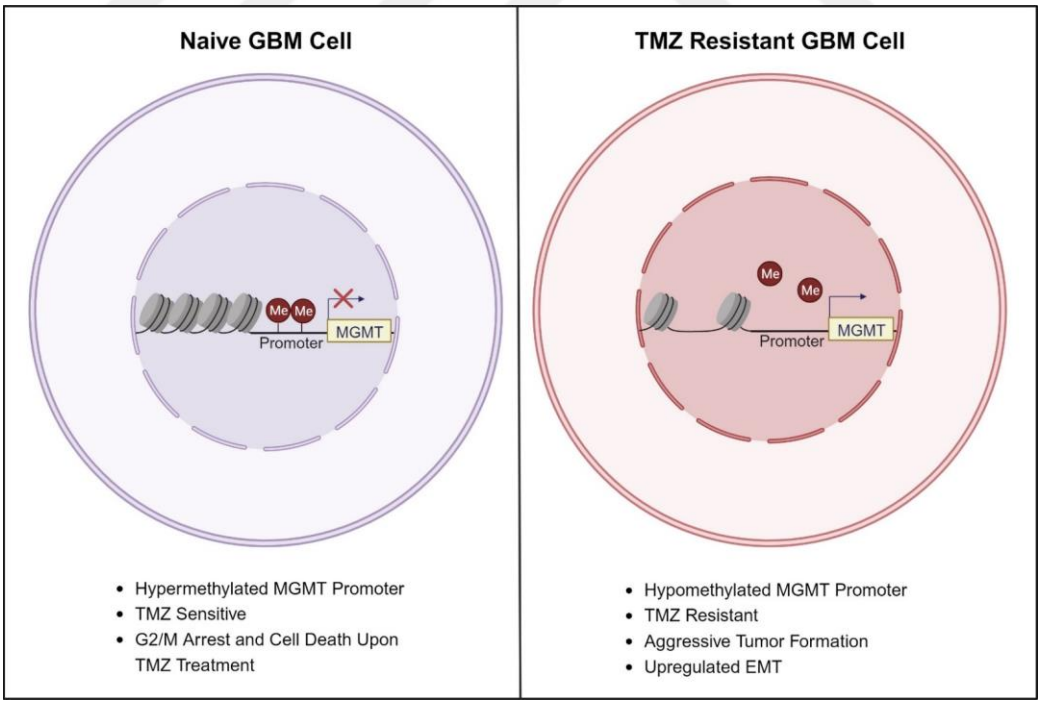

Figure 4.1: TMZ resistance mechanism and characteristics. *MGMT* promoter is hypermethylated in naïve glioblastoma cells which results in TMZ sensitization leading

to cell death. In TMZ resistant cells, *MGMT* promoter is hypomethylated, therefore no sensitization is observed. Resistant cells show upregulated EMT and aggressive growth *in vivo*. Figure created in Biorender.com.

EPIKOL screens with TMZ resistant cell lines reveal selective vulnerability genes.

Identification of genes that can breach TMZ resistance was one of our goals. For this reason, we performed EPIKOL screens in resistant models in the absence and presence of TMZ. To identify sensitizers, we compared two endpoints, DMSO and TMZ. From these comparisons, we compiled a list of genes as hits from U87MG-R and TMZRT cell lines. We picked gRNAs based on count data for each cell line and cloned the gRNAs to pLG plasmid. Initially, we performed a colony formation assay to test whether cells would sensitize to TMZ upon inhibition of these genes. However, we could not validate the screen results. Either the inhibition of the genes did not cause any significant sensitization, or it was essential by itself and cause decreased colony forming ability. The potential reasons for failed validations could be related to quality of the screen, off-targets or insufficient knock-out that does not result with a phenotype (Doench, 2018) (Bock et al., 2022). Although the depletion scores of the screens were good, we encountered many false positives. One reason for low screen performance could be the p53 status of the cell lines used in the experiment. It was previously reported that wildtype p53 harboring RPE1 cells (retinal pigment epithelium) show induced DNA damage response therefore, decreasing the effectiveness of CRISPR/Cas9 genome editing (Haapaniemi et al., 2018). They also reported that p53, along with pRB and p21 gRNAs were enriched in the screen performed with p53 deficient cells. Contrast to these results, Brown et al showed that successful CRISPR screen is possible with the same cell line, and other p53 wild type cells (Brown et al., 2019). Later, parallel screens with +/-p53 in RPE1 cell line were performed and showed that although p53 status negatively impacts the screen, efficient screening results also rely on the library itself, number of gRNAs and sequencing (Bowden et al., 2020). We know that U87MG cell line is p53 wildtype, whereas U373 is mutant. Although we cannot know for certain that the resistant cell lines generated from U87MG and U373 also have the same p53 status without further assessment, this might be one of the reasons why screen performance and poor validations were observed. We

also observe that gRNAs targeting p53 as enriched in U87MG-R screen (data not shown), consistent with findings from Haapaniemi et al (Haapaniemi et al., 2018). To improve the screen quality, knocking out p53 prior to CRISPR screen could be an important strategy that may eliminate low efficiency.

We moved on to the common genes depleted in both cell lines, which are PCGF6, SET, MGMT and APEX1. We know that MGMT KO sensitizes the cells to TMZ from our previous experiments. One important observation we had in this screen is that gRNAs targeting TET or DNMT enzymes were not significantly changed in the screens (data not shown). DNMT family is responsible for the addition of methyl groups to DNA and TET family is responsible for the removal of the methyl adducts, and MGMT is associated with these enzymes in terms of promoter methylation (Christmann & Kaina, 2019). The reason why the genes associated with *MGMT* promoter methylation not scoring as hits in CRISPR screens can be explained as knock-out one of the single gene family members may not be enough to disrupt the methylation/demethylation function. Knock-out of all TET family members, for example, can result in loss of demethylation activity, leading to hypermethylated *MGMT* promoter, therefore increased TMZ activity. This hypothesis can be tested using CRISPR/Cas9 for TET enzymes with individual cloning of gRNAs and ablating all TET genes. Since MGMT was one of the four common genes, we wanted to test the other three. Due to technical problems, we were not able to clone and KO APEX1, but it is still ongoing. In the meantime, we performed knock-out PCGF6 and SET with two gRNAs. However, PCGF6 did not produce any phenotype while SET showed a very slight sensitization for TMZ. Again, these studies will be further detailed with APEX1 and whether these genes induce sensitization for TMZ will be further investigated.

Next, we wanted to investigate the vulnerability genes for resistant models, in the absence of TMZ. This time, we eliminated the genes scoring as hits from the NHA screen and focused on GBM specific genes. A total of 7 genes were common in U87MG-R and TMZRT as TOP2A, PCNA, RBBP4, BAP1, NSL1, EXOCS2 and CDK2. Among these genes, only BAP1 is not common essential according to DepMap (cancer dependency map). We performed a colony formation assay with these genes and showed that only

RBBP4 and CDK2 led to significant growth reduction in U87MG-R cell line. RBBP4 is involved in many chromatin remodeling complexes and recent studies showed that it is involved in TMZ sensitivity in glioblastoma (Cai et al., 2023). CDK2 is one of the serine/threonine kinases that are involved in regulation of cell cycle. Together with Cyclin E, CDK2/CyclinE complex mediates G1/S transition by phosphorylating RB, allowing E2F targets to be expressed and initiates S phase (Fagundes & Teixeira, 2021). CDK2 also plays critical roles in regulation of DNA replication and DNA damage response (Tadesse et al., 2020). Due to its important function in cell cycle regulation and replication, mutations in CDK2 result in genomic instability in various cancer types (Fagundes & Teixeira, 2021). It's shown that CDK2 is overexpressed in high grade gliomas (H. Liu & Weng, 2022), and it is associated with radio-resistance and proliferation of GBM (J. Wang et al., 2016). Between these two targets, we were highly interested in RBBP4 due to its interaction with MGMT and TMZ resistance and continued our study with RBBP4.

RBBP4 inhibition induces cell cycle arrest and apoptosis.

The viability of U87MG-R and TMZRT cells upon RBBP4 knock-out was decreased, leading us to investigate the mechanism behind it. For this purpose, we analyzed cell cycle distribution of the cells after RBBP4 inhibition. Results showed that cells accumulate in G2/M phases, indicating an arrest at this cell cycle stage. From the literature, we know that RBBP4 is part of chromatin regulator complexes DREAM and MuvB, which plays important roles in cell cycle progression (Fischer & Müller, 2017).

We tested the apoptosis profile of these cells following RBBP4 silencing and saw increased total apoptotic levels in both cell lines compared to NT1 control. This indicates that following cell cycle arrest, cells die via induction of apoptosis. For the next steps, we needed to understand the molecular mechanisms that drive cell cycle arrest and apoptosis upon RBBP4 silencing to make deductions about the role of RBBP4 in our GBM models.

Loss of RBBP4 downregulates important cell cycle pathways.

GBM and RBBP4 relations indicate that GBM therapy resistance and survival is either associated with p300-RBBP4-MGMT axis (Mladek et al., 2022) or by MRN complex as MGMT independent manner (J. Li et al., 2023). To test this, we checked MGMT expression levels upon RBBP4 inhibition. Our results did not show any significant reduction in MGMT levels, meaning this regulation of vulnerability did not involve an accompanying reduction of MGMT expression. Next, we checked the MRN complex members' mRNA levels via qPCR. Again, there was no significant change upon KO of RBBP4. This led us to believe that the mechanism for RBBP4 dependent cell death was led by another mechanism. To identify this, we performed transcriptome analysis in U87MG-R cell line. MRN complex members or MGMT was not significantly differentially expressed in RNAseq results for both gRNAs, verifying our qPCR results. We carried out gene set enrichment analysis (GSEA) for the whole transcriptome. Many upregulated pathways were involved in inflammation and inflammatory response. Downregulated pathways were mostly involved in cell cycle regulation such as G2/M checkpoint. This result also verified our findings about cell cycle regulation upon RBBP4 silencing. Later, we determined the common genes downregulated with both gRNAs and performed an overlap analysis for these genes. Top downregulated pathways were G2/M checkpoint and E2F targets. It is clear that cell cycle is highly disrupted upon RBBP4 silencing. RBBP4 is involved in DREAM and MuvB complexes which play critical roles in cell cycle regulation (Fischer & Müller, 2017). When in complex with DREAM, RBBP4 functions as a repressor while with MuvB it functions as an activator. In our study, we see that upon RBBP4 silencing, G2/M arrest was induced and RNAseq results show G2/M checkpoint pathways to be downregulated. These may indicate that inhibition of cell survival in the resistant models may be regulated by the MuvB-RBBP4 during cell cycle. As our future directions, we need to show cell cycle dysregulation via functional assays, identify which complex or regulators are also involved in this phenotype in TMZ resistant glioblastoma models and verify the phenotype *in vivo*.

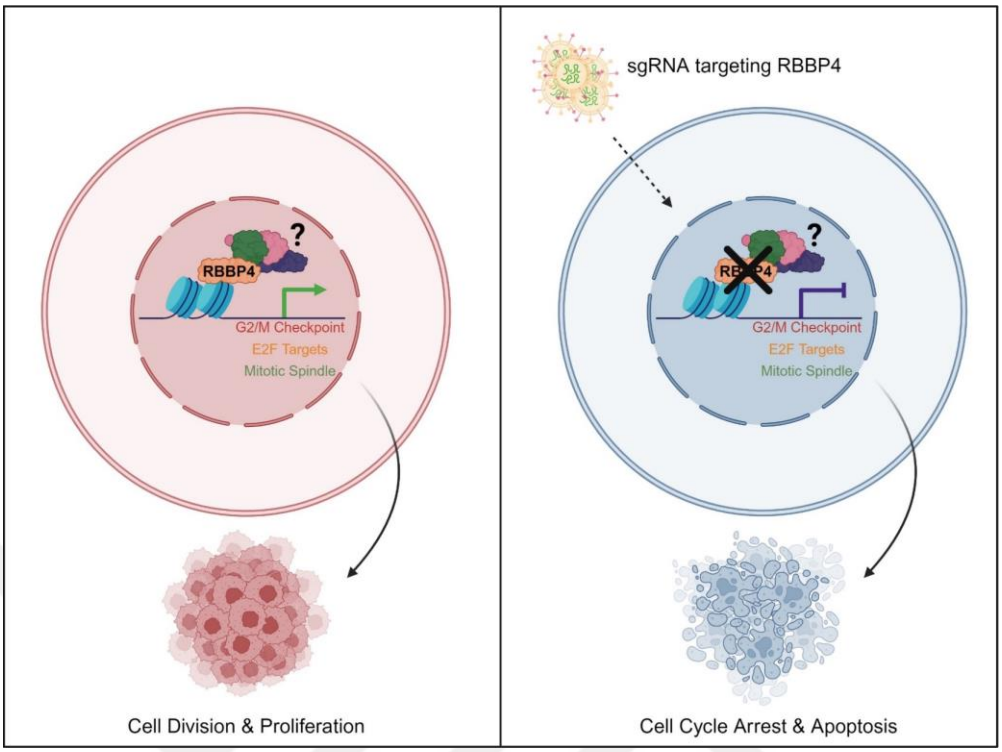

Figure 4.2: Proposed mechanism for RBBP4 mechanism. RBBP4 with a complex (probably with cell cycle regulators) involved in regulation of cell division and proliferation. Upon silencing via CRISPR/Cas9, several pathways involved in cell division and checkpoints were downregulated which results in cell cycle arrest and apoptosis. Figure created in Biorender.com.

As future directions, we are aiming to explore further the mechanism of RBBP4 regulation in TMZ resistant glioblastoma models. Transcriptome analysis gave us clues as to how this works. Detailed analysis of the downregulated genes/pathways and understanding of how they are involved in RBBP4 is important. qPCR, IF experiments for mitotic spindle associated proteins and *in vivo* RBBP4 silencing are some of the experiments that we will perform. Since RBBP4 is associated with many chromatin remodeler complexes, we may also investigate if any complexes are involved in this regulation. Co-immunoprecipitation experiments or inhibitors for specific complexes can be used for this purpose. Overall, we will investigate RBBP4-TMZ resistance relations in many aspects to enlighten the mechanism.

BIBLIOGRAPHY

Aleksandrov, R., Hristova, R., Stoynov, S., & Gospodinov, A. (2020). The Chromatin Response to Double-Strand DNA Breaks and Their Repair. In *Cells* (Vol. 9, Issue 8). NLM (Medline). https://doi.org/10.3390/cells9081853

Alkhatib, S. G., & Landry, J. W. (2011). The Nucleosome Remodeling Factor. *FEBS Letters*, *585*(20), 3197–3207. https://doi.org/https://doi.org/10.1016/j.febslet.2011.09.003

Allis, C. D., & Jenuwein, T. (2016). The molecular hallmarks of epigenetic control. *Nature Reviews Genetics*, *17*(8), 487–500. https://doi.org/10.1038/nrg.2016.59

Alyateem, G., Wade, H. M., Bickert, A. A., Lipsey, C. C., Mondal, P., Smith, M. K. D., Labib, R. M., Mock, B. A., Robey, R. W., & Gottesman, M. M. (2023). Use of CRISPR-based screens to identify mechanisms of chemotherapy resistance. *Cancer Gene Therapy*, *December 2022*, 1–8. https://doi.org/10.1038/s41417-023-00608-z

Anel, M., Steller, E., Esus, J., Arcia -F Oncillas, G., Ndion, S. A., Teven, S., Oodman, N. G., Icente, V., Anaclocha, V., Tephen, S., Aylin, B. B., Ames, J., & Erman, G. H. (2000). *The New England Journal of Medicine INACTIVATION OF THE DNA-REPAIR GENE MGMT AND THE CLINICAL RESPONSE OF GLIOMAS TO ALKYLATING AGENTS A BSTRACT Background The DNA-repair enzyme O 6-methyl*.

Awwad, S. W., Serrano-Benitez, A., Thomas, J. C., Gupta, V., & Jackson, S. P. (2023). Revolutionizing DNA repair research and cancer therapy with CRISPR–Cas screens. In *Nature Reviews Molecular Cell Biology* (Vol. 24, Issue 7, pp. 477–494). Nature Research. https://doi.org/10.1038/s41580-022-00571-x

Bagga, M., Kaur, A., Westermarck, J., & Abankwa, D. (2014). *ColonyArea : An ImageJ Plugin to Automatically Quantify Colony Formation in Clonogenic Assays*. *9*(3), 14–17. https://doi.org/10.1371/journal.pone.0092444

Banelli, B., Carra, E., Barbieri, F., Würth, R., Parodi, F., Pattarozzi, A., Carosio, R., Forlani, A., Allemanni, G., Marubbi, D., Florio, T., Daga, A., & Romani, M. (2015). The histone demethylase KDM5A is a key factor for the resistance to temozolomide in glioblastoma. *Cell Cycle*, *14*(21), 3418–3429. https://doi.org/10.1080/15384101.2015.1090063

Banelli, B., Daga, A., Forlani, A., Allemanni, G., Marubbi, D., Pistillo, M. P., Profumo, A., & Romani, M. (2017). Small molecules targeting histone demethylase genes (KDMs) inhibit growth of temozolomide-resistant glioblastoma cells. *Oncotarget*, *8*(21), 34896–34910. https://doi.org/10.18632/oncotarget.16820

Bannister, A. J., & Kouzarides, T. (2011). Regulation of chromatin by histone modifications. In *Cell Research* (Vol. 21, Issue 3, pp. 381–395). https://doi.org/10.1038/cr.2011.22

Barrangou, R., & Doudna, J. A. (2016). Applications of CRISPR technologies in research and beyond. *Nature Biotechnology*, *34*(9), 933–941. https://doi.org/10.1038/nbt.3659

Bates, S. E. (2020). Epigenetic Therapies for Cancer. *New England Journal of Medicine*, *383*(7), 650–663. https://doi.org/10.1056/nejmra1805035

Belinsky, S. A., Grimes, M. J., Casas, E., Stidley, C. A., Franklin, W. A., Bocklage, T. J., Johnson, D. H., & Schiller, J. H. (2007). Predicting gene promoter methylation in non-small-cell lung cancer by evaluating sputum and serum. *British Journal of Cancer*, *96*(8), 1278–1283. https://doi.org/10.1038/sj.bjc.6603721

Berdasco, M., & Esteller, M. (2019). Clinical epigenetics: seizing opportunities for translation. *Nature Reviews Genetics*, *20*(2), 109–127. https://doi.org/10.1038/s41576-018-0074-2

Bock, C., Datlinger, P., Chardon, F., Coelho, M. A., Dong, M. B., Lawson, K. A., Lu, T., Maroc, L., Norman, T. M., Song, B., Stanley, G., Chen, S., Garnett, M., Li, W., Moffat, J., Qi, L. S., Shapiro, R. S., Shendure, J., Weissman, J. S., & Zhuang, X. (2022). High-content CRISPR screening. In *Nature Reviews Methods Primers* (Vol. 2, Issue 1). Springer Nature. https://doi.org/10.1038/s43586-021-00093-4

Bowden, A. R., Morales-Juarez, D. A., Sczaniecka-Clift, M., Agudo, M. M., Lukashchuk, N., Thomas, J. C., & Jackson, S. P. (2020). Parallel CRISPR-Cas9 screens clarify impacts of p53 on screen performance. *ELife*, *9*, e55325. https://doi.org/10.7554/eLife.55325

Brandes, A. A., Bartolotti, M., Tosoni, A., & Franceschi, E. (2016). Nitrosoureas in the Management of Malignant Gliomas. *Current Neurology and Neuroscience Reports*, *16*(2), 13. https://doi.org/10.1007/s11910-015-0611-8

Brandsma, I., & Gent, D. C. (2012a). Pathway choice in DNA double strand break repair: Observations of a balancing act. *Genome Integrity*, *3*(1), 1. https://doi.org/10.1186/2041-9414-3-9

Brandsma, I., & Gent, D. C. (2012b). Pathway choice in DNA double strand break repair: Observations of a balancing act. *Genome Integrity*, *3*(1), 1. https://doi.org/10.1186/2041-9414-3-9

Breen, W. G., Anderson, S. K., Carrero, X. W., Brown, P. D., Ballman, K. V, O'Neill, B. P., Curran, W. J., Abrams, R. A., Laack, N. N., Levitt, R., Galanis, E., Buckner, J. C., & Shaw, E. G. (2020). Final report from Intergroup NCCTG 86-72-51 (Alliance): a phase III randomized clinical trial of high-dose versus low-dose radiation for adult low-grade glioma. *Neuro-Oncology*, *22*(6), 830–837. https://doi.org/10.1093/neuonc/noaa021

Brown, K. R., Mair, B., Soste, M., & Moffat, J. (2019). CRISPR screens are feasible in *TP53* wild‐type cells. *Molecular Systems Biology*, *15*(8), e8679. https://doi.org/https://doi.org/10.15252/msb.20188679

Cai, L., Liu, B., Cao, Y., Sun, T., & Li, Y. (2023). Unveiling the molecular structure and role of RBBP4/7: implications for epigenetic regulation and cancer research. *Frontiers in Molecular Biosciences*, *10*. https://doi.org/10.3389/fmolb.2023.1276612

Casas, S., Ollila, J., Aventín, A., Vihinen, M., Sierra, J., & Knuutila, S. (2003). Changes in apoptosis-related pathways in acute myelocytic leukemia. *Cancer Genetics and Cytogenetics*, *146*(2), 89–101. https://doi.org/10.1016/S0165-4608(03)00102-X

Cell Lines by Gene Mutation. (n.d.). www.atcc.org,

Chen, J., McKay, R. M., & Parada, L. F. (2012). Malignant glioma: Lessons from genomics, mouse models, and stem cells. *Cell*, *149*(1), 36–47. https://doi.org/10.1016/j.cell.2012.03.009

Chen, X., Zhang, M., Gan, H., Wang, H., Lee, J. H., Fang, D., Kitange, G. J., He, L., Hu, Z., Parney, I. F., Meyer, F. B., Giannini, C., Sarkaria, J. N., & Zhang, Z. (2018). A novel enhancer regulates MGMT expression and promotes temozolomide resistance in glioblastoma. *Nature Communications*, *9*(1). https://doi.org/10.1038/s41467-018-05373-4

Choi, S.-H., Cho, S.-Y., Song, J., & Hur, M.-W. (2020). KLHL4, a novel p53 target gene, inhibits cell proliferation by activating p21WAF/CDKN1A. *Biochemical and Biophysical Research Communications*, *530*(3), 588–596. https://doi.org/https://doi.org/10.1016/j.bbrc.2020.07.100

Christmann, M., & Kaina, B. (2019). Epigenetic regulation of DNA repair genes and implications for tumor therapy. In *Mutation Research - Reviews in Mutation Research* (Vol. 780, pp. 15–28). Elsevier B.V. https://doi.org/10.1016/j.mrrev.2017.10.001

Clapier, C. R., Iwasa, J., Cairns, B. R., & Peterson, C. L. (2017). Mechanisms of action and regulation of ATP-dependent chromatin-remodelling complexes. *Nature*

Reviews Molecular Cell Biology, *18*(7), 407–422. https://doi.org/10.1038/nrm.2017.26

Colella, B., Faienza, F., & Di Bartolomeo, S. (2019). EMT regulation by autophagy: A new perspective in glioblastoma biology. In *Cancers* (Vol. 11, Issue 3). MDPI AG. https://doi.org/10.3390/cancers11030312

Crespo, I., Vital, A. L., Gonzalez-Tablas, M., Patino, M. D. C., Otero, A., Lopes, M. C., De Oliveira, C., Domingues, P., Orfao, A., & Tabernero, M. D. (2015). Molecular and Genomic Alterations in Glioblastoma Multiforme. *American Journal of Pathology*, *185*(7), 1820–1833. https://doi.org/10.1016/j.ajpath.2015.02.023

Dawson, M. A., & Kouzarides, T. (2012). Cancer epigenetics: From mechanism to therapy. *Cell*, *150*(1), 12–27. https://doi.org/10.1016/j.cell.2012.06.013

de Vries, N. A., Hulsman, D., Akhtar, W., de Jong, J., Miles, D. C., Blom, M., van Tellingen, O., Jonkers, J., & van Lohuizen, M. (2015). Prolonged Ezh2 Depletion in Glioblastoma Causes a Robust Switch in Cell Fate Resulting in Tumor Progression. *Cell Reports*, *10*(3), 383–397. https://doi.org/10.1016/j.celrep.2014.12.028

Dmello, C., Zhao, J., Chen, L., Gould, A., Castro, B., Arrieta, V. A., Zhang, D. Y., Kim, K. S., Kanojia, D., Zhang, P., Miska, J., Yeeravalli, R., Habashy, K., Saganty, R., Kang, S. J., Fares, J., Liu, C., Dunn, G., Bartom, E., … Sonabend, A. M. (2023). Checkpoint kinase 1/2 inhibition potentiates anti-tumoral immune response and sensitizes gliomas to immune checkpoint blockade. *Nature Communications*, *14*(1). https://doi.org/10.1038/s41467-023-36878-2

Doench, J. G. (2018). Am i ready for CRISPR? A user's guide to genetic screens. *Nature Reviews Genetics*, *19*(2), 67–80. https://doi.org/10.1038/nrg.2017.97

Doench, J. G., Fusi, N., Sullender, M., Hegde, M., Vaimberg, E. W., Donovan, K. F., Smith, I., Tothova, Z., Wilen, C., Orchard, R., Virgin, H. W., Listgarten, J., & Root, D. E. (2016). Optimized sgRNA design to maximize activity and minimize off-target

effects of CRISPR-Cas9. *Nature Biotechnology*, *34*(2), 184–191. https://doi.org/10.1038/nbt.3437

Dominguez, A. A., Lim, W. A., & Qi, L. S. (2016). Beyond editing: Repurposing CRISPR-Cas9 for precision genome regulation and interrogation. *Nature Reviews Molecular Cell Biology*, *17*(1), 5–15. https://doi.org/10.1038/nrm.2015.2

Fagundes, R., & Teixeira, L. K. (2021). Cyclin E/CDK2: DNA Replication, Replication Stress and Genomic Instability. In *Frontiers in Cell and Developmental Biology* (Vol. 9). Frontiers Media S.A. https://doi.org/10.3389/fcell.2021.774845

Fischer, M., & Müller, G. A. (2017). Cell cycle transcription control: DREAM/MuvB and RB-E2F complexes. In *Critical Reviews in Biochemistry and Molecular Biology* (Vol. 52, Issue 6, pp. 638–662). Taylor and Francis Ltd. https://doi.org/10.1080/10409238.2017.1360836

Fisher, J. P., & Adamson, D. C. (2021). Current FDA-approved therapies for high-grade malignant Gliomas. In *Biomedicines* (Vol. 9, Issue 3). MDPI AG. https://doi.org/10.3390/biomedicines9030324

García-Claver, A. (n.d.). *Copy Number Alterations in Glioma Cell Lines*. www.intechopen.com

Glancy, E., Ciferri, C., & Bracken, A. P. (2021). Structural basis for PRC2 engagement with chromatin. In *Current Opinion in Structural Biology* (Vol. 67, pp. 135–144). Elsevier Ltd. https://doi.org/10.1016/j.sbi.2020.10.017

González-Mariscal, L., Miranda, J., Gallego-Gutiérrez, H., Cano-Cortina, M., & Amaya, E. (2020). Relationship between apical junction proteins, gene expression and cancer. *Biochimica et Biophysica Acta (BBA) - Biomembranes*, *1862*(9), 183278. https://doi.org/https://doi.org/10.1016/j.bbamem.2020.183278

Guo, Q., Cheng, K., Wang, X., Li, X., Yu, Y., Hua, Y., & Yang, Z. (2020). Expression of HDAC1 and RBBP4 correlate with clinicopathologic characteristics and

prognosis in breast cancer. *International Journal of Clinical and Experimental Pathology*, *13*(3), 563—572. https://europepmc.org/articles/PMC7137008

Gusyatiner, O., & Hegi, M. E. (2018). Glioma epigenetics: From subclassification to novel treatment options. *Seminars in Cancer Biology*, *51*(November), 50–58. https://doi.org/10.1016/j.semcancer.2017.11.010

Haapaniemi, E., Botla, S., Persson, J., Schmierer, B., & Taipale, J. (2018). CRISPR–Cas9 genome editing induces a p53-mediated DNA damage response. *Nature Medicine*, *24*(7), 927–930. https://doi.org/10.1038/s41591-018-0049-z

Haase, S., Garcia-Fabiani, M. B., Carney, S., Altshuler, D., Núñez, F. J., Méndez, F. M., Núñez, F., Lowenstein, P. R., & Castro, M. G. (2018). Mutant ATRX: uncovering a new therapeutic target for glioma. *Expert Opinion on Therapeutic Targets*, *22*(7), 599–613. https://doi.org/10.1080/14728222.2018.1487953

Hamiche, A., Sandaltzopoulos, R., Gdula, D. A., & Wu, C. (1999). ATP-Dependent Histone Octamer Sliding Mediated by the Chromatin Remodeling Complex NURF. *Cell*, *97*(7), 833–842. https://doi.org/10.1016/S0092-8674(00)80796-5

Hashizume, R., Andor, N., Ihara, Y., Lerner, R., Gan, H., Chen, X., Fang, D., Huang, X., Tom, M. W., Ngo, V., Solomon, D., Mueller, S., Paris, P. L., Zhang, Z., Petritsch, C., Gupta, N., Waldman, T. A., & James, C. D. (2014). Pharmacologic inhibition of histone demethylation as a therapy for pediatric brainstem glioma. *Nature Medicine*, *20*(12), 1394–1396. https://doi.org/10.1038/nm.3716

Hegi, M. E., Diserens, A. C., Gorlia, T., Hamou, M. F., De Tribolet, N., Weller, M., Kros, J. M., Hainfellner, J. A., Mason, W., Mariani, L., Bromberg, J. E. C., Hau, P., Mirimanoff, R. O., Cairncross, J. G., Janzer, R. C., & Stupp, R. (2005). MGMT gene silencing and benefit from temozolomide in glioblastoma. *New England Journal of Medicine*, *352*(10), 997–1003. https://doi.org/10.1056/NEJMoa043331

Henikoff, S., & Smith, M. M. (2015). Histone variants and epigenetics. *Cold Spring Harbor Perspectives in Biology*, *7*(1), 1–25. https://doi.org/10.1101/cshperspect.a019364

Holland, E. C. (2000). Glioblastoma multiforme: The terminator. *Proceedings of the National Academy of Sciences of the United States of America*, *97*(12), 6242–6244. https://doi.org/10.1073/pnas.97.12.6242

Huang, K., Liu, X., Li, Y., Wang, Q., Zhou, J., Wang, Y., Dong, F., Yang, C., Sun, Z., Fang, C., Liu, C., Tan, Y., Wu, X., Jiang, T., & Kang, C. (2019). Genome-Wide CRISPR-Cas9 Screening Identifies NF-κB/E2F6 Responsible for EGFRvIII-Associated Temozolomide Resistance in Glioblastoma. *Advanced Science*, *6*(17). https://doi.org/10.1002/advs.201900782

Huang, R. X., & Zhou, P. K. (2020). DNA damage response signaling pathways and targets for radiotherapy sensitization in cancer. In *Signal Transduction and Targeted Therapy* (Vol. 5, Issue 1). Springer Nature. https://doi.org/10.1038/s41392-020-0150-x

Hyun, K., Jeon, J., Park, K., & Kim, J. (2017). Writing, erasing and reading histone lysine methylations. *Experimental and Molecular Medicine*, *49*(4). https://doi.org/10.1038/emm.2017.11

Iness, A. N., & Litovchick, L. (2018). MuvB: A key to cell cycle control in ovarian cancer. In *Frontiers in Oncology* (Vol. 8, Issue JUN). Frontiers Media S.A. https://doi.org/10.3389/fonc.2018.00223

Iyer, V. S., Jiang, L., Shen, Y., Boddul, S. V, Panda, S. K., Kasza, Z., Schmierer, B., & Wermeling, F. (2020). Designing custom CRISPR libraries for hypothesis-driven drug target discovery. *Computational and Structural Biotechnology Journal*, *18*, 2237–2246. https://doi.org/https://doi.org/10.1016/j.csbj.2020.08.009

Jackson, S. P., & Bartek, J. (2009). The DNA-damage response in human biology and disease. *Nature*, *461*(7267), 1071–1078. https://doi.org/10.1038/nature08467

Jiang, F., & Doudna, J. A. (2017). *CRISPR – Cas9 Structures and Mechanisms*. 505–531.

Jinek, M., Chylinski, K., Fonfara, I., Hauer, M., Doudna, J. A., & Charpentier, E. (2012). *A Programmable Dual-RNA – Guided*. *337*(August), 816–822.

Jones, P. A., Issa, J. P. J., & Baylin, S. (2016). Targeting the cancer epigenome for therapy. *Nature Reviews Genetics*, *17*(10), 630–641. https://doi.org/10.1038/nrg.2016.93

Kaur, H., Phillips-Mason, P. J., Burden-Gulley, S. M., Kerstetter-Fogle, A. E., Basilion, J. P., Sloan, A. E., & Brady-Kalnay, S. M. (2012). Cadherin-11, a marker of the mesenchymal phenotype, regulates glioblastoma cell migration and survival in vivo. *Molecular Cancer Research*, *10*(3), 293–304. https://doi.org/10.1158/1541-7786.MCR-11-0457

Kayabolen, A., Yilmaz, E., Sahin, G. N., Seker-Polat, F., Cingoz, A., Isik, B., Acar, S., Wakimoto, H., Cahill, D. P., Solaroglu, I., Cribbs, A. P., Oppermann, U., & Bagci-Onder, T. (n.d.). *Orthogonal targeting of KDM6A/B and HDACs mediates potent therapeutic effects in IDH1-mutant glioma*. https://doi.org/10.1101/2020.11.26.400234

Khateb, A., Deshpande, A., Feng, Y., Finlay, D., Lee, J. S., Lazar, I., Fabre, B., Li, Y., Fujita, Y., Zhang, T., Yin, J., Pass, I., Livneh, I., Jeremias, I., Burian, C., Mason, J. R., Almog, R., Horesh, N., Ofran, Y., … Ronai, Z. A. (2021). The ubiquitin ligase RNF5 determines acute myeloid leukemia growth and susceptibility to histone deacetylase inhibitors. *Nature Communications*, *12*(1), 5397. https://doi.org/10.1038/s41467-021-25664-7

Kitange, G. J., Mladek, A. C., Schroeder, M. A., Pokorny, J. C., Carlson, B. L., Zhang, Y., Nair, A. A., Lee, J. H., Yan, H., Decker, P. A., Zhang, Z., & Sarkaria, J. N. (2016). Retinoblastoma Binding Protein 4 Modulates Temozolomide Sensitivity in Glioblastoma by Regulating DNA Repair Proteins. *Cell Reports*, *14*(11), 2587–2598. https://doi.org/10.1016/j.celrep.2016.02.045

Kondo, Y., Katsushima, K., Ohka, F., Natsume, A., & Shinjo, K. (2014). Epigenetic dysregulation in glioma. *Cancer Science*, *105*(4), 363–369. https://doi.org/10.1111/cas.12379

Kouznetsova, V. L., Tchekanov, A., Li, X., Yan, X., & Tsigelny, I. F. (2019). Polycomb repressive 2 complex—Molecular mechanisms of function. In *Protein Science* (Vol. 28, Issue 8, pp. 1387–1399). Blackwell Publishing Ltd. https://doi.org/10.1002/pro.3647

Kunadis, E., Lakiotaki, E., Korkolopoulou, P., & Piperi, C. (2021). Targeting post-translational histone modifying enzymes in glioblastoma. *Pharmacology and Therapeutics*, *220*(xxxx), 107721. https://doi.org/10.1016/j.pharmthera.2020.107721

Lee, S. Y. (2016). Temozolomide resistance in glioblastoma multiforme. *Genes and Diseases*, *3*(3), 198–210. https://doi.org/10.1016/j.gendis.2016.04.007

Lee, Y.-J., Seo, H. W., Baek, J.-H., Lim, S. H., Hwang, S.-G., & Kim, E. H. (2020). Gene expression profiling of glioblastoma cell lines depending on TP53 status after tumor-treating fields (TTFields) treatment. *Scientific Reports*, *10*(1), 12272. https://doi.org/10.1038/s41598-020-68473-6

Leica Biosystems. (n.d.). *H&E Staining Overview: A Guide to Best Practices*. Retrieved December 12, 2023, from https://www.leicabiosystems.com/knowledge-pathway/he-staining-overview-a-guide-to-best-practices/

Lejon, S., Thong, S. Y., Murthy, A., AlQarni, S., Murzina, N. V, Blobel, G. A., Laue, E. D., & Mackay, J. P. (2011). Insights into Association of the NuRD Complex with FOG-1 from the Crystal Structure of an RbAp48·FOG-1 Complex *. *Journal of Biological Chemistry*, *286*(2), 1196–1203. https://doi.org/10.1074/jbc.M110.195842

Li, J., Song, C., Gu, J., Li, C., Zang, W., Shi, L., Chen, L., Zhu, L., Zhou, M., Wang, T., Li, H., Qi, S., & Lu, Y. (2023). RBBP4 regulates the expression of the Mre11-

Rad50-NBS1 (MRN) complex and promotes DNA double-strand break repair to mediate glioblastoma chemoradiotherapy resistance. *Cancer Letters*, *557*(January), 216078. https://doi.org/10.1016/j.canlet.2023.216078

Li, W., Xu, H., Xiao, T., Cong, L., Love, M. I., Zhang, F., Irizarry, R. A., Liu, J. S., Brown, M., & Liu, X. (2014). MAGeCK enables robust identification of essential genes from genome-scale CRISPR/Cas9 knockout screens. *Genome Biology*, *15*(12), 554. https://doi.org/10.1186/preaccept-1316450832143458

Li, Y., Gong, H., Wang, P., Zhu, Y., Peng, H., Cui, Y., Li, H., Liu, J., & Wang, Z. (2021). The emerging role of ISWI chromatin remodeling complexes in cancer. In *Journal of Experimental and Clinical Cancer Research* (Vol. 40, Issue 1). BioMed Central Ltd. https://doi.org/10.1186/s13046-021-02151-x

Litovchick, L., Sadasivam, S., Florens, L., Zhu, X., Swanson, S. K., Velmurugan, S., Chen, R., Washburn, M. P., Liu, X. S., & DeCaprio, J. A. (2007). Evolutionarily Conserved Multisubunit RBL2/p130 and E2F4 Protein Complex Represses Human Cell Cycle-Dependent Genes in Quiescence. *Molecular Cell*, *26*(4), 539–551. https://doi.org/10.1016/j.molcel.2007.04.015

Liu, A., Hou, C., Chen, H., Zong, X., & Zong, P. (2016). Genetics and epigenetics of glioblastoma: Applications and Overall Incidence of IDH1 Mutation. *Frontiers in Oncology*, *6*(JAN), 1–9. https://doi.org/10.3389/fonc.2016.00016

Liu, H., & Weng, J. (2022). A comprehensive bioinformatic analysis of cyclin-dependent kinase 2 (CDK2) in glioma. *Gene*, *822*, 146325. https://doi.org/https://doi.org/10.1016/j.gene.2022.146325

Liu, L., & Gerson, S. L. (2006). Targeted modulation of MGMT: Clinical implications. In *Clinical Cancer Research* (Vol. 12, Issue 2, pp. 328–331). https://doi.org/10.1158/1078-0432.CCR-05-2543

Louis, D. N., Perry, A., Reifenberger, G., von Deimling, A., Figarella-Branger, D., Cavenee, W. K., Ohgaki, H., Wiestler, O. D., Kleihues, P., & Ellison, D. W. (2016).

The 2016 World Health Organization Classification of Tumors of the Central Nervous System: a summary. *Acta Neuropathologica*, *131*(6), 803–820. https://doi.org/10.1007/s00401-016-1545-1

Louis, D. N., Perry, A., Wesseling, P., Brat, D. J., Cree, I. A., Figarella-Branger, D., Hawkins, C., Ng, H. K., Pfister, S. M., Reifenberger, G., Soffietti, R., Von Deimling, A., & Ellison, D. W. (2021). The 2021 WHO classification of tumors of the central nervous system: A summary. *Neuro-Oncology*, *23*(8), 1231–1251. https://doi.org/10.1093/neuonc/noab106

MacLeod, G., Bozek, D. A., Rajakulendran, N., Monteiro, V., Ahmadi, M., Steinhart, Z., Kushida, M. M., Yu, H., Coutinho, F. J., Cavalli, F. M. G., Restall, I., Hao, X., Hart, T., Luchman, H. A., Weiss, S., Dirks, P. B., & Angers, S. (2019). Genome-Wide CRISPR-Cas9 Screens Expose Genetic Vulnerabilities and Mechanisms of Temozolomide Sensitivity in Glioblastoma Stem Cells. *Cell Reports*, *27*(3), 971-986.e9. https://doi.org/10.1016/j.celrep.2019.03.047

Mahabir, R., Tanino, M., Elmansuri, A., Wang, L., Kimura, T., Itoh, T., Ohba, Y., Nishihara, H., Shirato, H., Tsuda, M., & Tanaka, S. (2014). Sustained elevation of Snail promotes glial-mesenchymal transition after irradiation in malignant glioma. *Neuro-Oncology*, *16*(5), 671–685. https://doi.org/10.1093/neuonc/not239

Malta, T. M., De Souza, C. F., Sabedot, T. S., Silva, T. C., Mosella, M. S., Kalkanis, S. N., Snyder, J., Castro, A. V. B., & Noushmehr, H. (2018). Glioma CpG island methylator phenotype (G-CIMP): Biological and clinical implications. *Neuro-Oncology*, *20*(5), 608–620. https://doi.org/10.1093/neuonc/nox183

Mann, J., Ramakrishna, R., Magge, R., & Wernicke, A. G. (2018). Advances in Radiotherapy for Glioblastoma. *Frontiers in Neurology*, *8*. https://www.frontiersin.org/articles/10.3389/fneur.2017.00748

Margueron, R., & Reinberg, D. (2011). The Polycomb complex PRC2 and its mark in life. In *Nature* (Vol. 469, Issue 7330, pp. 343–349). https://doi.org/10.1038/nature09784

Marine, J. C., Dawson, S. J., & Dawson, M. A. (2020). Non-genetic mechanisms of therapeutic resistance in cancer. *Nature Reviews Cancer*, *20*(12), 743–756. https://doi.org/10.1038/s41568-020-00302-4

Maurage, C.-A., Adam, E., Minéo, J.-F., Sarrazin, S., Debunne, M., Siminski, R.-M., Baroncini, M., Lassalle, P., Blond, S., & Delehedde, M. (2009). Endocan Expression and Localization in Human Glioblastomas. *Journal of Neuropathology & Experimental Neurology*, *68*(6), 633–641. https://doi.org/10.1097/NEN.0b013e3181a52a7f

McDermott, M., Eustace, A. J., Busschots, S., Breen, L., Crown, J., Clynes, M., O'Donovan, N., & Stordal, B. (2014). In vitro development of chemotherapy and targeted therapy drug-resistant cancer cell lines: A practical guide with case studies. *Frontiers in Oncology*, *4 MAR*. https://doi.org/10.3389/fonc.2014.00040

McLendon, R., Friedman, A., Bigner, D., Van Meir, E. G., Brat, D. J., Mastrogianakis, G. M., Olson, J. J., Mikkelsen, T., Lehman, N., Aldape, K., Yung, W. K. A., Bogler, O., Weinstein, J. N., VandenBerg, S., Berger, M., Prados, M., Muzny, D., Morgan, M., Scherer, S., … Thomson, E. (2008). Comprehensive genomic characterization defines human glioblastoma genes and core pathways. *Nature*, *455*(7216), 1061–1068. https://doi.org/10.1038/nature07385

Mehta, M., Wen, P., Nishikawa, R., Reardon, D., & Peters, K. (2017). Critical review of the addition of tumor treating fields (TTFields) to the existing standard of care for newly diagnosed glioblastoma patients. *Critical Reviews in Oncology/Hematology*, *111*, 60–65. https://doi.org/https://doi.org/10.1016/j.critrevonc.2017.01.005

Miles, L. A., Garippa, R. J., & Poirier, J. T. (2016). Design, execution, and analysis of pooled in vitro CRISPR/Cas9 screens. *FEBS Journal*, *283*, 3170–3180. https://doi.org/10.1111/febs.13770

Millard, C. J., Fairall, L., Ragan, T. J., Savva, C. G., & Schwabe, J. W. R. (2020). The topology of chromatin-binding domains in the NuRD deacetylase complex. *Nucleic Acids Research*, *48*(22), 12972–12982. https://doi.org/10.1093/nar/gkaa1121

Millard, C. J., Varma, N., Saleh, A., Morris, K., Watson, P. J., Bottrill, A. R., Fairall, L., Smith, C. J., & Schwabe, J. W. (n.d.). *The structure of the core NuRD repression complex provides insights into its interaction with chromatin*. https://doi.org/10.7554/eLife.13941.001

Mladek, A. C., Yan, H., Tian, S., Decker, P. A., Burgenske, D. M., Bakken, K., Hu, Z., He, L., Connors, M. A., Carlson, B. L., Wilson, J., Bommi-Reddy, A., Conery, A., Eckel-Passow, J. E., Sarkaria, J. N., & Kitange, G. J. (2022). RBBP4-p300 axis modulates expression of genes essential for cell survival and is a potential target for therapy in glioblastoma. *Neuro-Oncology*, *24*(8), 1261–1272. https://doi.org/10.1093/neuonc/noac051

Musselman, C. A., Lalonde, M. E., Côté, J., & Kutateladze, T. G. (2012). Perceiving the epigenetic landscape through histone readers. In *Nature Structural and Molecular Biology* (Vol. 19, Issue 12, pp. 1218–1227). https://doi.org/10.1038/nsmb.2436

Nakamura, M., Gao, Y., Dominguez, A. A., & Qi, L. S. (2021). CRISPR technologies for precise epigenome editing. *Nature Cell Biology*, *23*(1), 11–22. https://doi.org/10.1038/s41556-020-00620-7

Ortiz, R., Perazzoli, G., Cabeza, L., Jiménez-Luna, C., Luque, R., Prados, J., & Melguizo, C. (2020). Temozolomide: An Updated Overview of Resistance Mechanisms, Nanotechnology Advances and Clinical Applications. *Current Neuropharmacology*, *19*(4), 513–537. https://doi.org/10.2174/1570159x18666200626204005

Ostrom, Q. T., Cioffi, G., Gittleman, H., Patil, N., Waite, K., Kruchko, C., & Barnholtz-Sloan, J. S. (2019). CBTRUS Statistical Report: Primary Brain and Other Central Nervous System Tumors Diagnosed in the United States in 2012-2016. In *Neuro-Oncology* (Vol. 21, pp. V1–V100). Oxford University Press. https://doi.org/10.1093/neuonc/noz150

Ozyerli-Goknar, E., Kala, E. Y., Aksu, A. C., Bulut, I., Cingöz, A., Nizamuddin, S., Biniossek, M., Seker-Polat, F., Morova, T., Aztekin, C., Kung, S. H. Y., Syed, H., Tuncbag, N., Gönen, M., Philpott, M., Cribbs, A. P., Acilan, C., Lack, N. A., Onder, T. T., … Bagci-Onder, T. (2023). Epigenetic-focused CRISPR/Cas9 screen identifies (absent, small, or homeotic)2-like protein (ASH2L) as a regulator of glioblastoma cell survival. *Cell Communication and Signaling*, *21*(1). https://doi.org/10.1186/s12964-023-01335-6

Parsons, D. W., Jones, S., Zhang, X., Lin, J. C. H., Leary, R. J., Angenendt, P., Mankoo, P., Carter, H., Siu, I. M., Gallia, G. L., Olivi, A., McLendon, R., Rasheed, B. A., Keir, S., Nikolskaya, T., Nikolsky, Y., Busam, D. A., Tekleab, H., Diaz, L. A., … Kinzler, K. W. (2008). An integrated genomic analysis of human glioblastoma multiforme. *Science*, *321*(5897), 1807–1812. https://doi.org/10.1126/science.1164382

Pfister, S. X., & Ashworth, A. (2017). Marked for death: Targeting epigenetic changes in cancer. *Nature Reviews Drug Discovery*, *16*(4), 241–263. https://doi.org/10.1038/nrd.2016.256

Pilié, P. G., Tang, C., Mills, G. B., & Yap, T. A. (2019). State-of-the-art strategies for targeting the DNA damage response in cancer. In *Nature Reviews Clinical Oncology* (Vol. 16, Issue 2, pp. 81–104). Nature Publishing Group. https://doi.org/10.1038/s41571-018-0114-z

Plass, C., Pfister, S. M., Lindroth, A. M., Bogatyrova, O., Claus, R., & Lichter, P. (2013). Mutations in regulators of the epigenome and their connections to global chromatin

patterns in cancer. *Nature Reviews Genetics*, *14*(11), 765–780. https://doi.org/10.1038/nrg3554

Qian, Y.-W., & Lee, E. Y.-H. P. (1995). Dual Retinoblastoma-binding Proteins with Properties Related to a Negative Regulator of Ras in Yeast (∗). *Journal of Biological Chemistry*, *270*(43), 25507–25513. https://doi.org/10.1074/jbc.270.43.25507

Qin, T., Mullan, B., Ravindran, R., Castro, M. G., Yadav, V. N., Koschmann, C., Qin, T., Mullan, B., Ravindran, R., Messinger, D., Siada, R., & Cummings, J. R. (2022). Article ATRX loss in glioma results in dysregulation of cell- cycle phase transition and ATM inhibitor radio- sensitization ll ATRX loss in glioma results in dysregulation of cell-cycle phase transition and ATM inhibitor radio-sensitization. *CellReports*, *38*(2), 110216. https://doi.org/10.1016/j.celrep.2021.110216

Roberti, A., Valdes, A. F., Torrecillas, R., Fraga, M. F., & Fernandez, A. F. (2019). Epigenetics in cancer therapy and nanomedicine. *Clinical Epigenetics*, *11*(1), 1–18. https://doi.org/10.1186/s13148-019-0675-4

Romani, M., Pistillo, M. P., & Banelli, B. (2018). Epigenetic targeting of glioblastoma. *Frontiers in Oncology*, *8*(OCT), 1–9. https://doi.org/10.3389/fonc.2018.00448

Sadasivam, S., & Decaprio, J. A. (2013). The DREAM complex: master coordinator of cell cycle-dependent gene expression. In *NATURE REVIEWS | CANCER* (Vol. 13). www.nature.com/reviews/cancer

Sadasivam, S., Duan, S., & DeCaprio, J. A. (2012). The MuvB complex sequentially recruits B-Myb and FoxM1 to promote mitotic gene expression. *Genes & Development*, *26*(5), 474–489. https://doi.org/10.1101/gad.181933.111

Schaff, L. R., & Mellinghoff, I. K. (2023). Glioblastoma and Other Primary Brain Malignancies in Adults: A Review. In *JAMA* (Vol. 329, Issue 7, pp. 574–587). American Medical Association. https://doi.org/10.1001/jama.2023.0023

Senbabaoglu, F., Aksu, A. C., Cingoz, A., Seker-Polat, F., Borklu-Yucel, E., Solaroglu, İ., & Bagci-Onder, T. (2020). Drug Repositioning Screen on a New Primary Cell Line Identifies Potent Therapeutics for Glioblastoma. *Frontiers in Neuroscience*, *14*(December), 1–13. https://doi.org/10.3389/fnins.2020.578316

Shalem, O., Sanjana, N. E., Hartenian, E., Shi, X., Scott, D. A., Mikkelsen, T. S., Heckl, D., Ebert, B. L., Root, D. E., Doench, J. G., & Zhang, F. (2014). Genome-scale CRISPR-Cas9 knockout screening in human cells. *Science*, *343*(6166), 84–87. https://doi.org/10.1126/science.1247005

SHARMA, S., SALEHI, F., SCHEITHAUER, B. W., ROTONDO, F., SYRO, L. V, & KOVACS, K. (2009). Role of MGMT in Tumor Development, Progression, Diagnosis, Treatment and Prognosis. *Anticancer Research*, *29*(10), 3759. http://ar.iiarjournals.org/content/29/10/3759.abstract

Shi, Y., Wang, X. X., Zhuang, Y. W., Jiang, Y., Melcher, K., & Xu, H. E. (2017). Structure of the PRC2 complex and application to drug discovery. In *Acta Pharmacologica Sinica* (Vol. 38, Issue 7, pp. 963–976). Nature Publishing Group. https://doi.org/10.1038/aps.2017.7

Shou, J., Gao, H., Cheng, S., Wang, B., & Guan, H. (2021). LncRNA HOXA-AS2 promotes glioblastoma carcinogenesis by targeting miR-885-5p/RBBP4 axis. *Cancer Cell International*, *21*(1). https://doi.org/10.1186/s12935-020-01690-1

Singh, N., Miner, A., Hennis, L., & Mittal, S. (2021). Mechanisms of temozolomide resistance in glioblastoma - a comprehensive review. In *Cancer Drug Resistance* (Vol. 4, Issue 1, pp. 17–43). OAE Publishing Inc. https://doi.org/10.20517/cdr.2020.79

Stirnimann, C. U., Petsalaki, E., Russell, R. B., & Müller, C. W. (2010). WD40 proteins propel cellular networks. *Trends in Biochemical Sciences*, *35*(10), 565–574. https://doi.org/https://doi.org/10.1016/j.tibs.2010.04.003

Stupp, R., Mason, W. P., Van Den Bent, M. J., Weller, M., Fisher, B., Taphoorn, M. J. B., Belanger, K., Brandes, A. A., Marosi, C., Bogdahn, U., Curschmann, J., Janzer, R. C., Ludwin, S. K., Gorlia, T., Allgeier, A., Lacombe, D., Cairncross, J. G., Eisenhauer, E., & Mirimanoff, R. O. (n.d.). *Radiotherapy plus Concomitant and Adjuvant Temozolomide for Glioblastoma*. www.nejm.org

Stupp, R., Taillibert, S., Kanner, A. A., Kesari, S., Steinberg, D. M., Toms, S. A., Taylor, L. P., Lieberman, F., Silvani, A., Fink, K. L., Barnett, G. H., Zhu, J.-J., Henson, J. W., Engelhard, H. H., Chen, T. C., Tran, D. D., Sroubek, J., Tran, N. D., Hottinger, A. F., … Ram, Z. (2015). Maintenance Therapy With Tumor-Treating Fields Plus Temozolomide vs Temozolomide Alone for Glioblastoma: A Randomized Clinical Trial. *JAMA*, *314*(23), 2535–2543. https://doi.org/10.1001/jama.2015.16669

Stupp, R., Wong, E. T., Kanner, A. A., Steinberg, D., Engelhard, H., Heidecke, V., Kirson, E. D., Taillibert, S., Liebermann, F., Dbalý, V., Ram, Z., Villano, J. L., Rainov, N., Weinberg, U., Schiff, D., Kunschner, L., Raizer, J., Honnorat, J., Sloan, A., … Gutin, P. H. (2012). NovoTTF-100A versus physician's choice chemotherapy in recurrent glioblastoma: A randomised phase III trial of a novel treatment modality. *European Journal of Cancer*, *48*(14), 2192–2202. https://doi.org/https://doi.org/10.1016/j.ejca.2012.04.011

Sykaras, A. G., Pergaris, A., & Theocharis, S. (2021). Challenging, Accurate and Feasible: CAF-1 as a Tumour Proliferation Marker of Diagnostic and Prognostic Value. *Cancers*, *13*(11). https://doi.org/10.3390/cancers13112575

Tadesse, S., Anshabo, A. T., Portman, N., Lim, E., Tilley, W., Caldon, C. E., & Wang, S. (2020). Targeting CDK2 in cancer: challenges and opportunities for therapy. *Drug Discovery Today*, *25*(2), 406–413. https://doi.org/https://doi.org/10.1016/j.drudis.2019.12.001

Toledo, C. M., Ding, Y., Hoellerbauer, P., Davis, R. J., Basom, R., Girard, E. J., Lee, E., Corrin, P., Hart, T., Bolouri, H., Davison, J., Zhang, Q., Hardcastle, J., Aronow, B. J., Plaisier, C. L., Baliga, N. S., Moffat, J., Lin, Q., Li, X. N., … Paddison, P. J.

(2015). Genome-wide CRISPR-Cas9 Screens Reveal Loss of Redundancy between PKMYT1 and WEE1 in Glioblastoma Stem-like Cells. *Cell Reports*, *13*(11), 2425–2439. https://doi.org/10.1016/j.celrep.2015.11.021

Tomar, M. S., Kumar, A., Srivastava, C., & Shrivastava, A. (2021). Elucidating the mechanisms of Temozolomide resistance in gliomas and the strategies to overcome the resistance. In *Biochimica et Biophysica Acta - Reviews on Cancer* (Vol. 1876, Issue 2). Elsevier B.V. https://doi.org/10.1016/j.bbcan.2021.188616

Torchy, M. P., Hamiche, A., & Klaholz, B. P. (2015). Structure and function insights into the NuRD chromatin remodeling complex. In *Cellular and Molecular Life Sciences* (Vol. 72, Issue 13, pp. 2491–2507). Birkhauser Verlag AG. https://doi.org/10.1007/s00018-015-1880-8

Tsai, H.-F., Chang, Y.-C., Li, C.-H., Chan, M.-H., Chen, C.-L., Tsai, W.-C., & Hsiao, M. (2021). Type V collagen alpha 1 chain promotes the malignancy of glioblastoma through PPRC1-ESM1 axis activation and extracellular matrix remodeling. *Cell Death Discovery*, *7*(1), 313. https://doi.org/10.1038/s41420-021-00661-3

Vedadi, M., Blazer, L., Eram, M. S., Barsyte-Lovejoy, D., Arrowsmith, C. H., & Hajian, T. (2017). Targeting human SET1/MLL family of proteins. *Protein Science*, *26*(4), 662–676. https://doi.org/10.1002/pro.3129

Verhaak, R. G. W., Hoadley, K. A., Purdom, E., Wang, V., Qi, Y., Wilkerson, M. D., Miller, C. R., Ding, L., Golub, T., Mesirov, J. P., Alexe, G., Lawrence, M., O'Kelly, M., Tamayo, P., Weir, B. A., Gabriel, S., Winckler, W., Gupta, S., Jakkula, L., … Hayes, D. N. (2010). Integrated Genomic Analysis Identifies Clinically Relevant Subtypes of Glioblastoma Characterized by Abnormalities in PDGFRA, IDH1, EGFR, and NF1. *Cancer Cell*, *17*(1), 98–110. https://doi.org/10.1016/j.ccr.2009.12.020

Verreault, A., Kaufman, P. D., Kobayashi, R., & Stillman, B. (1996). Nucleosome Assembly by a Complex of CAF-1 and Acetylated Histones H3/H4. *Cell*, *87*(1), 95–104. https://doi.org/10.1016/S0092-8674(00)81326-4

Villano, J. L., Seery, T. E., & Bressler, L. R. (2009). Temozolomide in malignant gliomas: Current use and future targets. *Cancer Chemotherapy and Pharmacology*, *64*(4), 647–655. https://doi.org/10.1007/s00280-009-1050-5

Vlassenbroeck, I., Califice, S., Diserens, A. C., Migliavacca, E., Straub, J., Di Stefano, I., Moreau, F., Hamou, M. F., Renard, I., Delorenzi, M., Flamion, B., DiGuiseppi, J., Bierau, K., & Hegi, M. E. (2008). Validation of real-time methylation-specific PCR to determine O 6-methylguanine-DNA methyltransferase gene promoter methylation in glioma. *Journal of Molecular Diagnostics*, *10*(4), 332–337. https://doi.org/10.2353/jmoldx.2008.070169

Wang, J., Yang, T., Xu, G., Liu, H., Ren, C., Xie, W., & Wang, M. (2016). Cyclin-Dependent Kinase 2 Promotes Tumor Proliferation and Induces Radio Resistance in Glioblastoma. *Translational Oncology*, *9*(6), 548–556. https://doi.org/https://doi.org/10.1016/j.tranon.2016.08.007

Wang, T., Wei, J. J., Sabatini, D. M., & Lander, E. S. (2014). Genetic screens in human cells using the CRISPR-Cas9 system. *Science*, *343*(6166), 80–84. https://doi.org/10.1126/science.1246981

Weller, M., van den Bent, M., Preusser, M., Le Rhun, E., Tonn, J. C., Minniti, G., Bendszus, M., Balana, C., Chinot, O., Dirven, L., French, P., Hegi, M. E., Jakola, A. S., Platten, M., Roth, P., Rudà, R., Short, S., Smits, M., Taphoorn, M. J. B., … Wick, W. (2021). EANO guidelines on the diagnosis and treatment of diffuse gliomas of adulthood. *Nature Reviews Clinical Oncology*, *18*(3), 170–186. https://doi.org/10.1038/s41571-020-00447-z

Wen, P. Y., Weller, M., Lee, E. Q., Alexander, B. M., Barnholtz-Sloan, J. S., Barthel, F. P., Batchelor, T. T., Bindra, R. S., Chang, S. M., Antonio Chiocca, E., Cloughesy,

T. F., DeGroot, J. F., Galanis, E., Gilbert, M. R., Hegi, M. E., Horbinski, C., Huang, R. Y., Lassman, A. B., Le Rhun, E., … van den Bent, M. J. (2020). Glioblastoma in adults: A Society for Neuro-Oncology (SNO) and European Society of Neuro-Oncology (EANO) consensus review on current management and future directions. In *Neuro-Oncology* (Vol. 22, Issue 8, pp. 1073–1113). Oxford University Press. https://doi.org/10.1093/neuonc/noaa106

Wesolowski, J. R., Rajdev, P., & Mukherji, S. K. (2010). Temozolomide (Temodar). *American Journal of Neuroradiology*, *31*(8), 1383–1384. https://doi.org/10.3174/ajnr.A2170

Wiedemeyer, W. R., Dunn, I. F., Quayle, S. N., Zhang, J., Chheda, M. G., Dunn, G. P., Zhuang, L., Rosenbluh, J., Chen, S., Xiao, Y., Shapiro, G. I., Hahn, W. C., & Chin, L. (2010). Pattern of retinoblastoma pathway inactivation dictates response to CDK4/6 inhibition in GBM. *Proceedings of the National Academy of Sciences*, *107*(25), 11501–11506. https://doi.org/10.1073/pnas.1001613107

Wijethilake, N., Islam, M., & Ren, H. (2020). Radiogenomics model for overall survival prediction of glioblastoma. *Medical & Biological Engineering & Computing*, *58*(8), 1767–1777. https://doi.org/10.1007/s11517-020-02179-9

Woo, PeterY. M., Li, Y., Chan, AnnaH. Y., Ng, StephanieC. P., Loong, HerbertH. F., Chan, DannyT. M., Wong, GeorgeK. C., & Poon, W.-S. (2019). A multifaceted review of temozolomide resistance mechanisms in glioblastoma beyond O-6-methylguanine-DNA methyltransferase. *Glioma*, *2*(2), 68. https://doi.org/10.4103/glioma.glioma_3_19

Yan, H., Williams, D., Jin, G., Mclendon, R., Rasheed, B. A., Yuan, W., Kos, I., Batinic-Haberle, I., Jones, S., Riggins, G. J., Friedman, H., Friedman, A., Reardon, D., Herndon, J., Kinzler, K. W., Velculescu, V. E., Vogelstein, B., & Bigner, D. D. (2009). IDH1 and IDH2 Mutations in Gliomas A bs tr ac t. In *N Engl J Med* (Vol. 360).

Yang, K., Wu, Z., Zhang, H., Zhang, N., Wu, W., Wang, Z., Dai, Z., Zhang, X., Zhang, L., Peng, Y., Ye, W., Zeng, W., Liu, Z., & Cheng, Q. (2022). Glioma targeted therapy: insight into future of molecular approaches. In *Molecular Cancer* (Vol. 21, Issue 1). BioMed Central Ltd. https://doi.org/10.1186/s12943-022-01513-z

Yedier-Bayram, O., Gokbayrak, B., Kayabolen, A., Aksu, A. C., Cavga, A. D., Cingöz, A., Kala, E. Y., Karabiyik, G., Günsay, R., Esin, B., Morova, T., Uyulur, F., Syed, H., Philpott, M., Cribbs, A. P., Kung, S. H. Y., Lack, N. A., Onder, T. T., & Bagci-Onder, T. (2022). EPIKOL, a chromatin-focused CRISPR/Cas9-based screening platform, to identify cancer-specific epigenetic vulnerabilities. *Cell Death and Disease*, *13*(8). https://doi.org/10.1038/s41419-022-05146-4

Yu, W., Zhang, L., Wei, Q., & Shao, A. (2020). O6-Methylguanine-DNA Methyltransferase (MGMT): Challenges and New Opportunities in Glioma Chemotherapy. In *Frontiers in Oncology* (Vol. 9). Frontiers Media S.A. https://doi.org/10.3389/fonc.2019.01547

Yu, Z., Liu, J., Deng, W. M., & Jiao, R. (2015). Histone chaperone CAF-1: Essential roles in multi-cellular organism development. *Cellular and Molecular Life Sciences*, *72*(2), 327–337. https://doi.org/10.1007/s00018-014-1748-3

Zhang, W., Aubert, A., Gomez de Segura, J. M., Karuppasamy, M., Basu, S., Murthy, A. S., Diamante, A., Drury, T. A., Balmer, J., Cramard, J., Watson, A. A., Lando, D., Lee, S. F., Palayret, M., Kloet, S. L., Smits, A. H., Deery, M. J., Vermeulen, M., Hendrich, B., … Laue, E. D. (2016). The Nucleosome Remodeling and Deacetylase Complex NuRD Is Built from Preformed Catalytically Active Sub-modules. *Journal of Molecular Biology*, *428*(14), 2931–2942. https://doi.org/https://doi.org/10.1016/j.jmb.2016.04.025

Zheng, Z., Yao, X., & Liu, Y. (2022). RBBP4 plays a vital role in the malignant progression of triple-negative breast cancer by regulating epithelial-mesenchymal transition. *Genes & Genomics*, *44*(10), 1301–1309. https://doi.org/10.1007/s13258-022-01262-9